UC Berkeley
UC Berkeley Electronic Theses and Dissertations

**Title**
Characterization of the Molecular Composition of Secondary Organic Aerosols using High Resolution Mass Spectrometry

**Permalink**
https://escholarship.org/uc/item/3v83v7s2

**Author**
Sellon, Rachel Elizabeth

**Publication Date**
2012

Peer reviewed|Thesis/dissertation

eScholarship.org Powered by the California Digital Library
University of California

# Characterization of the Molecular Composition of Secondary Organic Aerosols using High Resolution Mass Spectrometry

By

Rachel Elizabeth Sellon

A Dissertation submitted in partial satisfaction of the

requirements for the degree of

Doctor of Philosophy

in Chemistry

in the

Graduate Division

of the

University of California, Berkeley

Committee in charge:

Professor Allen Goldstein, Co-chair

Professor Ron Cohen, Co-chair

Professor Kristie Boering

Professor Rob Rhew

Fall, 2012

# Characterization of the Molecular Composition of Secondary Organic Aerosols using High Resolution Mass Spectrometry

Copyright 2012
by
Rachel Elizabeth Sellon

# Abstract

## Characterization of the Molecular Composition of Secondary Organic Aerosols using High Resolution Mass Spectrometry

by

Rachel Elizabeth Sellon

Doctor of Philosophy in Chemistry

University of California, Berkeley

Professor Allen Goldstein, co-chair

Professor Ron Cohen, co-chair

Atmospheric aerosols can affect visibility and the Earth's climate by scattering and absorbing light and they also can have adverse effects on human health. The organic portion of atmospheric aerosols is very complex and is a major fraction of fine particulate matter. High molecular weight (high-MW)/oligomeric organic compounds can make up a large part of this organic fraction and the composition, sources, and formation mechanisms for these compounds are not well understood. This knowledge and understanding is necessary to decrease the uncertainty in the climate affects of aerosols and to improve climate models. This dissertation investigates the composition and formation mechanisms for the high-MW/oligomeric fraction of secondary organic aerosols (SOA) collected in Bakersfield, CA and presents a comparative analysis of chamber and ambient SOA, from both Los Angeles (LA) and Bakersfield, to investigate sources at both locations.

A novel sampling technique, nanospray-Desorption Electrospray Ionization (nano-DESI), was used with high resolution mass spectrometry (HR-MS) to determine the molecular formulas of the high molecular weight (HMW)/oligomeric fraction of SOA. Nano-DESI involves direct desorption from the sample surface and was used to limit reactions that can take place with extraction and storage in solvent. The samples were collected in Bakersfield and LA during CalNex 2010. Both Bakersfield and LA are out of compliance with EPA standards of ozone and particulate matter and provide opportunities to examine air masses affected by both anthropogenic and biogenic sources.

This dissertation has provided the first evidence of observable changes in the composition of high-MW/oligomeric compounds throughout the day. Using positive mode nano-DESI, afternoon increases in the number of compounds that contain carbon, hydrogen and oxygen (CHO) were observed consistent with photochemistry/ozonolysis as a major source for these compounds. Compounds containing reduced nitrogen groups were dominant at night and had precursors consistent with imine formation products from the reaction of carbonyls and ammonia. In the negative mode, organonitrates (CHON) and nitroxy organosulfates (CHONS) had larger numbers of compounds in the night/morning samples consistent with nitrate radical

formation reactions. A subset of the CHONS compounds and compounds containing sulfur (CHOS) had the same composition as known biogenic organosulfates and nitroxy organosulfates indicating contributions from both biogenic and anthropogenic sources to the SOA.

This dissertation also provides the first analysis of the high-MW/oligomeric fraction in size resolved samples; the majority of the compounds were found in aerosol diameters between 0.18-1.0 μm and the CHON were bimodal with size. Finally, this dissertation presents the first comparative analysis of the overlap in the composition of this fraction of SOA between ambient and chamber samples. Samples collected in Pasadena, LA and Bakersfield were compared with samples collected in a smog chamber using diesel and isoprene sources. The results indicate that diesel had the highest overlap at both sites, Bakersfield samples were more oxidized, and LA showed evidence of a SOA plume arriving from downtown LA. The addition of ammonia to the diesel chamber experiment was necessary to form many of the 2N compounds found in Bakersfield.

These results increase our understanding of the types of compounds found in urban environments and give evidence for the timescales of formation reactions in an ambient environment. They show that the majority of the high-MW oligomeric compounds are found in submicron size particles and that the composition of this fraction of SOA varies with aerosol size. Results from the chamber comparisons show that both diesel and isoprene are important sources for these compounds and also that there other sources are present. Future work that combines this type of analysis, in other ambient environments, with studies of the optical properties of aerosols could be used to help improve climate models and to start to close the gap in our understanding of the climate effects of atmospheric aerosols.

# Acknowledgements

I would like to thank my advisor, Prof. Allen Goldstein, for giving me the chance to work in his group and from whom I have learned how to frame research questions, how to conduct that research, and how to present and publish the results. His guidance has been critical to my success and my development as a scientist.

My husband, Jeremy, has been a source of constant support through my time at Berkeley. He is a wonderfully eloquent person with whom it has been a pleasure to discuss ideas and results. His work ethic, attention to detail, and positive attitude have been an inspiration to me.

My parents, Gordon and Dulcy Sellon, have my deepest gratitude for supporting and encouraging me in all my pursuits over so many years. From evenings during my childhood when they helped me understand homework questions to being a voice of reason as I worked my way towards this degree, they have been both guides and inspirations for me. I thank my siblings, Alicia and Chris, for their support, humor, and entertainment.

I would like to thank my collaborators at Pacific Northwest National Labs, Alex and Julia Laskin, without whose help and support this work would not have been completed. Their feedback on the manuscripts taught me a great deal about how to clearly convey scientific ideas and results. My other collaborators on these projects include Dr. Tran Nguyen and Prof. Sergey Nizkorodov at UC Irvine, Prof. Lynn Russell and Shang Liu at UC San Diego, and Dr. Patrick Hayes and Prof. Jose-Luis Jimenez at University of Colorado at Boulder. I would like to thank all of them for their collaboration and willingness to share both data and ideas. I also sincerely thank the other members of the Goldstein group for their helpful discussions and stimulating group meetings.

Finally I would like to thank my dissertation committee members, Prof. Ron Cohen, Prof. Kristie Boering, and Prof. Robert Rhew.

# TABLE OF CONTENTS


Abstract…….. 1

Acknowledgements…….. i

Table of Contents…….. ii

List of Tables and Figures……. v

Abbreviations used in this work……..... vi

**Chapter 1. Introduction** **1**
1.1 Organic Aerosols……..... 1
1.2 High Molecular Weight Compounds and Oligomers……..... 2
1.3 Organic Nitrogen and Sulfur in Aerosols……..... 3
1.4 Research Motivation……..... 5
1.5 Aim of the Work…….. 5
1.6 Dissertation Overview…… 6
1.7 References……..... 8

**Chapter 2. Molecular Characterization of Organic Aerosol Using Positive Mode Nanospray Desporption/Electrospray Ionization Mass Spectrometry: CalNex 2010 Field Study** **13**
2.1 Introduction…….. 13
2.2 Experimental…… 14
2.3 Results and Discussion……..... 16
2.3.1 Mass Spectra and Elemental Composition……... 16
2.3.2 CHO compounds…….. 18
2.3.3 Organic Nitrogen…….. 18
2.3.4 Formation of Nitrogen Containing Organic Compounds……. 19
2.4 Summary…….. 20
2.5 References…… 22
2.6 Tables and Figures……..... 26

**Chapter 3. Using Negative Mode Nano-DESI High-Resolution Mass Spectrometry to Analyze SOA Composition as Function of Aerosol Size and Local Time during CalNex 2010** **32**
3.1 Introduction…….. 32
3.2 Experimental…… 33
3.3 Results and Discussion……. 34
3.3.1 Sample Comparison……. 34
3.3.2 Characterization by group…… 36
3.3.2.1 CHO Compounds…….. 36
3.3.2.2 CHOS Compounds……..... 37
3.3.2.3 CHON Compounds……... 38
3.3.2.4 CHONS Compounds……. 38
3.3.3 Size Distributions……. 39
3.4 References…… 41
3.5 Tables and Figures……..... 45

**Chapter 4. Probing Molecular Associations of Field-Collected and Laboratory Generated SOA with Nano-DESI High-Resolution Mass Spectrometry** **51**
4.1 Introduction…….. 51
4.2 Experimental…… 52
4.2.1 Sampling and Instrumentation……. 52
4.2.2 Data Acquisition/Analysis……..... 54
4.3 Results and Discussion……. 55
4.3.1 Comparing Ambient to Chamber Data……. 55
4.3.2 Comparing LA to BF……..... 58
4.3.3 Comparing Unique Species Observed in Chamber and Ambient Samples…. 59
4.4 Conclusions…….. 60
4.5 References…… 62
4.6 Tables and Figures……..... 67

**Chapter 5.** Summary and Future Work…… 73

**Appendix A: Supplemental Information for Chapter 2**
Appendix A1 Additional information on the field site, meteorology, and sampling. 78
Appendix A2 Relative Humidity and Ozone……. 81
Appendix A3 Mass spectra for samples collected on June 22nd……. 82
Appendix A4 Van Krevelen diagrams for samples collected on June 23rd…… 83
Appendix A5 Van Krevelen comparison of $NOC^+$ and $NOC^-$…….. 84
Appendix A6 Sulfur and $N_3$ containing compounds…….. 85
Appendix A7 Compounds that fail the tests for ammonium adducts……. 86
Appendix A8 Average elemental ratios…….. 87

**Appendix B: Supplemental Information for Chapter 3**


| | | |
|---|---|---|
| Appendix B1 | Additional information on the field site, analysis, and MS/MS……. | 88 |
| Appendix B2 | Meteorological data…… | 92 |
| Appendix B3 | Van Krevelen diagrams for the four samples collected on June 20th | 93 |
| Appendix B4 | Van Krevelen diagrams for the four samples collected on June 21st | 94 |
| Appendix B5 | Van Krevelen diagrams for the four samples collected on June 22nd | 95 |
| Appendix B6 | Van Krevelen diagrams for the four samples collected on June 23rd | 96 |
| Appendix B7 | Isolation and product MS/MS of CHOS compounds……. | 97 |
| Appendix B8 | Number of compounds of each class for size resolved samples……. | 98 |
| Appendix B9 | Number of compounds, by group, observed in each sample…….. | 99 |
| Appendix B10 | Results of the 30V CID test…… | 100 |
| Appendix B11 | Intensity weighted elemental ratios compared with AMS…….. | 101 |
| Appendix B12 | Number of compounds in each sample above given AI values…….. | 102 |
| Appendix B13 | Compounds outside the ranges of the van Krevelen diagrams..... | 103 |
| Appendix B14 | Average elemental ratios separated by compound class……. | 104 |
| Appendix B15 | Organosulfates also found with LC/ESI/MS by Surratt et al…….. | 105 |
| Appendix B16 | Nitroxy organosuflates also found with LC/ESI/MS by Surratt et al. | 106 |
| Appendix B17 | Average elemental ratios for size resolved samples……... | 107 |


**Appendix C: Supplemental Information for Chapter 4**


| | | |
|---|---|---|
| Appendix C1 | Sampling and Instrumentation…… | 108 |
| Appendix C2 | Number of common peaks between samples…… | 109 |
| Appendix C3 | Average elemental ratios: positive and negative mode ESI……... | 110 |
| Appendix C4 | Average O/C values for AMS data collected in LA…….. | 111 |
| Appendix C5 | Correlation of O/C to $f_{44}$ for Bakersfield AMS data…….. | 112 |
| Appendix C6 | Comparison MS BF to DSL-NOx chamber…… | 113 |
| Appendix C7 | Comparison MS LA to DSL-NOx chamber……... | 114 |
| Appendix C8 | Comparison MS BF to ISO-NOx chamber……. | 115 |
| Appendix C9 | Comparison MS LA to ISO-NOx chamber…… | 116 |
| Appendix C10 | Comparison MS BF to DSL-NOx-$NH_3$ chamber……... | 117 |
| Appendix C11 | Comparison MS LA to DSL-NOx-$NH_3$chamber…… | 118 |
| Appendix C12 | Van Krevelen diagrams for chamber experiments……. | 119 |
| Appendix C13 | Van Krevelen diagrams for BF samples……. | 120 |
| Appendix C14 | Van Krevelen diagrams for LA samples……. | 121 |
| Appendix C15 | Percent overlap of BF onto LA data……... | 122 |
| Appendix C16 | Percent Unsaturation of BF and LA data…… | 123 |
| Appendix C17 | Percent overlap of BF with ISO-NOx and DSL-NOx…… | 124 |
| Appendix C18 | Overlap between BF and unique DSL-NOx-NH3 and DSL-NOx…. | 125 |
| Appendix C19 | Overlap between LA and unique DSL-NOx-NH3 and DSL-NOx…. | 126 |

# LIST OF TABLES AND FIGURES


Table 2.1 Number of occurrences of NOC with mass shifts for imine formation…… 26

Table 3.1 Average elemental ratios for each sample time…… 45
Table 3.2 Average elemental ratios for each compound group…… 46

Table 4.1 Average elemental ratios for each sample…… 67

Figure 1.1 Nano-DESI sampling apparatus…… 3
Figure 1.2 Map of the sampling sites…… 7

Figure 2.1 Mass spectra for the samples collected on June 23rd…… 27
Figure 2.2 Van Krevelen diagram, June 23rd midnight-6am…….. 28
Figure 2.3 Comparison unique CHO peaks between midnight-6am and noon-6pm…… 29
Figure 2.4 Van Krevelen diagram for $NOC^+$ and $NOC^-$, June 23rd midnight-6am…… 30
Figure 2.5 Van Krevelen for compounds with/without imine formation precursors……. 31

Figure 3.1 Comparison of average percentage of each compound class……... 47
Figure 3.2 Van Krevelen diagram for negative mode samples, June 22nd……. 48
Figure 3.3 Mass spectra and DBE for sample collected on June 22nd noon-6pm…….. 49
Figure 3.4 Van Krevelen diagrams for size resolved sample……. 50

Figure 4.1 Comparisons of MS from BF and LA with DSL-NOx……..... 68
Figure 4.2 Number of chemical formula assigned to each group for each sample…… 69
Figure 4.3 Percent overlap of BF and LA with three chamber studies……. 71
Figure 4.4 Percent unsaturation of unique compounds between LA and BF…… 71
Figure 4.5 Percent overlap of unique DLS-NOx and DSL-NOx-$NH_3$ with BF and LA…… 72

# ABBREVIATIONS

| | |
|---|---|
| AI | Aromaticity index |
| AIM-IC | Ambient Ion Monitor/Ion Chromatograph |
| AMS | Aerosol Mass Spectrometry |
| BF | Bakersfield |
| CalNex | California Nexus (Research at the Nexus of Air Quality and Climate Change) |
| CHO | Compounds containing carbon, hydrogen, and oxygen |
| CID | Collision induced dissociation |
| CCN | Cloud condensation nuclei |
| Da | Daltons |
| $D_a$ | Aerodynamic diameter |
| DBE | Double bond equivalents |
| DOM | Dissolved organic matter |
| DSL | Diesel |
| EC | Elemental carbon |
| ESI | Electrospray ionization |
| FT-ICR-MS | Fourier transform ion cyclotron resonance mass spectrometry |
| FTIR | Fourier Transform Infrared Spectroscopy |
| FWHM | Full width half max |
| *f*44 | Organic mass fraction of *m/z* 44 |
| GC | Gas chromatography |
| H/C | Hydrogen-to-carbon ratio |
| HR-ToF-AMS | High-Resolution Time-of-Flight Aerosol Mass Spectrometer |
| HULIS | Humic-like substances |
| High-MW | High molecular weight |
| ISO | Isoprene |
| KM | Kendrick Mass |
| KMD | Kendrick Mass Defect |
| LA | Los Angeles |
| LC/ESI/MS | Liquid Chromatography/Electrospray Ionization/Mass Spectrometry |
| MOUDI | Micro-Orifice Uniform Deposit Impactor |
| MS | Mass spectrometry |
| MS/MS | Tandem MS (fragmentation) |
| *m/z* | Mass-to-charge ratio |
| nano-DESI | Nanospray-Desorption electrospray ionization |
| NOC ($^+$, $^-$) | Nitrogen-containing organic compounds (positive, negative ion mode) |
| OA | Organic aerosol |
| O/C | Oxygen-to-carbon ratio |
| OM | Organic matter |
| O/S | Oxygen-to-sulfur ratio |
| PAH | Polycyclic aromatic hydrocarbon |
| PDT | Pacific daylight time |
| $PM_{10}$ | Aerosols with diameter $\leq 10$ μm |

| | |
|---|---|
| $PM_{2.5}$ | Aerosols with diameter ≤ 2.5 μm |
| $PM_{1.5}$ | Aerosols with diameter ≤ 1.5 μm |
| $PM_1$ | Aerosols with diameter ≤ 1 μm |
| PNNL | Pacific Northwest National Labs |
| POA | Primary organic aerosol |
| ppb | Parts per billion |
| ppm | Parts per million |
| QC-TIDLAS | Quantum Cascade laser based Tunable Infrared Differential Absorption Spectroscopy |
| Q-TOFMS | Quadruple-Time of Flight Mass Spectrometer |
| RH | Relative Humidity |
| SLM | Standard Liters per Minute |
| SOA | Secondary organic aerosol |
| UCI | University of California Irvine |
| UNC | University of North Carolina at Chapel Hill |
| UPLC | Ultra Performance Liquid Chromatography |
| VOC | Volatile organic compound |
| 1D | One dimensional |
| 1N, 2N, 3N | Compounds containing (one, two, three) nitrogen atoms |

# Chapter 1

# Introduction

## 1.1 Organic Aerosols

Atmospheric aerosols are suspensions of liquid or solid particles in a gas. In atmospheric science, the term organic aerosol is often used to describe the particulate phase which is differentiated from the volatile organic compounds (VOC) in the gas phase. Atmospheric aerosols have a wide variety of natural and anthropogenic sources and can generally be separated into two groups, primary and secondary, based on how they are formed. Primary organic aerosols (POA) are directly emitted in the condensed phase. Natural sources for POA include forest fires, wind driven lofting of biological materials including plant debris and microorganisms, and sea spray with dissolved organic compounds. POA are also formed from anthropogenic biomass burning and fossil fuel combustion (Jacobson et al., 2000).

Secondary organic aerosols (SOA) can be formed by (1) chemical reactions creating VOCs with lower vapor pressure or high solubility which either nucleate and grow new particles or partition onto preexisting aerosol particles and (2) by heterogeneous and particle phase reactions on the surface or in the bulk of the aerosols forming new compounds (Seinfeld and Pankow, 2003; Poschl, 2005; Ervens et al., 2011). Organic aerosols (OA) have two main sinks from the atmosphere, wet and dry deposition. Wet deposition is loss of aerosol particles to rain, and is the main sink. Dry deposition is the loss of aerosols particles to the earth through settling and adhesion to surfaces. The life-times of OA in the atmosphere depend on the sources and meteorology but generally range from hours to weeks (Williams et al., 2002).

Aerosols exist in a wide range of particle sizes from a few nanometers for freshly nucleated particles to tens of microns for coarse mode particles. In atmospheric studies, the aerosols are typically separated into two groups: $PM_{2.5}$, which are commonly called fine mode particles, have aerodynamic diameters smaller than 2.5 microns, and $PM_{10}$, or coarse mode particles, which include particles with diameters ~10 microns or less. A third group with aerodynamic diameters < 0.1 μm, called ultra fine particles, is also differentiated. Organic aerosols have been found to be a major fraction of fine particulate matter (Zhang et al., 2007) and the majority of OA particles (by number) are found in the $PM_{2.5}$ fraction (Seinfeld and Pandis, 2006).

Organic aerosols have significant impacts on health and climate. Studies have shown a positive correlation between mortality and the amount of particulate matter found in a city (Pope and Dockery, 2006). The size of the aerosol has an impact on where it might settle in the respiratory system after being inhaled. $PM_{10}$ particles are small enough to penetrate and settle in the lungs and bronchi. $PM_{2.5}$ particles tend to penetrate the alveoli and ultra fine mode particles can pass the membrane barriers and enter the blood circulation (Poschl, 2005; Pope and Dockery, 2006). This mechanism can introduce carcinogenic compounds such as polycyclic aromatic hydrocarbons (PAH) into the human body, a major health concern.

Organic aerosols have strong impacts on radiative forcing in the Earth's climate. Radiative forcing alters the balance in the energy fluxes of incoming solar radiation and outgoing terrestrial radiation. The impacts are generally classified as direct or indirect effects. Direct

effects include negative radiative forcing due to scattering and reflection, and positive forcing from decreased albedo due to black carbon on white snow banks, for example. Indirect effects have result from ability of aerosols to serve as cloud condensation nuclei (CCN); increasing CCN leads to both more extensive cloud formation and clouds with higher reflectance, increasing the Earth's albedo. Overall, aerosols pollution cools the Earth; the globally averaged, net radiative forcing from aerosols (including both direct and indirect effects) is ~ -0.4 to -2.7 $W/m^2$ (IPCC, 2007). These effects of aerosols are the largest uncertainty in the 2007 IPCC analysis of anthropogenic radiative forcing.

The aerosol properties relevant to both indirect and the direct effects are determined by particle size, structure, and chemical composition. The composition of the organic fraction is very complex and changes as the aerosol ages. Chemical aging of aerosols increases hygroscopicity, CCN activity, and can change optical properties (Rudich et al., 2007; Titscher et al., 2011; Wong et al., 2011). The timescales for these changes can be shorter than the life-time of the particles in the atmosphere. Thus, the chemical and physical properties of atmospherically aged aerosols can be very different from the properties of the same aerosols collected nearer to their sources. To correctly model and predict climate effects of aerosols the types of aging reactions, the timescales for these changes, and their effects on the properties and composition of the aerosol must be understood.

## 1.2 High Molecular Weight Compounds and Oligomers

The formation of SOA from oxidation and gas-particle partitioning of the thousands of VOC compounds in the atmosphere creates a huge amount of chemical complexity in the organic fraction (Goldstein and Galbally, 2007). Subsequent heterogeneous and particle phase reactions can increase this complexity still further (Ervens et al., 2011). Speciated analysis of the organic fraction is necessary to identify oxidation/reaction mechanisms and sources for organic aerosols (Worton et al., 2012). Traditionally, speciation of OA has been achieved using gas-chromatography mass spectrometry (GC-MS). This technique, however, is limited to relatively small, non-polar compounds and as a result, only characterizes ~10-30% of the organic mass (Rogge et al., 1993).

A large fraction of the OA, which cannot be studied using GC-MS, is thought to be high molecular weight (HMW) oligomeric compounds. This fraction has also been termed Humic-Like substances (HULIS) due to similarities with terrestrial and aquatic humic and fulvic acids (Graber and Rudich, 2006). This complex mixture of oligomers ranges in size from approximately 500-1000 Da and may have strong impacts on hygroscopicity, CCN activity and light absorption properties of atmospheric aerosols (Kiss et al., 2005; Dinar et al., 2006, 2008). There are many possible sources for these compounds including direct emission by biomass burning (Mayol-Bracero et al., 2002), atmospheric reactions such as photooxidation (Kalberer et al., 2004) and ozonolysis (Zahardis et al., 2008), and particle phase reactions such as acid-catalyzed aldol condensation (Tolocka et al., 2004).

Given the high molecular weight and polar nature of the oligomeric fraction of SOA, soft ionization techniques combined with high resolution mass spectrometry have proven to be useful for finding the exact masses of the molecular ions. The chemical formulas of each ion can then be calculated from the exact masses. High resolution mass spectrometers such as Fourier-transform ion cyclotron resonance mass spectrometers (Kalberer et al., 2004; Tolocka et al.,

2004; Reinhardt et al., 2007; Schmitt-Kopplin et al., 2010) and Orbitrap mass spectrometers (Walser et al., 2008; Bateman et al., 2009; Nguyen et al., 2010) have been used to characterize aerosol samples. In this dissertation, nanospray desorption electrospray ionization (nano-DESI), a novel soft ionization technique (Roach et al., 2010a), coupled to an Orbitrap mass spectrometer, was used to analyze samples from the CalNex campaign in Bakersfield and Los Angeles (LA) and smog chamber samples.

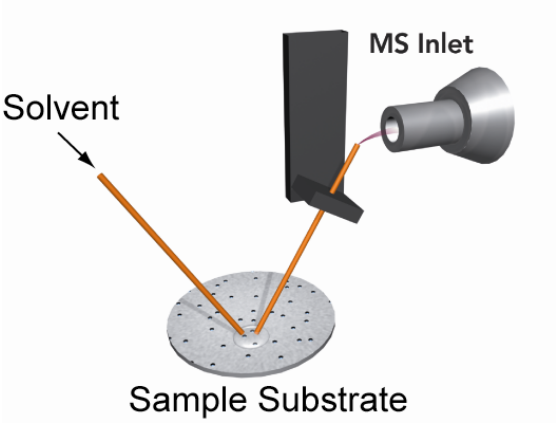


**Figure 1.1** Diagram of the nano-DESI sampling apparatus. Figure courtesy of Alex Laskin.

Figure 1.1 shows a diagram for nano-DESI; with this technique, the sample is dissolved and ionized very rapidly, thus minimizing potential reactions of the sample compounds with the solvent (Roach et al., 2010b). The sampling is done at ambient pressure, and minimal sample preparation is required. The Orbitrap mass spectrometer has high resolution (60,000 m/Δm at FWHM) and high mass accuracy (< 2 ppm) and measure either positive or negative ions (positive or negative mode). The high resolution and accuracy of the Orbitrap enables the separation and identification of hundreds to thousands of compounds in a sample.

Both positive and negative mode ESI was used since observable compounds in the sample can be different depending on the ionization mode. Organic acids tend to ionize in the negative mode and compounds with primarily basic functional groups, such as alcohols, and amines tend to ionize in the positive mode. The minimal sample preparation necessary and the high resolution and accuracy of the Orbitrap make this a very useful system for the characterization of complex aerosol samples.

## 1.3 Organic Nitrogen and Sulfur in Aerosols

The amount of reactive nitrogen emitted to Earth's atmosphere has increased greatly since preindustrial times due to agriculture, fossil fuel combustion, and the Haber-Bosch process of fertilizer production. In the last few decades, the production by humans has been greater than

all natural terrestrial systems (Galloway et al., 2003). The impacts of this increased production and deposition include acidification and lack of biodiversity in lakes and streams (Vitousek et al., 1997), eutrophication and loss of biodiversity in costal ecosystems (Howarth et al., 2000), and the increased production of tropospheric aerosols and ozone, which have serious health effects in humans (Pope et al., 1995) . Reactive nitrogen is widely dispersed by hydrologic and atmospheric transport processes. The cycling (emission, transport, and deposition) of reactive nitrogen is usually studied in terms of inorganic nitrogen compounds, including ammonia and ammonium, nitrogen oxide, nitric acid, nitrous oxide and nitrate.

Organic nitrogen is also a major contributor to the atmospheric cycling of reactive nitrogen (Cornell et al., 2003). However, the sources and impacts are much more difficult to constrain due to the complexity of the composition and the possible sources and formation mechanisms. Organic nitrogen can be found in both reduced and oxidized forms. Oxidized forms include organonitrates, which are formed in the atmosphere during the day through photochemical reactions of $NO_x$ (NO and $NO_2$) with volatile anthropogenic or biogenic organic compounds and during the night through reactions between nitrate radicals ($NO_3$) and gas-phase alkenes (Roberts, 1990; Gong et al., 2005; Ng et al., 2008). Organonitrates with low enough vapor pressures can condense onto aerosols under ambient conditions, and smog chamber studies have demonstrated the importance of organonitrates in SOA production (Lim and Ziemann, 2005; Fry et al., 2009).

Reduced organic nitrogen includes amines and imines which can be directly emitted or formed in the aerosol phase through heterogeneous and particle phase reactions. A Mannich reaction between a primary amine, a secondary amine, or ammonia and a carbonyl is a possible mechanism for the formation of higher molecular weight amines in aerosols (Wang et al., 2010). Imine formation reactions between ammonia and carbonyl oxygen atoms in the aerosol have also been shown to be a possible formation reaction for reduced nitrogen compounds in aerosols (Laskin et al., 2010).

Recently, another class of organic compounds which contain either sulfur atoms in sulfate functional groups (organosulfates) or sulfate and nitrate functional groups (nitroxy organosulfates) have been observed in both laboratory and ambient aerosol samples (Surratt et al., 2007; Surratt et al., 2008; Chan et al., 2010; Kristensen and Glasius, 2011; Worton et al., 2011). These organosulfates can be an important fraction of SOA, contributing up to 30% of the organic mass in some locations (Surratt et al., 2008). While the majority of the sulfur is anthropogenic in origin, the organic precursors for these compounds can be either anthropogenic or biogenic in origin. Thus, organosulfates can serve as a tracer for both anthropogenic SOA and anthropogenically enhanced biogenic SOA. Multiple reaction mechanisms have been proposed, including the reactive uptake of gas-phase epoxides on acidic aerosols (Iinuma et al., 2009; Surratt et al., 2010), reactions between photoinduced sulfate radicals and unsaturated organics (Nozière et al., 2010), and nucleophilic attack by sulfate on protonated carbonyls (Liggio et al., 2005). This dissertation provides molecular level characterization of ambient aerosol samples showing the presence of both reduced and oxidized organic nitrogen compounds as well as organosulfates and nitroxy organosulfates. The number of and relative intensities of these compounds are compared throughout the day and potential sources/formation mechanisms are discussed.

## 1.4 Research Motivation

Chamber experiments have shown the presence of oligomers in SOA from both biogenic and anthropogenic VOC precursors (Gao et al., 2004; Kalberer et al., 2004; Tolocka et al., 2004; Baltensperger et al., 2005; Dommen et al., 2006; Nguyen et al., 2011). The formation of these compounds through acid-catalyzed particle phase reactions (Jang et al., 2002; Tolocka et al., 2004) can explain some of the enhanced SOA formation found in chamber experiments. Studies characterizing the composition of oligomeric compounds in ambient samples are fewer and include ambient aerosol samples (Reemtsma et al., 2006; Wozniak et al., 2008; Schmitt-Kopplin et al., 2010), precipitation samples (Altieri et al., 2009), and fog water samples (Mazzoleni et al., 2010). In the aerosol studies, high volume filters with samples times from a day to a week were typically collected. The samples collected by Wozniak et al. (2008) had no size cut-off; the other two had $PM_{2.5}$ and $PM_{1.5}$ cyclones placed upstream of the filters.

The research in this dissertation is the first to use HR-MS analysis of size resolved samples of ambient aerosols in the San Joaquin Valley which has high aerosol loading due to a combination of biogenic and anthropogenic sources as well as high levels of ozone and ammonia. My samples were collected in Bakersfield during the CalNex 2010 campaign with a size resolved aerosol impactor and this work is also the first to analyze the changes in the chemical composition of the oligomeric fraction with aerosol size. Reemtsma et al (2006) analyzed the oligomeric fraction of SOA in Riverside during the 2005 SOAR campaign. The sampling in LA for my research took place in Pasadena, also during CalNex, which is located closer to downtown LA than the study in Riverside. Thus, the research presented here expands the types of ambient environments that have been studied and provides further data on oligomer formation in the LA basin.

In chamber studies, the molecular composition of the oligomeric fraction has been found to change with varying humidity and $NO_x$ levels (Nguyen et al., 2011). In ambient aerosol samples, changes in the composition have been reported in samples impacted by a new source such as biomass burning (Schmitt-Kopplin et al., 2010). The majority of ambient data are from samples integrated over days to weeks. The research reported in this dissertation is the first that has consecutive six hour samples analyzed and compared to observe and characterize differences in the composition of the HMW fraction throughout the day. Using the high time resolution combined with concurrent measurements by other researchers at the campaign field site, including meteorology and both in-situ and lab based aerosol measurements, and chamber studies, I propose and discuss potential sources and mechanisms for the formation of these compounds.

## 1.5 Aim of the Work

This dissertation seeks to address the following questions:

1) What is the molecular composition of SOA in the fine mode? What are the dominant classes of chemical species?
2) How does the composition of this SOA change throughout the day? Can insights into chemical transformations and sources be achieved using multiple samples in the course of a day?

3) In what size range is the high molecular weight oligomeric faction of SOA predominantly found? Does the chemical composition of this fraction change with aerosol size?
4) Can a comparison of the overlap between compounds measured in a chamber study and those in ambient samples provide information on the types of sources, source strengths, and dominant chemical transformation processes in the ambient environment?

## 1.6 Dissertation Overview

This dissertation documents an investigation of the chemical composition of the high molecular weight, oligomeric fraction of SOA from ambient aerosols collected during CalNex 2010 in Bakersfield and Pasadena. Figure 1.2 shows a Google Earth image of the two field sites with Bakersfield shown at the bottom of the San Joaquin Valley and Pasadena located northeast of downtown LA in the South Coast Air Basin. The two sites were chosen for the CalNex campaign in part because both valleys are out of compliance with ozone and particulate matter standards. This dissertation presents an analysis of the composition of ambient samples in both an urban (LA) and a mixed urban and rural environment (Bakersfield) and presents potential sources for these compounds. The molecular level composition of ambient aerosols was analyzed using nano-DESI and high resolution mass spectrometry. The chemical composition was separated into classes of compounds and changes in the composition throughout the day were compared with both chamber studies and concurrent measurements to investigate both sources and potential formation reactions.

Chapter 2 describes the molecular level composition of samples collected in Bakersfield using positive mode nano-DESI. The analysis focused on two classes of compounds: molecules that contain reduced and oxidized nitrogen and molecules that contain only carbon, hydrogen and oxygen (CHO). Six hour samples were collected, diurnal changes in the chemical composition were observed, and these changes were related to meteorological observations. This is the first time that this level of time resolution on the oligomeric fraction of OA in ambient samples has been investigated. CHO compounds were predominant in the afternoon samples which coincide with potential production via ozonolysis and/or photochemistry. Nitrogen containing compounds were dominant in the night samples and formation of imines via reactions with ammonia is discussed as a potential formation pathway.

In Chapter 3, the chemical composition of OA collected in Bakersfield and analyzed using negative mode nano-DESI are discussed. Four days worth of six-hour samples were analyzed as well as a set of size resolved samples collected over twelve hours. Four compound classes were observed: CHO compounds, compounds with sulfur (CHOS), compounds with nitrogen (CHON), and compounds with both (CHONS). Changes in the composition of the aerosol during the day across these four compound classes were analyzed. A comparison with measurements of specific tracers by other methods provides evidence of SOA produced from oxidation of both anthropogenic and biogenic VOC sources. For the size resolved samples, the composition of the high molecular weight fraction changed with the aerodynamic diameter of the aerosols. The majority of the compounds were observed in aerosols below $PM_{1.0}$ and the number of observed CHON compounds were bimodal with aerosol size. This is the first time the chemical composition of the oligomeric fraction of OA in size resolved fractions have been reported.

In Chapter 4, a systematic comparison of the degree of overlap between the molecular level composition of ambient OA collected in both Bakersfield and Los Angeles (LA) and OA generated in lab studies is presented. Chamber samples were produced using diesel fuel and isoprene precursors under high $NO_x$ conditions. A sample with ammonia ($NH_3$) in the chamber with diesel was also collected because Bakersfield is characterized by elevated mixing rations of $NH_3$. Composition differences were observable in the mass spectra and both diesel and isoprene were found to be important SOA sources. This is the first direct comparison of the chemical composition of the high molecular weight/oligomeric fraction of OA in ambient and chamber samples and the first to use this type of comparison to analyze the strength of different SOA sources for this fraction of organic aerosols in ambient environments.

In Chapter 5 a summary of the work discussed in this thesis and a discussion of potential future directions is presented. Future work is proposed that includes studies to continue to analyze the composition of ambient samples in different locations and to determine the sources and chemical transformations of these compounds. Studies that determine the impacts of these compounds on the physical properties of aerosol samples are also proposed.


**Figure 1.2** Google Earth image of the two CalNex sampling sites, Bakersfield and Pasadena.

## 1.7 References


Altieri, K. E., et al. (2008), Oligomers formed through in-cloud methylglyoxal reactions: Chemical composition, properties, and mechanisms investigated by ultra-high resolution FT-ICR mass spectrometry, *Atmos. Environ.*, *42*(7), 1476-1490.

Altieri, K. E., B. J. Turpin and S. P. Seitzinger (2009), Oligomers, organosulfates, and nitrooxy organosulfates in rainwater identified by ultra-high resolution electrospray ionization FT-ICR mass spectrometry, *Atmos. Chem. Phys.*, *9*(7), 2533-2542.

Baltensperger, U., et al. (2005), Secondary organic aerosols from anthropogenic and biogenic precursors, *Faraday Discuss.*, *130*265-278.

Bateman, A. P., S. A. Nizkorodov, J. Laskin and A. Laskin (2009), Time-resolved molecular characterization of limonene/ozone aerosol using high-resolution electrospray ionization mass spectrometry, *Phys. Chem. Chem. Phys.*, *11*(36), 7931-7942.

Chan, M. N., et al. (2010), Characterization and quantification of isoprene-derived epoxydiols in ambient aerosol in the southeastern United States, *Environ. Sci. Technol.*, *44*(12), 4590-4596.

Cornell, S. E., et al. (2003), Organic nitrogen deposition on land and coastal environments: a review of methods and data, *Atmos. Environ.*, *37*(16), 2173-2191.

Dinar, E., et al. (2008), The complex refractive index of atmospheric and model humic-like substances (HULIS) retrieved by a cavity ring down aerosol spectrometer (CRD-AS), *Faraday Discuss.*, *137*279-295.

Dinar, E., et al. (2006), Cloud condensation nuclei properties of model and atmospheric HULIS, *Atmos. Chem. Phys.*, *6*2465-2481.

Dommen, J., et al. (2006), Laboratory observation of oligomers in the aerosol from isoprene/NO(x) photooxidation, *Geophys. Res. Lett.*, *33*(13), L13805 DOI: 10.1029/2006GL026523.

Ervens, B., B. J. Turpin and R. J. Weber (2011), Secondary organic aerosol formation in cloud droplets and aqueous particles (aqSOA): A review of laboratory, field and model studies, *Atmos. Chem. Phys.*, *11*(21), 11069-11102.

Fry, J. L., et al. (2009), Organic nitrate and secondary organic aerosol yield from NO3 oxidation of beta-pinene evaluated using a gas-phase kinetics/aerosol partitioning model, *Atmos. Chem. Phys.*, *9*(4), 1431-1449.

Galloway, J. N., et al. (2003), The nitrogen cascade, *Bioscience*, *53*(4), 341-356.

Gao, S., et al. (2004), Low-molecular-weight and oligomeric components in secondary organic aerosol from the ozonolysis of cycloalkenes and alpha-pinene, *J. Phys. Chem. A*, *108*(46), 10147-10164.

Goldstein, A. H. and I. E. Galbally (2007), Known and unexplored organic constituents in the earth's atmosphere, *Environ. Sci. Technol.*, *41*(5), 1514-1521.

Gong, H. M., A. Matsunaga and P. J. Ziemann (2005), Products and mechanism of secondary organic aerosol formation from reactions of linear alkenes with NO3 radicals, *J. Phys. Chem. A*, *109*(19), 4312-4324.

Graber, E. R. and Y. Rudich (2006), Atmospheric HULIS: How humic-like are they? A comprehensive and critical review, *Atmos. Chem. Phys.*, *6*729-753.

Howarth, R. W., D. P. Swaney, T. J. Butler and R. Marino (2000), Climatic control on eutrophication of the Hudson River estuary, *Ecosystems*, *3*(2), 210-215.

Iinuma, Y., O. Boge, A. Kahnt and H. Herrmann (2009), Laboratory chamber studies on the formation of organosulfates from reactive uptake of monoterpene oxides, *Phys. Chem. Chem. Phys.*, *11*(36), 7985-7997.

IPCC (2007). IPCC, 2007: Climate Change 2007: The Physical Science Basis. Contribution of Working Group I to the Fourth Assessment Report of the Intergovernmental Panel on Climate Change. S. Solomon, D. Qin, M. Manning, Z. Chen, M. Marquis, K.B. Averyt, M. Tignor and H.L. Miller (eds.), Cambridge University Press, Cambridge, UK and New York, NY, USA.

Jacobson, M. C., H. C. Hansson, K. J. Noone and R. J. Charlson (2000), Organic atmospheric aerosols: Review and state of the science, *Rev. Geophys.*, *38*(2), 267-294.

Jang, M. S., N. M. Czoschke, S. Lee and R. M. Kamens (2002), Heterogeneous atmospheric aerosol production by acid-catalyzed particle-phase reactions, *Science*, *298*(5594), 814-817.

Kalberer, M., et al. (2004), Identification of polymers as major components of atmospheric organic aerosols, *Science*, *303*(5664), 1659-1662.

Kiss, G., E. Tombacz and H. C. Hansson (2005), Surface tension effects of humic-like substances in the aqueous extract of tropospheric fine aerosol, *J. Atmos. Chem.*, *50*(3), 279-294.

Kristensen, K. and M. Glasius (2011), Organosulfates and oxidation products from biogenic hydrocarbons in fine aerosols from a forest in North West Europe during spring, *Atmos. Environ.*, *45*(27), 4546-4556.

Laskin, J., et al. (2010), High-resolution desorption electrospray ionization mass spectrometry for chemical characterization of organic aerosols, *Anal. Chem.*, *82*(5), 2048-2058.

Liggio, J., S. M. Li and R. McLaren (2005), Heterogeneous reactions of glyoxal on particulate matter: Identification of acetals and sulfate esters, *Environ. Sci. Technol.*, *39*(6), 1532-1541.

Lim, Y. B. and P. J. Ziemann (2005), Products and mechanism of secondary organic aerosol formation from reactions of n-alkanes with OH radicals in the presence of NOx, *Environ. Sci. Technol.*, *39*(23), 9229-9236.

Mayol-Bracero, O. L., et al. (2002), Water-soluble organic compounds in biomass burning aerosols over Amazonia - 2. Apportionment of the chemical composition and importance of the polyacidic fraction, *J. Geophys. Res.-Atmos.*, *107*(D20), doi:10.1029/2001JD000522

Mazzoleni, L. R., et al. (2010), Water-soluble atmospheric organic matter in fog: exact masses and chemical formula identification by ultrahigh-resolution fourier transform ion cyclotron resonance mass spectrometry, *Environ. Sci. Technol.*, *44*(10), 3690-3697.

Ng, N. L., et al. (2008), Secondary organic aerosol (SOA) formation from reaction of isoprene with nitrate radicals (NO(3)), *Atmos. Chem. Phys.*, *8*(14), 4117-4140.

Nguyen, T. B., et al. (2010), High-resolution mass spectrometry analysis of secondary organic aerosol generated by ozonolysis of isoprene, *Atmos. Environ.*, *44*(8), 1032-1042.

Nguyen, T. B., J. Laskin, A. Laskin and S. A. Nizkorodov (2011), Nitrogen-containing organic compounds and oligomers in secondary organic aerosol formed by photooxidation of isoprene, *Environ. Sci. Technol.*, *45*(16), 6908-6918.

Nozière, B., S. Ekström, T. Alsberg and S. Holmström (2010), Radical-initiated formation of organosulfates and surfactants in atmospheric aerosols, *Geophys. Res. Lett.*, *37*, L05806 DOI:10.1029/2009GL041683.

Pope, C. A. and D. W. Dockery (2006), Health effects of fine particulate air pollution: Lines that connect, *J. Air Waste Manage. Assoc.*, *56*(6), 709-742.

Pope, C. A., et al. (1995), Particulate air-pollution as a predictor of mortality in a prospective-study of US adults, *Am. J. Respir. Crit. Care Med.*, *151*(3), 669-674.

Poschl, U. (2005), Atmospheric aerosols: Composition, transformation, climate and health effects, *Angew. Chem.-Int. Edit.*, *44*(46), 7520-7540.

Reemtsma, T., et al. (2006), Identification of fulvic acids and sulfated and nitrated analogues in atmospheric aerosol by electrospray ionization Fourier transform ion cyclotron resonance mass spectrometry, *Anal. Chem.*, *78*(24), 8299-8304.

Reinhardt, A., et al. (2007), Ultrahigh mass resolution and accurate mass measurements as a tool to characterize oligomers in secondary organic aerosols, *Anal. Chem.*, *79*(11), 4074-4082.

Roach, P. J., J. Laskin and A. Laskin (2010a), Nanospray desorption electrospray ionization: an ambient method for liquid-extraction surface sampling in mass spectrometry, *Analyst*, *135*(9), 2233-2236.

Roach, P. J., J. Laskin and A. Laskin (2010b), Molecular characterization of organic aerosols using nanospray-desorption/electrospray ionization-mass spectrometry, *Analytical Chemistry*, *82*(19), 7979-7986.

Roberts, J. M. (1990), The atmospheric chemistry of organic nitrates, *Atmospheric Environment Part a-General Topics*, *24*(2), 243-287.

Rogge, W. F., et al. (1993), Quantification of urban organic aerosols at a molecular-level - identification, abundance and seasonal-variation, *Atmospheric Environment Part a-General Topics*, *27*(8), 1309-1330.

Rudich, Y., N. M. Donahue and T. F. Mentel (2007). Aging of organic aerosol: Bridging the gap between laboratory and field studies, *Annu. Rev. Phys. Chem, 58*, 321-352.

Schmitt-Kopplin, P., et al. (2010), Analysis of the unresolved organic fraction in atmospheric aerosols with ultrahigh-resolution mass spectrometry and nuclear magnetic resonance spectroscopy: organosulfates as photochemical smog constituents, *Anal. Chem.*, *82*(19), 8017-8026.

Seinfeld, J. H. and S. N. Pandis (2006). Atmospheric Chemistry and Physics: From Air Pollution to Climate Change. Hoboken, John Wiley & Sons.

Seinfeld, J. H. and J. F. Pankow (2003), Organic atmospheric particulate material, *Annu. Rev. Phys. Chem.*, *54*121-140.

Surratt, J. D., et al. (2010), Reactive intermediates revealed in secondary organic aerosol formation from isoprene, *Proc. Natl. Acad. Sci. U. S. A.*, *107*(15), 6640-6645.

Surratt, J. D., et al. (2008), Organosulfate formation in biogenic secondary organic aerosol, *J. Phys. Chem. A*, *112*(36), 8345-8378.

Surratt, J. D., et al. (2007), Evidence for organosulfates in secondary organic aerosol, *Environ. Sci. Technol.*, *41*(2), 517-527.

Tolocka, M. P., et al. (2004), Formation of oligomers in secondary organic aerosol, *Environ. Sci. Technol.*, *38*(5), 1428-1434.

Tritscher, T., et al. (2011), Volatility and hygroscopicity of aging secondary organic aerosol in a smog chamber, *Atmos. Chem. Phys.*, *11*(22), 11477-11496.

Vitousek, P. M., et al. (1997), Human alteration of the global nitrogen cycle: Sources and consequences, *Ecol. Appl.*, *7*(3), 737-750.

Walser, M. L., et al. (2008), High-resolution mass spectrometric analysis of secondary organic aerosol produced by ozonation of limonene, *Phys. Chem. Chem. Phys.*, *10*(7), 1009-1022.

Wang, X. F., et al. (2010), Evidence for high molecular weight nitrogen-containing organic salts in urban aerosols, *Environ. Sci. Technol.*, *44*(12), 4441-4446.

Williams, J., et al. (2002), Application of the variability-size relationship to atmospheric aerosol studies: estimating aerosol lifetimes and ages, *Atmos. Chem. Phys.*, *2*133-145.

Wong, J. P. S., et al. (2011), Oxidation of ambient biogenic secondary organic aerosol by hydroxyl radicals: Effects on cloud condensation nuclei activity, *Geophys. Res. Lett.*, *38*, L22805 DOI: 10.1029/2011GL049351

Worton, D. R., D. R. Gentner, G. Isaacman and A. H. Goldstein (2012), Embracing complexity: deciphering origins and transformations of atmospheric organics through speciated measurements, *Environ. Sci. Technol.*, *46*(10), 5265-5266.

Worton, D. R., et al. (2011), Origins and composition of fine atmospheric carbonaceous aerosol in the Sierra Nevada Mountains, California, *Atmos. Chem. Phys.*, *11*(19), 10219-10241.

Wozniak, A. S., et al. (2008), Technical Note: Molecular characterization of aerosol-derived water soluble organic carbon using ultrahigh resolution electrospray ionization Fourier transform ion cyclotron resonance mass spectrometry, *Atmos. Chem. Phys.*, *8*(17), 5099-5111.

Zahardis, J., S. Geddes and G. A. Petrucci (2008), The ozonolysis of primary aliphatic amines in fine particles, *Atmos. Chem. Phys.*, *8*(5), 1181-1194.

Zhang, Q., et al. (2007), Ubiquity and dominance of oxygenated species in organic aerosols in anthropogenically-influenced Northern Hemisphere midlatitudes, *Geophys. Res. Lett.*, *34*(13), L13801 DOI:10.1029/2007GL029979.

# Chapter 2

# Molecular Characterization of Organic Aerosol Using Positive Mode Nanospray Desorption/Electrospray Ionization Mass Spectrometry: CalNex 2010 field study

## 2.1 Introduction

Organic compounds have been measured as the dominant fraction of sub-micron aerosols throughout the world (Kanakidou et al., 2005; Fuzzi et al., 2006; Zhang et al., 2007) with multiple studies showing secondary organic aerosol (SOA) as the most abundant portion of total organic aerosol (Turpin and Huntzicker, 1995; Kanakidou et al., 2005). SOA is formed in the atmosphere through gas-to-particle condensation of the oxidation products of volatile organic compounds (VOCs), by heterogeneous gas-particle interactions, and by particle phase reactions (Seinfeld and Pankow, 2003; Ervens et al., 2011). Thousands of primary organic compounds are present in the atmosphere, and the complexity of the organics is increased further by oxidation (Goldstein and Galbally, 2007). The effect that atmospheric aerosols have on the climate by absorbing and scattering radiation, as well as by influencing the lifetime and albedo of clouds, is a major uncertainty in climate modeling (IPCC, 2007). Tying the composition to the properties of the aerosol is inherently obscured by the complexity of the organic constituents. Molecular characterization of organic aerosol is an important step for improving our understanding of aerosol sources, transformations, and their environmental impact (Nizkorodov et al., 2011).

Traditional methods of OA analysis such as gas chromatography-mass spectrometry (GC-MS) are well-suited for identification of many organic molecules, but typically can only identify 10-30% of the OA mass (Rogge et al., 1993). Large (high molecular weight) and polar molecules are generally not measureable by GC. These high molecular weight compounds are often oligomeric, and are sometimes referred to as humic like substances (HULIS) due to their similarities with aqueous and terrestrial humic and fulvic acids. Oligomeric organics may have a large effect on aerosol properties such as cloud nucleation and light absorption (Graber and Rudich, 2006), yet fundamental understanding of their chemical composition is incomplete.

A soft ionization technique such as electrospray ionization (ESI) (Fenn et al., 1990) coupled to mass spectrometry is particularly well suited for the analysis of large polar compounds in complex samples. High-resolution mass spectrometry techniques such as Fourier transform ion cyclotron resonance mass spectrometry (FT-ICR MS) (Kalberer et al., 2004; Tolocka et al., 2004; Reemtsma et al., 2006; Altieri et al., 2008; Schmitt-Kopplin et al., 2010) and Orbitrap MS (Laskin et al., 2010; Nguyen et al., 2010) have been successfully used to identify the molecular composition of thousands of organic compounds. Insights into the sources and transformations of aerosols can be gained from changes observed in the chemical composition of ambient samples throughout the day. For example, using an Orbitrap MS, Roach et al. (2010a) observed changes in the chemical composition of ambient aerosols between early morning and midday in samples in Mexico City.

The addition of heteroatoms such as nitrogen through gas-phase, heterogeneous gas-particle, and condensed-phase chemical reactions adds another level of complexity to the

molecular composition of OA (Cape et al., 2011). Nitrogen-containing organic compounds (NOC) have been found to make up 10-20% of the particle mass (Zhang et al., 2002; Holzinger et al., 2010). They can be broadly separated into groups containing either oxidized or reduced nitrogen functional groups. Organonitrates, containing oxidized nitrogen, have been observed in both chamber studies (Fry et al., 2011; Nguyen et al., 2011) and ambient samples (Day et al., 2010; Zaveri et al., 2010). Proposed mechanisms of organonitrate formation include reactions of NO with organic peroxy radicals during the day and reactions of alkenes with $NO_3$ radicals at night (Ng et al., 2008; Matsunaga and Ziemann, 2009).

NOC constituents of OA with reduced nitrogen groups have also been observed in chamber studies (Laskin et al., 2010) and in field-collected aerosol samples (Pratt et al., 2009; Wang et al., 2010). These compounds can be either primary emissions or products of reactions of, for example, ammonia and amines with carbonyl groups via imine formation reactions (Laskin et al., 2010) and Mannich reactions (Wang et al., 2010). Recently, the use of high-resolution mass spectrometry to characterize the chemical composition of aerosol samples has revealed the presence of a large range of NOC found in atmospheric aerosols (Reemtsma et al., 2006; Schmitt-Kopplin et al., 2010), rainwater (Altieri et al., 2009), and fog water (Mazzoleni et al., 2010). Given the complexity of possible sources and reactions, changes in atmospheric conditions should impact the chemical composition of NOC. Measurements with temporal resolution that separates different times of day should provide valuable insight into the sources and chemical transformations of these compounds.

In typical ESI studies, the aerosol is first extracted into organic solvent and then electrosprayed into the mass spectrometer inlet. Previous studies have shown that chemical modifications of organic compounds such as the acid catalyzed loss of reduced NOC can occur during storage in solvent (Laskin et al., 2010). In principle, the potential alteration of compounds due to reactions in solvent can be reduced by dissolving and ionizing the sample simultaneously, directly from the substrate. A novel method for this type of ambient ionization is nano-desorption/electrospray ionization (nano-DESI) mass spectrometry (Roach et al., 2010b). Roach et al. (2010a) have demonstrated the utility of nano-DESI for soft ionization of organic compounds with no sample preparation and the potential preservation of some labile species.

In this study we report the chemical composition of organic aerosols collected in Bakersfield, CA, during the CalNex 2010 campaign. Using nano-DESI and high-resolution mass spectrometry we measured the chemical composition of the OA samples. Our analysis focused on two classes of compounds: molecules that contain reduced and oxidized nitrogen and molecules that contain only carbon, hydrogen and oxygen. We report diurnal changes in chemical composition, their relationship to meteorological observations, and show that many of the observed compounds formed through ozonolysis and photochemistry were found predominantly in the afternoon samples.

## 2.2 Experimental Section

A description of the field site, the meteorology, and the ambient sampling methodology are provided in the supplemental section. Briefly, four samples per day were collected starting at midnight in Bakersfield (35.35°N, 118.97°W) during the CalNex 2010 campaign. The days of June 22$^{nd}$ and 23$^{rd}$ were chosen for in-depth analysis because concurrent measurements indicated high OA loadings. The meteorology on those days was typical for the campaign with higher

ozone levels during the day and higher relative humidity during the night (Appendix A2). Samples were collected on aluminum foil substrates using a Micro-Orifice Uniform Deposit Impactor (MOUDI) model 100R (MSP, Inc.) without rotation. Samples on the eighth stage of the MOUDI, (aerodynamic diameter of 0.18 -0.32 μm), had the highest number of the compounds of interest so samples from this stage were chosen for intensive study. All times discussed here are in local time (PDT). On-line composition of non-refractory components, including the elemental composition of the organic mass (Aiken et al., 2007), was measured using an Aerodyne High-Resolution Time-of-Flight Aerosol Mass Spectrometer (HR-ToF-AMS) at an adjacent trailer (Ahlm et al., 2012).

Samples were analyzed at Environmental Molecular Science Laboratory located in Richland, WA. Analysis was performed with an LTQ/Orbitrap mass spectrometer (Thermo Electron, Bremen, Germany) equipped with a nano-DESI source (Roach et al., 2010a; Roach et al., 2010b). The source is assembled from two fused-silica capillaries (193 μm o.d./50 μm i.d, Polymicro Technologies LLC, Phoenix, AZ). The primary capillary supplies the solvent and maintains a small droplet of solvent over the analyte area. Analyte molecules dissolved into the solvent are transferred into the mass spectrometer inlet through the nanospray capillary. A voltage of ~ ±6 kV was applied between the capillary end and the mass spectrometer inlet to obtain stable spray of charged droplets. The solvent was supplied at 1.5−2.5 μL/min flow rate to maintain a stable droplet on the surface. The system was operated in the positive and negative ion modes with a resolution of 60,000 m/$\Delta$m at 400 *m/z*. The majority of the data discussed hereafter were obtained in the positive ion mode, only the elemental ratios from negative mode ESI are discussed; a full analysis of the negative ion mode will be presented in a future publication. The instrument was mass calibrated using a standard ESI calibration mix of caffeine, MRFA, and Ultramark 1621.

Time-dependent MS signal was acquired for each of the samples, where the acquisition was started first for ~1 min. on the substrate outside of the sample deposition area (background MS). Then, the substrate was moved such that the probe was positioned over the sample containing area while data acquisition was continued for an additional 2-3 min. (sample MS). Mass spectral features with a signal-to-noise ratio of at least 3 were extracted from background and sample raw spectra using the Decon2LS program developed at PNNL (http://ncrr.pnl.gov/software/). Then, peaks recorded in the sample MS spectrum were eliminated from the sample peak list if the intensity in the sample MS was less than ten times the intensity in the background MS. An Excel macro was used for the background subtraction and to remove compounds with $^{13}C$ isotopes. The remaining peaks were assigned molecular formulas using Formula Calculator v. 1.1 developed at the National High Magnetic Field Laboratory (http://magnet.fsu.edu/~midas/download.html). The molecular formula search was performed using the following parameters: $C_{0\text{-}100}H_{0\text{-}200}O_{0\text{-}50}N_{0\text{-}3}S_{0\text{-}1}Na_{0\text{-}1}^{+}$.

Approximately 80-90% of the peaks could be assigned molecular formulas. Assignments were aided by Kendrick analysis (Kendrick, 1963) using O and $C_3H_4O_2$ as bases, and a second-order mass defect analysis using a sequence of $CH_2$ and $H_2$ bases (Roach et al., 2011). Details of the Kendrick analyses are provided in Appendix A. A mass range of 50-1000 *m/z* was collected for each sample; however, we limit our discussion to the mass range of 50-400 Da because we can unambiguously assign identities give the mass accuracy and resolution used in this study. Further discussion on the assignments of molecular formulas is provided in the supplemental section.

All assigned peaks have a mass error within ±2ppm. Between 60 and 80 percent of the peaks in these samples have exact masses with potential assignments of either $C_xH_yO_z\ Na^+$ or $C_{x-3}H_{y-2}\ N_2O_{z+2}\ H^+$ and $C_xH_yNO_z\ Na^+$ or $C_{x-3}H_{y-2}\ N_3O_{z+2}H^+$. Peaks with these possible assignments that had only one option within ±2ppm were kept while those that had both options within ±2ppm were removed from the peak list. This removed less than 0.1% of the peaks in each sample. The mass spectra have been separated by the number of nitrogen atoms in the chemical formula. Data representing compounds containing no nitrogen atoms will be referred to as CHO. Data for compounds containing one or two nitrogen atoms will be referred to as 1N or 2N respectively. For the comparison of the positive and negative mode NOC the data will be referred to as $NOC^+$ and $NOC^-$ and the $NOC^-$ contains no sulfur.

Compounds present in the samples were observed as either protonated or sodiated molecules in the positive mode spectra, and as deprotonated molecules in the negative mode spectra. The compounds were converted to neutral species by subtracting either the exact mass of a proton or a sodium ion from $[M+H]^+$ or $[M+Na]^+$ respectively or by adding the mass of a proton to $[M+H]^-$. Approximately 2-18% of the peaks in each sample were detected as both a sodiated and protonated compound in the positive mode spectra. For these peaks, the sum of the intensities was used and the duplicate peaks were merged so that all the peaks shown in the figures and considered in the data analysis are unique.

## 2.3. Results and Discussion

### 2.3.1 Mass Spectra and Elemental Composition.

High resolution positive mode nano-DESI mass spectra for the four samples collected on June 23, 2010 in Bakersfield, CA are shown in Figure 2.1. The molecular formulas of approximately 700-800 compounds were identified in each mass spectrum between 50 and 400 Da. With electrospray ionization, the measured peak intensities are affected by the solution composition, the concentration, and the ionization efficiency of the sample molecules. Thus, the intensities do not directly correlate to the absolute concentrations in the sample. However, qualitative information on the relative concentrations of molecules between samples can still be obtained since similar compositions between samples mean that the samples have very similar matrices. The groups of peaks in the figure have been separated by the number of nitrogen atoms in their chemical formulae. Data plotted for CHO only compounds are colored black and data for 1N and 2N compounds are colored red and blue respectively. A very small number of compounds with one sulfur atom or three nitrogen atoms were measured. All of those compounds were below 15% relative intensity and are not shown in Figure 2.1, but are listed in Appendix A6. The pie charts in the upper right corners represent the percentage of detected species that fall into each category. Since individual species could have many different isomeric structures, the percentages reflect only the number of unique molecular formulae and do not reflect the number of unique molecules in each category.

The intensity distributions and the number of compounds in each group changed throughout the day. The percent of NOC species, including those containing two nitrogen atoms, was largest between midnight and 6 am (Figure 2.1a). From 6 am to noon (Figure 2.1b), the number of NOC species decreased slightly and the number of CHO species increased. An increase in both the percentage of and the relative intensities of the CHO species occurred in the

noon to 6 pm sample (Figure 2.1c) when the number and relative intensities of NOC reached their lowest values. This trend reversed in the 6pm to midnight sample (Figure 2.1d) when the percentage and relative intensity of the NOC species increased. Similar patterns were observed for the samples collected on June 22nd (Appendix A3).

A Van Krevelen diagram is presented in Figure 2.2 with the H/C ratios plotted against the O/C ratios of the neutral compounds identified in the sample collected on June 23rd from midnight to 6am. The Van Krevelen plots for the other samples are similar and are shown in Appendix A4. This type of diagram provides a comparison of the degree of saturation vs. oxidation of the compounds. The degree of saturation is represented by the H/C ratio on the y-axis, with increasing values representing increasing saturation. The degree of oxidation is represented by the O/C ratios on the x-axis, with increasing values representing increasing oxidation. The observable patterns (lines and stars) are due to the fact that the elemental compositions must have integer numbers of carbon, hydrogen, oxygen, and nitrogen atoms (Kim et al, 2003). The data is broken down by the number of nitrogen atoms in the compound following the color scheme used in Figure 2.1. Each point on the diagram can represent more than one molecule since multiple compounds can have the same combination of H/C and O/C ratios. The range of values plotted in the diagrams does not change significantly throughout the day for most of the CHO compounds (Appendix A4). The average elemental ratios, e.g. <O/C>, discussed below are weighted by the relative intensities in the mass spectra (Nguyen et al., 2010). The <H/C> value of all of the samples was 1.6 and the <O/C> values ranged between 0.32 from 6am to noon to 0.36 in the samples from noon to midnight.

Aerosol Mass Spectrometers (AMS) measure the composition of the aerosol in real time and the <O/C> and <H/C> values can be compared between the two techniques (Baer et al., 2006). Comparing these values to AMS data must be done with caution, however, because of a bias towards more sensitive detection of more oxidized compounds that are preferentially found in negative mode ESI which leads to higher <O/C> values in negative mode data. Additionally, the aerosol size fraction for this analysis was 0.18-0.32 μm and AMS was sampling up to 1.0 μm. However, no dependence of the <O/C> on the aerosol size was found from an analysis of the AMS data. For the four samples on June 23rd, the <O/C> values of 0.32-0.36 for the positive mode data and 0.57-0.71 for the negative mode data bracket the <O/C> of 0.40-0.48 measured with the AMS in Bakersfield on the same day (Appendix A8). The <O/C> values obtained in this study also compare favorably with AMS data collected in Riverside during the SOAR-1 campaign and the <O/C> measurements from the AMAZE-08 campaign in the Amazon basin (Heald et al., 2010). Our data also compare well to the averaged AMS data and the nano-DESI data from the MILAGRO campaign that have <O/C> values of 0.42-0.47 and 0.37 respectively (Roach et al., 2010a).

In Figures 2.2 and Appendix A4, the majority of points from the NOC are shown to occur in the same O/C vs. H/C region as the CHO points. The intensity weighted <N/C> values for the positive mode ESI data on June 23rd ranged from 0.011 in the noon to 6pm sample to 0.042 in the midnight to 6am sample. These values are 3 to 10 times higher than the average N/C values measured with AMS in Bakersfield. The best comparisons were in the afternoon and evening samples (Appendix A8). The high ionization efficiency of reduced nitrogen containing compounds with ESI (Oss et al., 2010) could be one reason for these differences. More work comparing the responses of the two different techniques to nitrogen containing compounds is necessary to fully explain these results.

### 2.3.2 CHO Compounds

Ozone concentration during sample collection was high in the afternoon and low at night (Appendix A2). On June 23rd the highest levels of ozone occurred from noon to 6 pm with an eight hour average of 85 ppb and a peak of 92 ppb at 1:30 pm, exceeding the regulatory standard set by the California Air Resources Board of 70 ppb ozone over eight hours (CARB, 2012). The high ozone levels correlated with appearance of the predominant CHO compounds in the mass spectra from noon to 6 pm suggesting that these compounds were secondary products of daytime oxidation including ozonolysis and/or photochemical reactions. Figure 2.3a shows a comparison between the midnight-6am and the noon-6pm samples of the CHO peaks that were unique to each sample. The double-bond equivalence (DBE) values shown in Figure 2.3b were calculated from the chemical formulas of the neutral compounds using equation 3:

$$DBE = 1 + c - h/2 \quad (3)$$

Where c and h refer to the number of carbon and hydrogen atoms in the chemical formula. The DBE represents the sum of all rings and double bonds in the molecule. The midnight to 6am sample had 165 unique compounds with a median neutral mass of 214 Da and the noon to 6pm sample had 160 unique compounds with a median neutral mass 333 Da. The DBE values ranged from about 2-9 in both of the samples. Almost all of the low-mass compounds (< 200 Da) were unique to the midnight to 6 am sample. These compounds could be either local emissions or small molecules that do not remain in the aerosol phase during the higher temperatures of mid-day.

### 2.3.3 Organic Nitrogen

The observed diurnal trend of the NOC fractions in the four samples shown in Figure 2.1 likely reflects different processes in the atmospheric chemistry occurring at night and during the day. Both the number and the relative intensities of NOC were largest during the night, indicating that nitrate radical chemistry could have been a significant source of these compounds. It should be noted, however, that since this is positive mode ESI, the ionization of organonitrate compounds will be relatively disfavored unless they contain a group that can solvate the positive charge. Ion chromatography measurements of the gas phase concentrations of ammonia showed an average diurnal concentration range for the campaign of ~700-900 nmol/$m^3$ (Markovic, manuscript in preparation, 2012) which could have been available for reactions that add reduced nitrogen to chemical compounds such as Mannich reactions (Wang et al., 2010) and imine formation reactions (Laskin et al., 2010).

The number of oxygen atoms in the 1N subgroup ranges from zero to ten with approximately 15% of those compounds containing less than three oxygen atoms in the molecular formula. Approximately 70-90% of the 2N compounds, in each sample, had enough oxygen atoms for every nitrogen to potentially be in an organonitrate group. However, the O/C range for the positive mode ($NOC^+$) was lower overall than the O/C range for the negative mode ($NOC^-$), where the ionization of organonitrates was favored. Figure 2.4 shows a Van Krevelen diagram for the $NOC^+$ and $NOC^-$ data collected from midnight to 6am on June 23rd. Similar Van Krevelen diagrams for the other samples on June 23 are shown in Appendix A5. The lower

average O/C range of the positive mode data suggests that a large percentage of the $NOC^+$ contain reduced nitrogen.

In the above discussion, the NOC were assumed to be covalently bound. To investigate the possible formation of $[M+NH_4^+]$ compounds, in source fragmentation was performed by applying an accelerating voltage in the ion optics which should dissociate non-covalent complexes formed in electrospray (Duffin et al., 1991). The NOC that disappeared as a result of collision-induced dissociation (CID) in a 30 V field gradient were analyzed using three criteria to determine which of these compounds were more likely to be ammonium adducts. Compounds that were below 5% relative intensity were removed from the list because the natural variability of the peak intensities precludes them being used in this type of analysis. NOC with sodium as the charge carrier were removed from the list since all of the molecules were singly charged and thus could not have simultaneous adduction of both sodium and ammonium ions. Finally, compounds that were observed in the negative mode were also removed since negatively charged ions with ammonium adducts are highly unlikely. The remaining NOC made up 0.5-5% of the total number of NOC in each sample. However, a large number of the remaining compounds that disappeared as a result of CID in one sample remained in another. Only 32 compounds failed the tests and were unique to one sample and only seven failed the tests in more than one sample (Appendix A7). This suggests that the amount of ammonium adduction was likely very small. A complete analysis requires knowledge of the structure of the molecules since that determines how tightly the ammonium may be adducted and thus, what voltages are necessary to break noncovalent clusters. Future work will involve MS/MS on the isolated compounds to determine structures of both the CHO only compounds and the NOC.

## 2.3.4 Formation of Nitrogen Containing Organic Compounds

The addition of reduced nitrogen to organic molecules can occur via imine formation reactions where carbonyl oxygen atoms are replaced by NH groups. The following reaction was reported in laboratory studies of SOA aging through heterogeneous uptake and reaction of gaseous ammonia with wet SOA particles (r1) (Laskin et al., 2010).

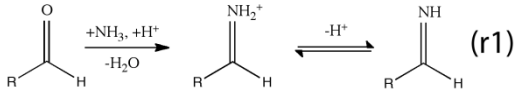


Products of the above reaction were found to undergo additional cyclization and disproportionation reactions in the condensed aqueous phase of SOA (r2 and r3) (Laskin et al., 2010).

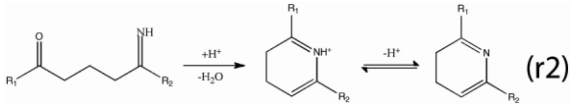


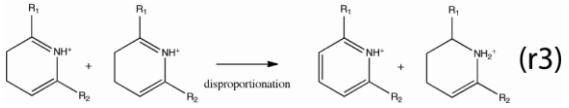

The 2N and 3N compounds could be formed through subsequent reactions of carbonyl groups on newly formed imines (Laskin et al., 2010). The potential prevalence of these reactions in forming the observed NOC was analyzed using the mass differences between the reactants and products in reactions r1-r3 to find possible precursor-product pairs in the mass spectra. Table 2.1 shows a summary of the number of NOC that had mass differences from reactions r1-r3 relating potential precursor-product pairs. The "total number of unique occurrences" shows the full number of NOC that can be explained by these reactions; note that there is a great deal of overlap between the three reactions. The total number of compounds that have corresponding precursors for these samples was on the same order of magnitude as results from chemically aged SOA (Laskin et al., 2010), and approximately 50 to 80% of the identified NOC could potentially be explained by this type of chemistry. A large part of the variability in the total coverage was likely driven by the presence or lack of potential precursors since the number of CHO compounds observed changed throughout the day.

Figure 2.5 shows a Van Krevelen diagram for the NOC compounds for the midnight-6am sample on June 23rd. The light blue points were compounds found to have precursors in the sample that correspond to reactions r1-r3, while the pink points were compounds that had no corresponding precursors. The black points were compounds with no corresponding precursor that were also observed in the negative mode. The compounds observed in the negative mode were all located at relatively high O/C ratios consistent with organonitrates. The NOC that do not have a precursor were predominantly located in the upper H/C range and are likely either local emissions, compounds where the precursor was depleted below the limit of detection, or they could be formed through other reactions such as Mannich reactions with small aldehydes (Wang et al., 2010).

The oxidation state of nitrogen is not evident from a given chemical formula and there are many potential sources and formation mechanisms for the observed NOC. Additionally, presence of precursor/product pairs is not definitive proof of a reaction pathway; future work with MS/MS analysis to gain structural information is necessary to fully characterize formation mechanisms. We present these reactions as possible mechanisms for the formation of compounds containing reduced nitrogen groups and conclude that it is likely ammonia plays a role in the chemistry of the organic fraction in Bakersfield.

## 2.4 Summary

The molecular composition of size-resolved aerosol samples collected in Bakersfield California during CalNex 2010 was investigated using nano-DESI and high resolution mass spectrometry. Positive mode ESI was used and three groups of compounds were observed: compounds containing only carbon, hydrogen, and oxygen (CHO) and compounds containing one or two nitrogen atoms (NOC). Changes in the chemical composition were observed throughout the day with more NOC identified in the night samples and more CHO only compounds identified during the day. The high number of CHO compounds coincided with high ozone and photoactive radiation levels consistent with photochemistry/ozonolysis as major sources. The NOC had lower O/C values than the NOC measured using negative mode ESI and thus likely contained reduced nitrogen groups. Over 50% of the NOC had precursor/product pairs consistent with imidization and cyclization reactions. These reactions involve ammonia and carbonyl groups on the precursor indicating the potential role of ammonia in forming NOC.

The analysis used here was not quantitative and future work to determine the atmospheric concentrations of these compounds is necessary to compare the impact of these compounds in aerosols from different environments. Detailed analysis of the changes in the chemical composition throughout the day have elucidated the roles of nitrogen, photochemistry, and particle phase reactions on the formation and transformation of high molecular weight oligomers in Bakersfield California.

## 2.5 References


Ahlm, L., et al. (2012), Formation and growth of ultrafine particles from secondary sources in Bakersfield, California, *J. Geophys. Res.-Atmos.*, *117*, D00V08 DOI: 10.1029/2011JD017144.

Aiken, A. C., P. F. DeCarlo and J. L. Jimenez (2007), Elemental analysis of organic species with electron ionization high-resolution mass spectrometry, *Anal. Chem.*, *79*(21), 8350-8358.

Altieri, K. E., et al. (2008), Oligomers formed through in-cloud methylglyoxal reactions: Chemical composition, properties, and mechanisms investigated by ultra-high resolution FT-ICR mass spectrometry, *Atmos. Environ.*, *42*(7), 1476-1490.

Altieri, K. E., B. J. Turpin and S. P. Seitzinger (2009), Oligomers, organosulfates, and nitrooxy organosulfates in rainwater identified by ultra-high resolution electrospray ionization FT-ICR mass spectrometry, *Atmos. Chem. Phys.*, *9*(7), 2533-2542.

Baer, T., M. V. Johnston and D. G. Nash (2006), Aerosol mass spectrometry: An introductory review, *Int. J. Mass Spectrom. (Netherlands)*, *258*(1-3), 2-1212.

Cape, J. N., S. E. Cornell, T. D. Jickells and E. Nemitz (2011), Organic nitrogen in the atmosphere - Where does it come from? A review of sources and methods, *Atmos. Res.*, *102*(1-2), 30-48.

CARB: California Air Resources Board (2012), ambient air quality standards, *Available at:* http://www.arb.ca.gov/research/aaqs/aaqs2.pdf, accessed on July 4, 2012.

Day, D. A., S. Liu, L. M. Russell and P. J. Ziemann (2010), Organonitrate group concentrations in submicron particles with high nitrate and organic fractions in coastal southern California, *Atmos. Environ.*, *44*(16), 1970-1979.

Duffin, K. L., J. D. Henion and J. J. Shieh (1991), Electrospray and tandem mass-spectrometric characterization of acylglycerol mixtures that are dissolved in nonpolar-solvents, *Anal. Chem.*, *63*(17), 1781-1788.

Ervens, B., B. J. Turpin and R. J. Weber (2011), Secondary organic aerosol formation in cloud droplets and aqueous particles (aqSOA): a review of laboratory, field and model studies, *Atmos. Chem. Phys.*, *11*(21), 11069-11102.

Fenn, J. B., et al. (1990), Electrospray ionization-principles and practice, *Mass Spectrom. Rev.*, *9*(1), 37-70.

Fry, J. L., et al., 201. SOA from limonene: role of NO3 in its generation and degradation. Atmos. Chem. Phys., 11(8), 3879-3894.

Fuzzi, S., et al. (2006), Critical assessment of the current state of scientific knowledge, terminology, and research needs concerning the role of organic aerosols in the atmosphere, climate, and global change, *Atmos. Chem. Phys., 6*, 2017-2038.

Goldstein, A. H. and I. E. Galbally (2007), Known and unexplored organic constituents in the earth's atmosphere, *Environ. Sci. Technol., 41*(5), 1514-1521.

Graber, E. R. and Y. Rudich (2006), Atmospheric HULIS: How humic-like are they? A comprehensive and critical review, *Atmos. Chem. Phys., 6*, 729-753.

Heald, C. L., et al. (2010), A simplified description of the evolution of organic aerosol composition in the atmosphere, *Geophys. Res. Lett., 37*, L08803 DOI: 10.1029/2010gl042737.

Holzinger, R., et al. (2010), Analysis of the chemical composition of organic aerosol at the Mt. Sonnblick observatory using a novel high mass resolution thermal-desorption proton-transfer-reaction mass-spectrometer (hr-TD-PTR-MS), *Atmos. Chem. Phys., 10*(20), 10111-10128.

IPCC (2007). IPCC, 2007: Climate Change 2007: The Physical Science Basis. Contribution of Working Group I to the Fourth Assessment Report of the Intergovernmental Panel on Climate Change. S. Solomon, D. Qin, M. Manning, Z. Chen, M. Marquis, K.B. Averyt, M. Tignor and H.L. Miller (eds.), Cambridge University Press, Cambridge, UK and New York, NY, USA.

Kalberer, M., et al. (2004), Identification of polymers as major components of atmospheric organic aerosols, *Science, 303*(5664), 1659-1662.

Kanakidou, M., et al. (2005), Organic aerosol and global climate modelling: a review, *Atmos. Chem. Phys., 5*, 1053-1123.

Kendrick, E. (1963), A mass scale based on ch2=14.0000 for high resolution mass spectrometry of organic compounds, *Anal. Chem., 35*(13), 2146-&.

Kim, S., R. W. Kramer and P. G. Hatcher (2003), Graphical method for analysis of ultrahigh-resolution broadband mass spectra of natural organic matter, the van Krevelen diagram, *Anal. Chem., 75*(20), 5336-5344.

Laskin, J., et al. (2010), High-resolution desorption electrospray ionization mass spectrometry for chemical characterization of organic aerosols, *Anal. Chem., 82*(5), 2048-2058.

Markovic, M. Z. V., T. C.; Baker, K. R.; Murphey, J. G. Measurements and modeling of the water-soluble composition of $PM_{2.5}$ and associated precursor gases in Bakersfield, CA during CalNex 2010, *manuscript in preparation*.

Matsunaga, A. and P. J. Ziemann (2009), Yields of beta-hydroxynitrates and dihydroxynitrates in aerosol formed from OH radical-initiated reactions of linear alkenes in the presence of NO(x), *Journal of Physical Chemistry A*, *113*(3), 599-606.

Mazzoleni, L. R., et al. (2010), Water-soluble atmospheric organic matter in Fog: exact masses and chemical formula identification by ultrahigh-resolution fourier transform ion cyclotron resonance mass spectrometry, *Environ. Sci. Technol.*, *44*(10), 3690-3697.

Ng, N. L., et al. (2008), Secondary organic aerosol (SOA) formation from reaction of isoprene with nitrate radicals (NO(3)), *Atmos. Chem. Phys.*, *8*(14), 4117-4140.

Nguyen, T. B., et al. (2010), High-resolution mass spectrometry analysis of secondary organic aerosol generated by ozonolysis of isoprene, *Atmos. Environ.*, *44*(8), 1032-1042.

Nguyen, T. B., J. Laskin, A. Laskin and S. A. Nizkorodov (2011), Nitrogen-containing organic compounds and oligomers in secondary organic aerosol formed by photooxidation of isoprene, *Environ. Sci. Technol.*, *45*(16), 6908-6918.

Nizkorodov, S. A., J. Laskin and A. Laskin (2011), Molecular chemistry of organic aerosols through the application of high resolution mass spectrometry, *Phys. Chem. Chem. Phys.*, *13*(9), 3612-3629.

Oss, M., A. Kruve, K. Herodes and I. Leito (2010), Electrospray ionization efficiency scale of organic compounds, *Anal. Chem.*, *82*(7), 2865-2872.

Pratt, K. A., L. E. Hatch and K. A. Prather (2009), Seasonal volatility dependence of ambient particle phase amines, *Environ. Sci. Technol.*, *43*(14), 5276-5281.

Reemtsma, T., et al. (2006), Identification of fulvic acids and sulfated and nitrated analogues in atmospheric aerosol by electrospray ionization Fourier transform ion cyclotron resonance mass spectrometry, *Anal. Chem.*, *78*(24), 8299-8304.

Roach, P. J., J. Laskin and A. Laskin (2010a), Molecular characterization of organic aerosols using nanospray-desorption/electrospray ionization-mass spectrometry, *Anal. Chem.*, *82*(19), 7979-7986.

Roach, P. J., J. Laskin and A. Laskin (2010b), Nanospray desorption electrospray ionization: an ambient method for liquid-extraction surface sampling in mass spectrometry, *Analyst*, *135*(9), 2233-2236.

Roach, P. J., J. Laskin and A. Laskin (2011), Higher-order mass defect analysis for mass spectra of complex organic mixtures, *Anal. Chem.*, *83*(12), 4924-4929.

Rogge, W. F., et al. (1993), Quantification of urban organic aerosols at a molecular-level - identification, abundance and seasonal-variation, *Atmos. Environ, Part A*, *27*(8), 1309-1330.

Schmitt-Kopplin, P., et al. (2010), Analysis of the unresolved organic fraction in atmospheric aerosols with ultrahigh-resolution mass spectrometry and nuclear magnetic resonance spectroscopy: organosulfates as photochemical smog constituents, *Anal. Chem.*, *82*(19), 8017-8026.

Seinfeld, J. H. and J. F. Pankow (2003), Organic atmospheric particulate material, *Annu. Rev. Phys. Chem.*, *54*, 121-140.

Tolocka, M. P., et al. (2004), Formation of oligomers in secondary organic aerosol, *Environ. Sci. Technol.*, *38*(5), 1428-1434.

Turpin, B. J. and J. J. Huntzicker (1995), Identification of secondary organic aerosol episodes and quantitation of primary and secondary organic aerosol concentrations during Scaqs, *Atmos. Environ.*, *29*(23), 3527-3544.

Wang, X. F., et al. (2010), Evidence for high molecular weight nitrogen-containing organic salts in urban aerosols, *Environ. Sci. Technol.*, *44*(12), 4441-4446.

Zaveri, R. A., et al. (2010), Nighttime chemical evolution of aerosol and trace gases in a power plant plume: Implications for secondary organic nitrate and organosulfate aerosol formation, NO(3) radical chemistry, and N(2)O(5) heterogeneous hydrolysis, *J. Geophys. Res.-Atmos.*, *115*D12304 DOI: 10.1029/2009JD013250.

Zhang, Q., C. Anastasio and M. Jimemez-Cruz (2002), Water-soluble organic nitrogen in atmospheric fine particles ($PM_{2.5}$) from northern California, *J. Geophys. Res.-Atmos.*, *107*(D11), 4112, DOI: 10.1029/2001jd000870.

Zhang, Q., et al. (2007), Ubiquity and dominance of oxygenated species in organic aerosols in anthropogenically-influenced Northern Hemisphere midlatitudes, *Geophys. Res. Lett.*, *34*(13), L13801 DOI:10.1029/2007GL029979.

## 2.6 Tables and Figures

**Table 2.1** Number of occurrences of $NOC^+$, per sample, that have mass shifts corresponding to the formation of products by reactions r1- r3.

| | Number of Occurrences | | | | |
|---|---|---|---|---|---|
| | **Total NOC** | **r1 +NH; -O** | **r2 +N; -H;-$O_2$** | **r3 r2: +2H;-2H** | **Total number of unique occurrences** |
| **6/22 midnight-6am** | 375 | 183 | 138 | 130 | 242 |
| **6/22 6am-noon** | 407 | 146 | 104 | 106 | 200 |
| **6/22 noon-6pm** | 326 | 205 | 149 | 146 | 251 |
| **6/22 6pm-midnight** | 387 | 231 | 180 | 188 | 285 |
| **6/23 midnight-6am** | 456 | 234 | 155 | 158 | 270 |
| **6/23 6am-noon** | 398 | 220 | 159 | 172 | 269 |
| **6/23 noon-6pm** | 277 | 190 | 151 | 118 | 223 |
| **6/23 6pm-midnight** | 361 | 235 | 186 | 194 | 290 |

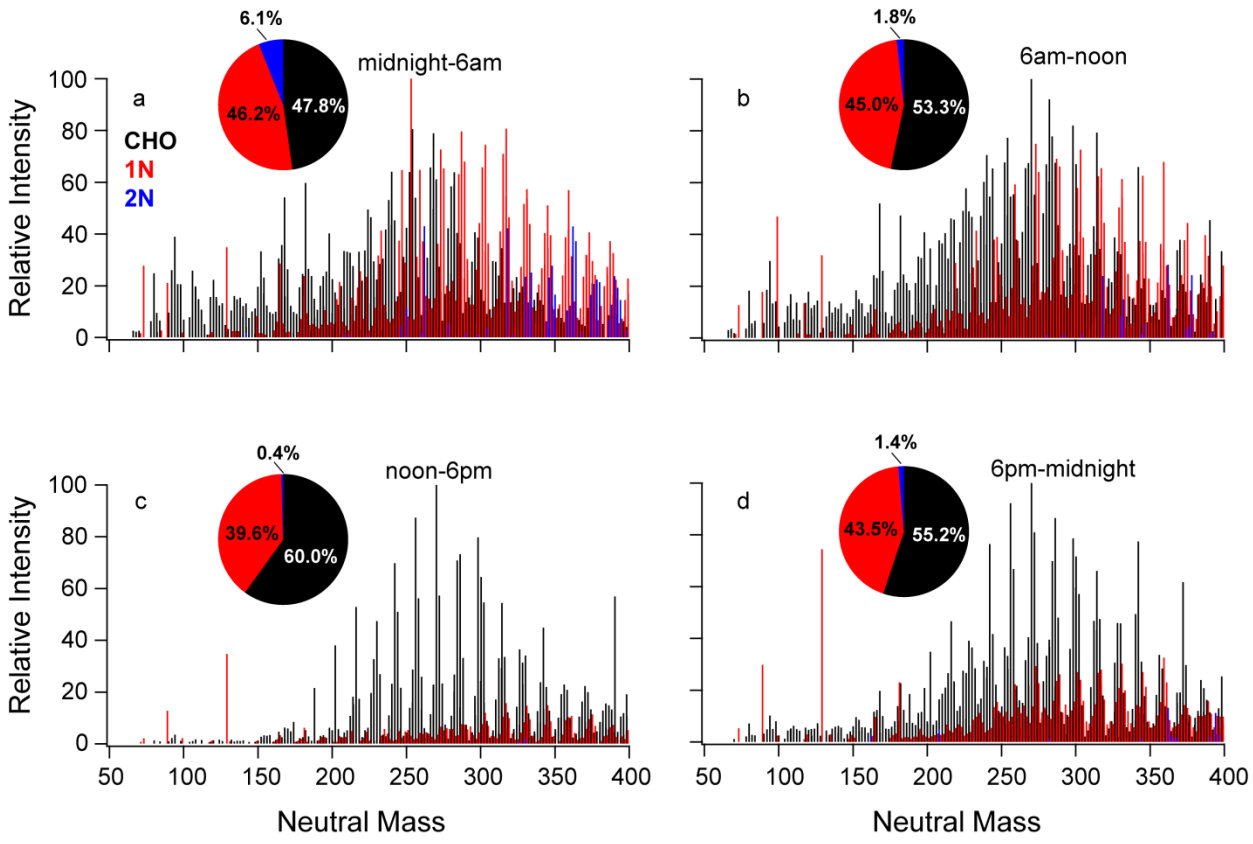


**Figure 2.1** Reconstructed mass spectra of the identified peaks in each of the four samples collected on June 23rd. CHO only compounds are shown in black, 1N and 2N compounds are shown in red and blue respectively. The pie charts show the percentage of compounds by number that fall in each group. The starred peak in (d) has an intensity of 150 on this scale.

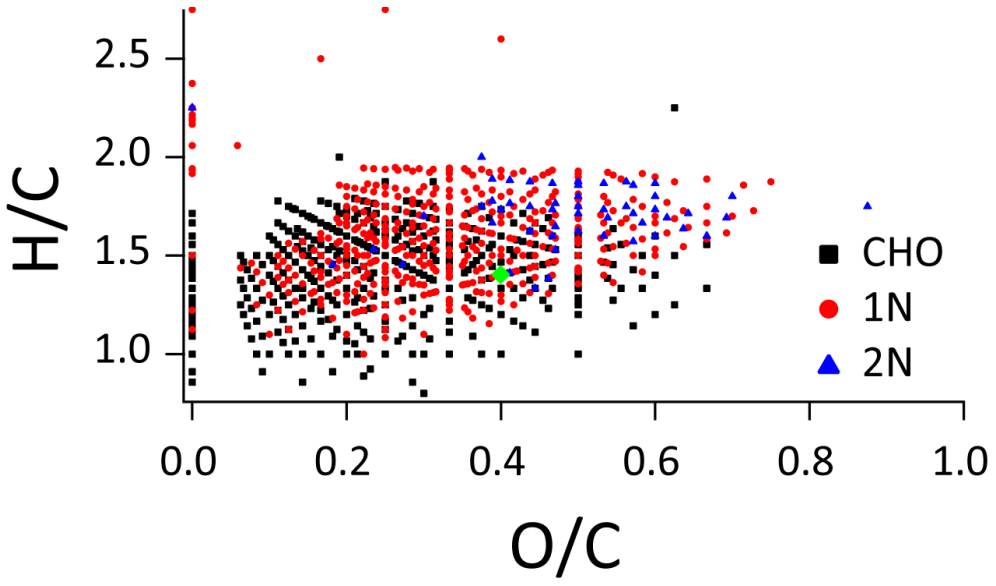


**Figure 2.2** Van Krevelen diagram for the sample collected on June 23rd midnight-6am. Blue markers are CHO only and red, green, and black correspond to compounds with one, two, and three nitrogen atoms respectively. The green diamond (0.4, 1.4) corresponds to AMS data averaged over the same sample time.

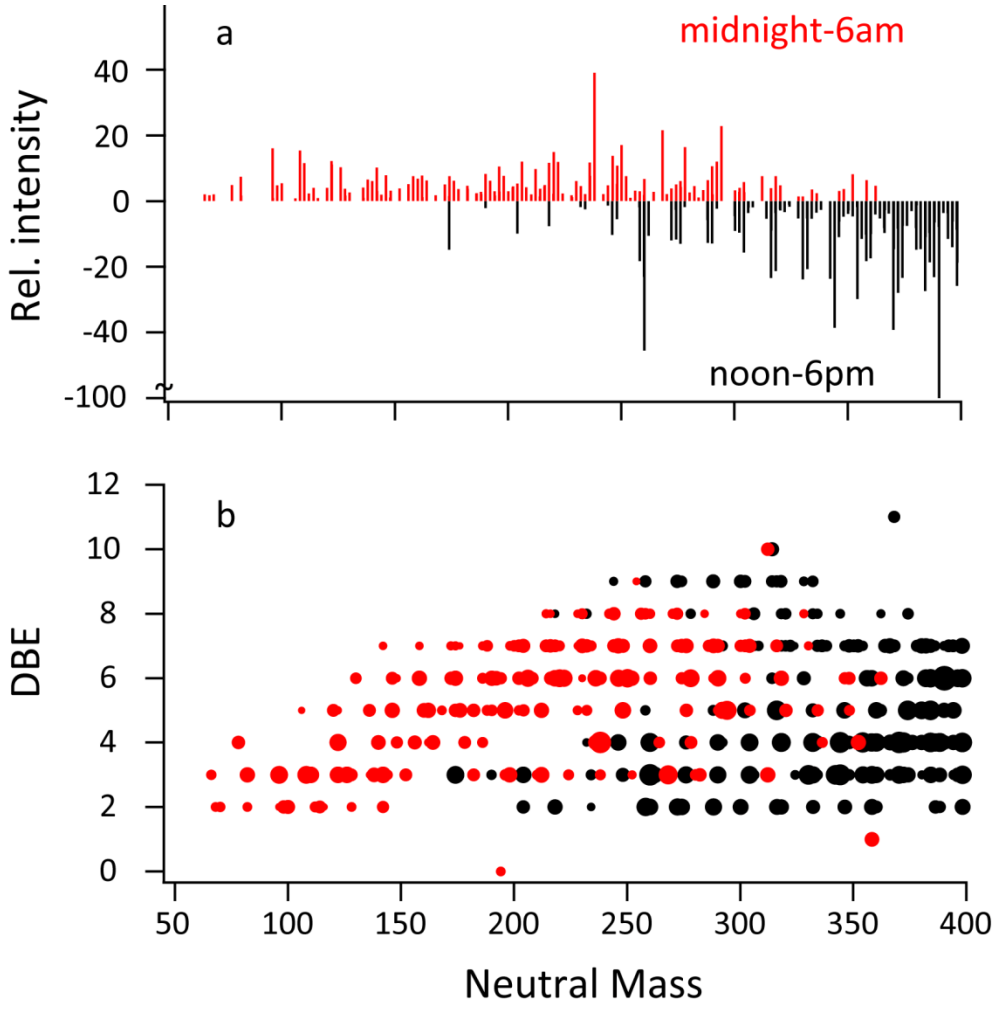


**Figure 2.3** Comparison of CHO peaks that are unique between midnight to 6am (red) and noon to 6pm (black). (a) Mass spectra of the unique peaks are shown as positive and negative signal to aid in the comparison. (b) DBE versus the neutral mass of the unique peaks is shown. The size of the points is proportional to the logarithm of the relative peak intensity.

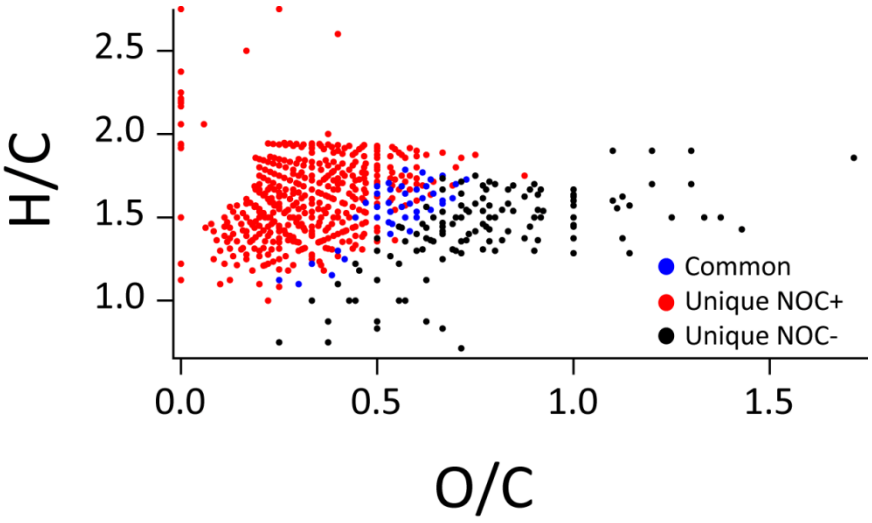


**Figure 2.4** Van Krevelen diagram for NOC from the sample collected on June 23rd from midnight-6am. Blue markers are compounds measured in both negative and positive mode, red and black are compounds measured in only the positive and negative mode respectively.

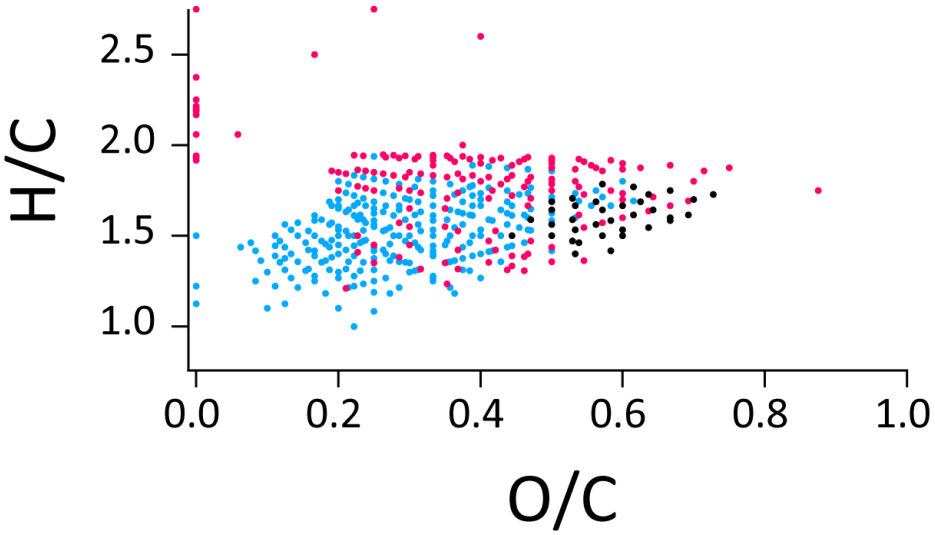


**Figure 2.5** Van Krevelen diagram for NOC from the sample collected on June 23rd from midnight-6am. The light blue points correspond to compounds that had a precursor with the mass differences given by reactions r1, r2, or r3, for the formation of imines. The pink dots are compounds for which we do not observe a precursor and the black dots are compounds without an observed precursor that are also measured in the negative mode.

# Chapter 3

# Using Negative Mode Nano-DESI High-Resolution Mass Spectrometry to Analyze SOA Composition as a Function of Aerosol Size and Local Time during CalNex 2010.

## 3.1 Introduction

Atmospheric aerosols affect the Earth's climate by absorbing and scattering radiation and by serving as cloud condensation nuclei (Poschl, 2005; IPCC, 2007). These effects are impacted by the chemical composition of the aerosols. Organic compounds are a major fraction of atmospheric particulate matter (< 2.5 μm) and organic aerosols have a very complex chemical composition (Kanakidou et al., 2005; Fuzzi et al., 2006; Zhang et al., 2007; Williams et al., 2010). Secondary organic aerosols (SOA) comprise a large fraction of organic aerosols and are formed by the condensation of low-volatility organic compounds and subsequent particle phase reactions (Seinfeld and Pankow, 2003; Ervens et al., 2011). Identifying the chemical composition of the organic fraction is necessary to improve our understanding of the sources, chemical transformation processes, and the environmental impacts of aerosols.

The complexity of organic aerosols is greatly increased by the addition of nitrogen and sulfur through gas-phase and condensed-phase reactions. Nitrogen containing compounds such as organonitrates have been found to comprise 10-20% of the aerosol particle mass (Zhang et al., 2002; Day et al., 2010; Holzinger et al., 2010). Two potential mechanisms for the formation of organonitrates include reactions of alkenes with $NO_3$ radicals during the night and reactions of NO with organic peroxy radicals during the day (Roberts, 1990; Gong et al., 2005; Ng et al., 2008). Sulfur containing compounds such as organosulfates have also been reported to make up a large portion (30%) of the organic mass fraction (Surratt et al., 2008). Multiple mechanisms for the formation of organosulfates have been proposed including reactive uptake of gaseous epoxides onto acidic aerosols (Iinuma et al., 2009; Surratt et al., 2010) and radical initiated formation driven by photochemistry of sulfate ions (Nozière et al., 2010).

Traditionally, gas-chromatography with mass spectrometry (GC-MS) has been used to measure the speciated chemical composition in the organic fraction of aerosol samples. This technique is well suited for the characterization of many organic compounds found in aerosols, but typically only 10-30% of the organic mass is speciated (Rogge et al., 1993). High molecular weight and polar compounds are thought to comprise a large portion of organic aerosols and are generally not measureable with GC-MS (Havers et al., 1998; Samburova et al., 2005; Kalberer, 2006). Soft ionization techniques, such as electrospray ionization (ESI) (Fenn et al., 1990), coupled to mass spectrometry have proven to be an effective technique for the determination of the molecular composition of complex atmospheric samples. The use of high resolution mass spectrometers, such as Fourier transform ion cyclotron resonance mass spectrometers (FT-ICR MS) and Orbitrap MS, have been used to identify thousands of organic compounds including organosulfates, organonitrates, and nitroxy organosulfates in aerosol, fog, and rainwater samples (Reemtsma et al., 2006; Altieri et al., 2009; Mazzoleni et al., 2010). From the changes observed in the composition of the organic aerosols over time, insights into the sources and the chemical transformations of these aerosols can be gained (O'Brien et al., *manuscript in prep.*, 2012a).

A novel dissolution-ionization technique, nano-DESI, has been introduced for the analysis of organic aerosol samples (Roach et al., 2010a). With nano-DESI, the analyte is quickly dissolved and ionized directly from the surface of the substrate. This technique limits potential solvent-analyte interactions that can occur with the typical solvent extraction done for ESI analysis (Laskin et al., 2010). Nano-DESI has been shown to be a powerful technique for the soft ionization of complex mixtures on substrates with the preservation of some labile species and no sample preparation (Roach et al., 2010b).

In this study, we report the chemical composition of organic aerosols collected over June 20$^{th}$-June 24$^{th}$ in Bakersfield California during CalNex 2010. Using nano-DESI on six hour, size resolved, samples we measured the molecular formulas of over 1000 unique compounds. We report changes in the composition of the aerosol during the day across four compound classes and provide evidence for local production and long range transport of SOA produced from oxidation of both anthropogenic and biogenic volatile organic compound (VOC) sources. We also report how the composition of the high molecular weight fraction changes with the aerodynamic diameter of the aerosols.

## 3.2 Experimental

Samples were collected in Bakersfield California (35.35°N, 118.97°W) during CalNex 2010. A description of the field site, meteorology, and sampling methodology are provided in elsewhere (O'Brien et al., *manuscript in prep.*, 2012a). Briefly, samples collected on June 20$^{th}$-24$^{th}$ were chosen for in-depth analysis because concurrent measurements including High-Resolution Time-of-Flight Aerosol Mass Spectrometer (HR-ToF-AMS) indicated high SOA loading and diurnal patterns similar to the rest of the campaign. The meteorology on these days was similar to the rest of the campaign with higher ozone and air temperatures during the afternoon and higher relative humidity at night. Samples were collected on aluminum foil substrates using a Micro-Orifice Uniform Deposit Impactor (MOUDI) model 100R (MSP, Inc.) without rotation. Samples on the eighth stage of the MOUDI, (0.18 -0.32 μm aerodynamic diameter ($D_a$)), had the largest number of the compounds of interest and were chosen for intensive study. For the twelve hour sample acquired on June 24$^{th}$, stages 5-8 ($0.18 < D_a < 1.8$ μm) were analyzed to provide size resolved data. All times discussed here are in local time (PDT). In-situ measurements of the elemental composition of the organic mass (Aiken et al., 2007) were undertaken using an Aerodyne HR-ToF-AMS at an adjacent trailer (Ahlm et al., 2012). High volume filter samples were collected on prebaked quartz fiber filters with 23 hour sample times (12 am-11pm). Filter samples were extracted with methanol and, after clean-up, analyzed with an Agilent ultra performance liquid chromatography (UPLC) coupled to an Agilent 6520 Series Accurate-Mass high resolution quadrupole time-of-flight mass spectrometer (Q-TOFMS) equipped with an ESI source operated in the negative ion mode. For brevity, the analysis technique will be termed liquid chromatography/electrospray ionization/mass spectrometry (LC/ESI/MS).

The samples were analyzed at Pacific Northwest National Labs (PNNL) in the Environmental Molecular Sciences Laboratory. A high resolution LTQ-Orbitrap™ MS (Thermo Fisher, Bremen, Germany) equipped with a recently developed nano-DESI source was used for the analysis. The source consists of two fused-silica capillaries (193 μm o.d./50 μm i.d, Polymicro Technologies LLC, Phoenix, AZ). The source capillary provided acetonitrile,

forming a droplet on the surface of the aluminum foil. The dissolved analyte was transferred into the inlet of mass spectrometer through a separate nanospray capillary. Electrospray was maintained using a flow rate of 1.0−2.0 μL/min and a voltage of ~6 kV. The system was operated in the negative ion mode with a resolution of 60,000 m/Δm at 400 m/z. The instrument was externally calibrated using a standard ESI calibration mix of sodium dodecylsulfate, sodium taurocholate, MRFA, caffeine, and Ultramark 1621.

Data analysis was performed in a similar manner to our previous work (Nguyen et al., 2010; Nizkorodov et al., 2011; O'Brien et al., *manuscript in prep*., 2012a). Briefly, raw mass spectra were obtained over the sample free area at the edge of the MOUDI substrate (blank MS) and over the sample area with deposited particulate matter (sample MS). Mass spectra peaks with a signal-to-noise ratio higher than 3 were extracted from the raw MS. Peaks in the sample MS that were less than ten times the intensity of blank MS were removed from the peak list. Molecular assignments of the observed ions were obtained using MIDAS molecular formula calculator (http://magnet.fsu.edu/~midas/) with the following constraints $C_{1\text{-}100}$ $H_{0\text{-}200}O_{0\text{-}50}N_{0\text{-}3}S_{0\text{-}1}$. Assignments were aided by Kendrick analyses (Kendrick, 1963) using $C_3H_4O_2$ and oxygen as bases, and a second-order Kendrick analysis using a sequence of $CH_2$ and $H_2$ bases (Roach et al., 2011). Approximately 65-80% of the peaks were unambiguously assigned molecular formulas. Compounds were observed as deprotonated molecules and the mass of the neutral species was obtained by adding the mass of a proton to the measured mass. Double bond equivalence values (DBE) provide information on the number of rings and double bonds in the molecules. DBE were calculated from the elemental formulas using equation 1(Laskin et at., 2009):

$$DBE = 1 + c - h/2 + n/2 \qquad (1)$$

Where c, h, and n correspond to the number of carbon, hydrogen, and nitrogen atoms in the molecular formula, respectively. Divalent atoms such as oxygen are not included The aromaticity index (AI) is a useful way to characterize the extent of aromaticity (Koch and Dittmar, 2006). AI values for the compounds were calculated using equation 2:

$$AI = (1+c-o-s-(0.5h)) / (c-o-s-n) \quad (=0 \textit{ if negative}) \qquad (2)$$

Here c, o, s, n, and h, correspond to the number of each type of atom. While there are exceptions, in general AI values greater than 0.5 indicate the presence of aromatic rings and values ≥ 0.67 are characteristic of condensed aromatic structures.

## 3.3 Results and Discussion

### 3.3.1 Sample Comparison

The 16 samples were collected over four consecutive days (June 20$^{th}$-June 23$^{rd}$) in Bakersfield during CalNex 2010. Using high resolution negative mode nano-DESI mass spectra, the molecular formulas of ~600-900 compounds were identified in the mass range of 50-400 Da for each sample. The compounds fall into four main groups: carbon, hydrogen and oxygen only (CHO), sulfur containing (CHOS), nitrogen containing (CHON), and compounds that contain both nitrogen and sulfur (CHONS). Figure 3.1 shows the number of compounds in each group

for each time period. The data are averaged over the four days; the data for each day individually are given in Appendix B9. Approximately 44-56% of the compounds were CHO with greater numbers of CHO peaks in the afternoon samples. This is consistent with results from positive mode data which showed higher numbers of CHO only compounds in the noon-midnight samples on June 22nd and 23rd (O'Brien et al., *manuscript in prep.*, 2012a). Approximately 20-29% of the compounds were CHOS with the highest number of compounds in the daytime samples, 6am-6pm. The number of CHON compounds ranged from approximately 16-20% and the percentages were highest at night. The remaining 4-11% of the compounds were CHONS compounds. Greater numbers of CHONS compounds were observed in the morning samples (midnight-noon). Since each compound may have multiple isomers, the values discussed above reflect only the number of unique molecular formulas observed and are likely an underestimate of the number of unique molecular structures in each category. Therefore, the term "compound" in this paper refers to all of the molecules with a specific molecular formula.

In these samples the sulfur and nitrogen are assumed to be covalently bound. To investigate the possible formation of $[M+HSO_4]^-$ or $[M+ NO_3]^-$ compounds, in source collision induced dissociation (CID) was performed by applying a 30 V field gradient in the ion optics which may dissociate non-covalent complexes formed in electrospray. In these samples the majority, on average ~72-97%, of the CHOS, CHONS, and CHON compounds are below 5% relative intensity (RI). Since there is a natural variability of peak intensities as the samples are collected, caution must be used when looking for the lack of a peak in one sample vs. another. The sample collected on June 24th midnight-6am was analyzed for loss of CHOS, CHON, and CHONS compounds with CID. Of the compounds in the starting MS (no CID) that had >5% RI, more than 89% of the compounds in each group remained (Appendix B10). This suggests that the amount of hydrogen sulfate and nitrate adduction was likely very small. The CHON compounds had the highest number of peaks lost with CID (Appendix B10); future work analyzing the structures of these compounds and their behavior with CID is necessary to fully explain these results.

In Table 3.1, the intensity weighted average elemental ratios (Bateman et al., 2009; Nguyen et al., 2010) are shown for each sample period. The data in Table 3.1 is averaged over four days, individual values for each sample are given in Appendix B11. The <H/C> values ranged from 1.5 to 1.6. The <O/C> values were highest in the morning with values of 0.69 and 0.71 in the midnight-6am and 6am-noon samples, respectively, and lowest in the afternoon samples with values of 0.58 and 0.59. Aerosol mass spectrometers (AMS) measure the chemical composition of individual aerosol particles in real time and the elemental ratios of the compounds can be compared between the two techniques. Some caution must be used when comparing these values, however, because ionization biases in ESI can lead to either overestimations or underestimations of the elemental ratios. Additionally, the <O/C> and <N/C> values measured by AMS may be an underestimation of the true value (Farmer et al., 2010). In Bakersfield, the <O/C> values measured by AMS did not depend on the size of the aerosol particles and so bulk AMS values were used for comparison. The four day average <O/C> values of 0.57-0.69 are comparable to but larger than the average AMS values of 0.33-0.44 measured over the same time periods. The data presented here is for negative nano-DESI only, previous results for the analysis of June 23rd showed that the positive and negative mode nano-DESI data tended to bracket the AMS values (O'Brien et al., *manuscript in prep.*, 2012a; O'Brien et al., *manuscript in prep.*, 2012b).

For the nano-DESI analysis, the <N/C> values in the morning samples ranged from 0.028 to 0.019 in the midnight-6am sample and 6am-noon sample, respectively. The average <N/C> values in the afternoon and evening samples were 3-4 times lower, with values between 0.0056 and 0.0065. The morning <N/C> values for the nano-DESI analysis are 4-6 times larger than the <N/C> values measured with AMS while the afternoon/evening values are only 1.2-1.3 times higher the AMS measurements. Additional experiments analyzing the response of both types of instruments to nitrogen containing compounds are necessary to further investigate these differences.

## 3.3.2 Characterization by group

### 3.3.2.1 CHO compounds

Over the four day average, between 280 and 465 compounds were assigned CHO molecular formulas for each sample time. Significantly more CHO compounds were observed in the afternoon samples than the rest of the day (Figure 3.1). The same trend was observed for the positive mode data and the increased abundances have been attributed to photochemistry and ozonolysis (O'Brien et al., *manuscript in prep.*, 2012a) Figure 3.2a shows a representative mass spectrum for the sample collected on June 22$^{nd}$ noon-6pm. The relative intensities were calculated by dividing the measured intensity by the maximum intensity observed in that sample. The CHO compounds, shown in black, cover a wide range of masses from 50-400 Da. The peaks with the highest intensity are centered ~150-300 Da. Reemtsma et al. (2006) found the highest intensity CHO peaks in a similar range in an analysis of aerosol samples collected in Riverside, CA. Aerosol samples collected in New York (NY) and Virginia (VA) showed a slightly higher range of ~230-350 for the most intense peaks. The data reported for NY and VA was for the bulk, CHO was not separated, but CHO compounds were the dominant species in the samples (Wozniak et al., 2008).

In Figure 3.2b, DBE (equation 1) values are plotted against the neutral mass for the same sample. The CHO compounds cover a range of DBE values of 1-8. This is similar to the CHO compounds measured in the positive mode in samples collected on June 23$^{rd}$ at Bakersfield which had DBE = 2-10 for the majority of the CHO compounds observed. AI values, calculated from equation 2, indicated that there were between 4 and 26 CHO compounds with an aromatic ring in each sample with slightly more, on average, in the afternoon samples (noon-midnight) (Appendix B12). In most of the samples there were also a few compounds (up to 10) with AI $\geq$ 0.67 indicating the presence of condensed aromatic compounds.

Additional insight into changes in the chemical composition of the aerosol throughout the day can be gained by examining the elemental ratios of each group. In Figure 3.3, Van Krevelen diagrams for two samples on June 23$^{rd}$ are shown: midnight-6am and noon-6pm. Van Krevelen diagrams for all of the samples are given in Appendices B3-B6. A few compounds were outside of the axis limits in the van Krevelen diagrams, they are listed in Appendix B13. The majority of the CHO compounds, shown in black, fall between 0.5< H/C <2.0 and 0.1< O/C <1.0. These are similar to the ranges previously reported for CHO compounds in rainwater and fog (Altieri et al., 2009; Mazzoleni et al., 2010). The range is also comparable to aerosol samples collected in NY and VA except that the O/C range here extends to slightly higher values (0.6 vs. 1.0) (Wozniak et al., 2008).

In Table 3.2, the intensity weighted average elemental ratios are shown, averaged over the four days. The average ratios for each sample individually are given in Appendix B14. The <H/C> value increases from 1.4 to 1.5 and the <O/C> value drops from 0.54 to about 0.5 going from the morning to the afternoon samples. These changes are also observed in Figure 3.2 as an increased number of peaks in the upper left section of the Van Krevelen diagram covered by CHO compounds. These changes suggest that the fresh CHO compounds in the afternoon are less oxidized and more saturated than the compounds observed in the morning samples. The CHO compounds measured in Bakersfield have similar elemental ratios and compositions to CHO compounds measured in other atmospheric samples (Reemtsma et al., 2006; Wozniak et al., 2008; Altieri et al., 2009; Mazzoleni et al., 2010) and the increased number of compounds in the afternoon suggests daytime production by photochemistry/ozonolysis.

### 3.3.2.2 CHOS Compounds

The majority of the CHOS compounds, displayed in green, were located at higher H/C and O/C values than the CHO compounds (Figure 3.3, Table 3.2). The average molecular weights were higher for the CHOS compounds (Figure 3.2) and more than 96.5% of the compounds measured in each sample had O/S values greater than 4. All of these observations are consistent with the majority of the sulfur atoms occurring in sulfate groups. A few of the CHOS compounds were isolated and product ion mass spectra were generated, an example is shown in Appendix B7. Losses of 79.9568 Da ($SO_3$) and the occurrence of 96.9620 ($HSO_4^-$) were observed in all of the product mass spectra and provide further evidence for the assignment of organosulfates (Reemtsma et al., 2006). The majority of the CHOS compounds have DBE values that range from approximately 0 to 4, lower than the CHO compounds discussed above. Low DBE or high H/C values for organosulfate compounds were also observed in fog, rainwater, and aerosol samples (Reemtsma et al., 2006; Wozniak et al., 2008; Altieri et al., 2009; Mazzoleni et al., 2010).

Over the four day averages, there were between 164 and 192 CHOS compounds detected with slightly more observed on average in the afternoon samples (Figure 3.1). The CHOS compounds have the smallest variation in diurnal pattern over the 4 day averages. Either the main source for these compounds was remote from the sampling site, or the number of compounds observed did not strongly depend on the meteorology at the site. The elemental ratios of the CHOS compounds were compared to the ratios for organosulfates formed from the gas-phase oxidation of isoprene, $\alpha$-pinene, $\beta$-pinene, $\alpha$-terpinene, $\gamma$-terpinene, and limonene (Surratt et al., 2008). Twenty-two organosulfates were observed in 24 hour filter samples analyzed by LC/ESI/MS at University of North Carolina, Chapel Hill (UNC). All of the compounds with the same elemental formulas as the organosulfates identified by LC/ESI/MS were observed in the nano-DESI aerosol samples (Appendix B15). The overlap between the two measurements was very good. The overlap between the two measurements was very good; in 97% of the cases where an organosulfate was reported using LC/ESI/MS, we observed a compound with the same molecular formula in at least one sample collected the same day. The small variations in the diurnal pattern were consistent with the upwind formation of some of the CHOS compounds and subsequent transport to the sampling site. The overlap with some of the biogenic organosulfates identified using LC/ESI/MS indicates both biogenic and anthropogenic VOC precursor sources for these compounds.

### 3.3.2.3 CHON Compounds

The majority of the O/C values measured for the CHON compounds (red markers) fall to the right, but within the range, of the values measured for the CHO compounds (Figure 3.2). On average, more than 98% of the CHON compounds in each sample had O/N > 3. The higher oxidation level of these compounds indicates that for the majority of them the nitrogen could be present in a nitrate ($ONO_2$) group. Compounds containing either one, two, or three nitrogen atoms (1N, 2N, 3N) in their molecular formula were observed. Almost all occurrences of 2N and 3N compounds were observed in the morning samples (midnight-6am and 6am-noon). The CHON compounds covered a wide range of masses with averages around 280 Da. In these samples the CHON compounds had low relative intensities; on average > 97% of the peaks had RI values below 5% (Figure 3.2a). The low intensities precluded these compounds from MS/MS analysis.

The majority of these compounds have DBE values between 4 and 6 (Figure 3.2b). This is within the range of DBE values of 3-11 reported for CHON in fog water (Mazzoleni et al., 2010) and is slightly higher than the range of 3-4 reported for the major components of the CHON compounds in aerosol samples collected during the SOAR campaign in Riverside, CA (Reemtsma et al., 2006). A small number (0-4) of CHON compounds in each sample had AI values > 0.5 and ≥ 0.67 indicating the presence of aromatic rings and condensed aromatic structures (Appendix B12). The majority of the aromatic compounds had O/N ≤ 3. The first sample, June 20$^{th}$ midnight-6am, had 12 compounds with AI values ≥ 0.67 and all of these had O/N ≤ 1 consistent with aromatic compounds that had nitrogen atoms in the rings.

Between 101 and 164 CHON compounds were observed, over the four day average, with higher percentages of compounds in the night time samples (6pm-midnight and midnight-6am). The increase in the 6pm-midnight sample indicates that nitrate radical chemistry was likely a major source for these compounds, consistent with concurrent measurements of particulate peroxy nitrates by Rollins et al. (submitted manuscript, 2012) which also showed increased production during the night in Bakersfield. The distribution of the elemental ratios for the CHON compounds was different between the morning and the evening samples (Figure 3.3). In the morning, the majority of the compounds had high O/C and H/C values while in the afternoon, many of those compounds were not observed and new compounds at lower O/C and H/C values appeared. This shift in composition is also shown in the decrease of the <O/C> values from the morning to afternoon samples (Table 3.2). The average O/C values for the 1N compounds show the same trends; they average between 0.67 and 0.70 in the morning (midnight-noon) and 0.59-0.60 in the evening (noon-midnight). Thus, the lack of 2N and 3N compounds in the afternoon samples does not fully explain the data. These results are consistent with both the cessation of the formation of some of the higher O/C compounds, and the local production of new CHON compounds with lower O/C values in the afternoon formed through reactions of NO with organic peroxy radicals.

### 3.3.2.4 CHONS

Data for the CHONS compounds, shown in blue, fall in the same region of the van Krevelen diagram as the CHOS compounds and have on average slightly higher <O/C> values

(Figure 3.3, Table 3.2). On average more than 80% of the CHONS compounds in each sample have enough oxygen atoms to have both sulfate and nitrate groups. The higher oxidation levels and the high numbers of oxygen atoms indicate that the majority of the CHONS compounds are nitroxy organosulfates. The CHONS compounds covered a relatively narrow range of masses (300-400 Da) and they also had low relative intensities in these samples. Like the CHON, the low intensities precluded MS/MS analysis. The majority of the compounds had DBE values of 2-3. These DBE values are in the same range as some of the CHONS compounds reported in fog water (Mazzoleni et al., 2010). The majority of the CHONS compounds contained 1N, only 27 of the 142 unique CHONS compounds contained 2N or 3N.

Between 32 and 70 CHONS compounds were observed, over the four day average, with more detected during the morning samples (midnight-6am and 6am-noon) (Figure 3.1). The greater numbers of compounds in the morning samples is consistent with a nitrate radical source for the nitrate part of the CHONS and a slower, particle-phase addition of sulfate. The lower numbers of CHONS compounds observed during the day indicate that the formation mechanism is not as active later in the afternoon. Twelve of the CHONS compounds measured in these samples have elemental formulas corresponding to nitroxy organosulfates, formed from biogenic organic compounds, also measured at UNC with LC/ESI/MS analysis of Bakersfield 24 hour filters (Appendix B16). Like the organosulfates, the overlap between the two techniques was good; in 80% of the cases where a nitroxy organosulfate was reported using LC/ESI/MS, we observed a compound with the same molecular formula in at least one sample collected the same day. Given the lack of prior separation with nano-DESI, it is likely that the compounds were not observed because of charge competition in ESI. The larger number of compounds in the morning samples is consistent with local night-time production of the compounds via nitrate radical chemistry and the overlap with some of the terpene derived CHONS compounds identified using LC/ESI/MS indicates that both biogenic and anthropogenic sources play a role in the formation.

### 3.3.3 Size Distributions

Size resolved data were analyzed for the twelve hour samples collected on June 24$^{th}$ from noon to midnight. The total number of compounds decreased with increasing size cut with 787 compounds on stage 8 (0.18 -0.32 μm), ~ 622 on stage 7 (0.32-0.56 μm), ~ 477 on stage 6 (0.56-1.0 μm), and 100 on stage 5 (1.0-1.8 μm). The data were separated into the same four groups: CHO, CHOS, CHON, and CHONS. Figure 3.4 shows van Krevelen diagrams for the data in each sample and the intensity weighted average elemental ratios for each group are given in Appendix B17. The range of elemental ratios for the CHO, CHOS, and CHONS groups were similar across the bottom three stages of the MOUDI (stages 8-6). All three groups fall in similar ranges in the Van Krevelen diagrams as the samples discussed previously. This is consistent with the majority of the compounds having sulfur and nitrogen in sulfate and nitrate groups. The CHO compounds showed a gradual decrease in the number of compounds as the aerosol size increased (Figures 3.3 and Appendix B8). In contrast, the number of CHOS and CHONS compounds increased slightly on stage 7 and then decreased slightly on stage 6. The size ranges observed for the CHOS compounds are consistent with results showing the highest concentrations of organosulfates below one micron (Lukacs et al., 2009; Hatch et al., 2011). These results indicate that the eighth stage had the largest number of organic compounds (CHO)

and that the two sulfur containing groups occupy a wider range of aerosol sizes over which roughly equal numbers of the compounds can be observed.

The CHON compounds showed different behavior as the aerosol size increased. From stage 8 to stage 7, there was a large decrease in the number of CHON compounds. Most of the CHON compounds at higher O/C values in the stage 8 sample were not observed in the stage 7 sample and thus, the <O/C> of the CHON compounds decreased on stage 7. For the next size cut (stage 6), the number of CHON compounds almost tripled, increasing to 105 (Appendix B8). The majority (97%) of the CHON compounds on stage 8 had O/N values > 3 consistent with organonitrates. However, many of the CHON compounds on stage 6 were located at lower H/C values than the CHON compounds on stage 8. The <N/C> values for the stage 6 CHON compounds were higher (0.28 vs. 0.10 on stage 8) and at least 50% of them did not have enough oxygen atoms in the molecular formula for all of the nitrogen atoms to be organic nitrate ($ONO_2$) groups. Additionally, the AI values for 33 of them were $\geq 0.67$ indicating the presence of condensed aromatic compounds. These results suggest that some of the CHON compounds in the $0.56 < D_a < 1.0$ μm size fraction were aromatic compounds with nitrogen atoms in the rings and nitro-aromatic compounds which can be formed from the photooxidation of aromatic compounds in the presence of $NO_x$ (Forstner et al., 1997; Wozniak et al., 2008). The CHON group shows a large change from the accumulation mode to the droplet mode and further work analyzing the chemical composition of aerosols in size resolved fractions is needed to provide information on the sources of these compounds.

## 3.4 References


Ahlm, L., et al. (2012), Formation and growth of ultrafine particles from secondary sources in Bakersfield, California, *Journal of Geophysical Research-Atmospheres*, *117*, D00V08 DOI: 10.1029/2011JD017144.

Aiken, A. C., P. F. DeCarlo and J. L. Jimenez (2007), Elemental analysis of organic species with electron ionization high-resolution mass spectrometry, *Analytical Chemistry*, *79*(21), 8350-8358.

Altieri, K. E., B. J. Turpin and S. P. Seitzinger (2009), Oligomers, organosulfates, and nitrooxy organosulfates in rainwater identified by ultra-high resolution electrospray ionization FT-ICR mass spectrometry, *Atmospheric Chemistry and Physics*, *9*(7), 2533-2542.

Bateman, A. P., S. A. Nizkorodov, J. Laskin and A. Laskin (2009), Time-resolved molecular characterization of limonene/ozone aerosol using high-resolution electrospray ionization mass spectrometry, *Physical Chemistry Chemical Physics*, *11*(36), 7931-7942.

Day, D. A., S. Liu, L. M. Russell and P. J. Ziemann (2010), Organonitrate group concentrations in submicron particles with high nitrate and organic fractions in coastal southern California, *Atmos. Environ.*, *44*(16), 1970-1979.

Ervens, B., B. J. Turpin and R. J. Weber (2011), Secondary organic aerosol formation in cloud droplets and aqueous particles (aqSOA): a review of laboratory, field and model studies, *Atmospheric Chemistry and Physics*, *11*(21), 11069-11102.

Farmer, D. K., et al. (2010), Response of an aerosol mass spectrometer to organonitrates and organosulfates and implications for atmospheric chemistry, *Proceedings of the National Academy of Sciences of the United States of America*, *107*(15), 6670-6675.

Fenn, J. B., et al. (1990), Electrospray ionization-principles and practice, *Mass Spectrometry Reviews*, *9*(1), 37-70.

Forstner, H. J. L., R. C. Flagan and J. H. Seinfeld (1997), Secondary organic aerosol from the photooxidation of aromatic hydrocarbons: Molecular composition, *Environmental Science & Technology*, *31*(5), 1345-1358.

Fuzzi, S., et al. (2006), Critical assessment of the current state of scientific knowledge, terminology, and research needs concerning the role of organic aerosols in the atmosphere, climate, and global change, *Atmospheric Chemistry and Physics*, *6*, 2017-2038.

Gong, H. M., A. Matsunaga and P. J. Ziemann (2005), Products and mechanism of secondary organic aerosol formation from reactions of linear alkenes with NO3 radicals, *Journal of Physical Chemistry A*, *109*(19), 4312-4324.

Hatch, L. E., et al. (2011), Measurements of isoprene-derived organosulfates in ambient aerosols by aerosol time-of-flight mass spectrometry - Part 1: single particle atmospheric observations in Atlanta, *Environmental Science & Technology*, *45*(12), 5105-5111.

Havers, N., P. Burba, J. Lambert and D. Klockow (1998), Spectroscopic characterization of humic-like substances in airborne particulate matter, *Journal of Atmospheric Chemistry*, *29*(1), 45-54.

Holzinger, R., et al. (2010), Analysis of the chemical composition of organic aerosol at the Mt. Sonnblick observatory using a novel high mass resolution thermal-desorption proton-transfer-reaction mass-spectrometer (hr-TD-PTR-MS), *Atmospheric Chemistry and Physics*, *10*(20), 10111-10128.

Iinuma, Y., O. Boge, A. Kahnt and H. Herrmann (2009), Laboratory chamber studies on the formation of organosulfates from reactive uptake of monoterpene oxides, *Physical Chemistry Chemical Physics*, *11*(36), 7985-7997.

IPCC (2007). IPCC, 2007: Climate Change 2007: The Physical Science Basis. Contribution of Working Group I to the Fourth Assessment Report of the Intergovernmental Panel on Climate Change. S. Solomon, D. Qin, M. Manning, Z. Chen, M. Marquis, K.B. Averyt, M. Tignor and H.L. Miller (eds.), Cambridge University Press, Cambridge, UK and New York, NY, USA.

Kalberer, M. (2006), Analysis of oligomers in atmospheric aerosol particles - analytical challenges, *Analytical and Bioanalytical Chemistry*, *385*(1), 22-25.

Kanakidou, M., et al. (2005), Organic aerosol and global climate modelling: a review, *Atmospheric Chemistry and Physics*, *5*, 1053-1123.

Kendrick, E. (1963), A mass scale based on ch2=14.0000 for high resolution mass spectrometry of organic compounds, *Analytical Chemistry*, *35*(13), 2146-&.

Koch, B. P. and T. Dittmar (2006), From mass to structure: an aromaticity index for high-resolution mass data of natural organic matter, *Rapid Communications in Mass Spectrometry*, *20*(5), 926-932.

Laskin, A., et al. (2009), Molecular characterization of nitrogen-containing organic compounds in biomass burning aerosols using high-resolution mass spectrometry, *Environmental Science and Technology*, *43*, 3764-3771.

Laskin, J., et al. (2010), High-resolution desorption electrospray ionization mass spectrometry for chemical characterization of organic aerosols, *Analytical Chemistry*, *82*(5), 2048-2058.

Lukacs, H., et al. (2009), Quantitative assessment of organosulfates in size-segregated rural fine aerosol, *Atmospheric Chemistry and Physics*, *9*(1), 231-238.

Mazzoleni, L. R., et al. (2010), Water-soluble atmospheric organic matter in fog: exact masses and chemical formula identification by ultrahigh-resolution fourier transform ion cyclotron resonance mass spectrometry, *Environmental Science & Technology*, *44*(10), 3690-3697.

Ng, N. L., et al. (2008), Secondary organic aerosol (SOA) formation from reaction of isoprene with nitrate radicals (NO(3)), *Atmospheric Chemistry and Physics*, *8*(14), 4117-4140.

Nguyen, T. B., et al. (2010), High-resolution mass spectrometry analysis of secondary organic aerosol generated by ozonolysis of isoprene, *Atmospheric Environment*, *44*(8), 1032-1042.

Nizkorodov, S. A., J. Laskin and A. Laskin (2011), Molecular chemistry of organic aerosols through the application of high resolution mass spectrometry, *Physical Chemistry Chemical Physics*, *13*(9), 3612-3629.

Nozière, B., S. Ekström, T. Alsberg and S. Holmström (2010), Radical-initiated formation of organosulfates and surfactants in atmospheric aerosols, *Geophys. Res. Lett.*, *37*, L05806 DOI:10.1029/2009GL041683

O'Brien, R. E., et al. (2012), Molecular characterization of organic aerosol using nanospray desorption/electrospray ionization mass spectrometery: CalNex 2010 field study, *in prep. for Atmospheric Enviornment*.

O'Brien, R. E., et al. (2012), Probing molecular associations of field-collected and laboratory-generated SOA with nano-DESI high-resolution mass spectrometry.,*in prep. for JGR-Atmos*.

Poschl, U. (2005), Atmospheric aerosols: Composition, transformation, climate and health effects, *Angewandte Chemie-International Edition*, *44*(46), 7520-7540.

Reemtsma, T., et al. (2006), Identification of fulvic acids and sulfated and nitrated analogues in atmospheric aerosol by electrospray ionization Fourier transform ion cyclotron resonance mass spectrometry, *Analytical Chemistry*, *78*(24), 8299-8304.

Roach, P. J., J. Laskin and A. Laskin (2010a), Nanospray desorption electrospray ionization: an ambient method for liquid-extraction surface sampling in mass spectrometry, *Analyst*, *135*(9), 2233-2236.

Roach, P. J., J. Laskin and A. Laskin (2010b), Molecular characterization of organic aerosols using nanospray-desorption/electrospray ionization-mass spectrometry, *Analytical Chemistry*, *82*(19), 7979-7986.

Roach, P. J., J. Laskin and A. Laskin (2011), Higher-order mass defect analysis for mass spectra of complex organic mixtures, *Analytical Chemistry*, *83*(12), 4924-4929.

Roberts, J. M. (1990), The atmospheric chemistry of organic nitrates, *Atmospheric Environment Part a-General Topics, 24*(2), 243-287.

Rogge, W. F., et al. (1993), Quantification of urban organic aerosols at a molecular-level - identification, abundance and seasonal-variation, *Atmospheric Environment Part a-General Topics, 27*(8), 1309-1330.

Rollins, A. W., et al. (2012), Nighttime growth of particulate organic nitrates: a significant source of atmospheric secondary organic aerosols, *Submitted*.

Samburova, V., R. Zenobi and M. Kalberer (2005), Characterization of high molecular weight compounds in urban atmospheric particles, *Atmospheric Chemistry and Physics, 5*2163-2170.

Seinfeld, J. H. and J. F. Pankow (2003), Organic atmospheric particulate material, *Annual Review of Physical Chemistry, 54,* 121-140.

Surratt, J. D., et al. (2010), Reactive intermediates revealed in secondary organic aerosol formation from isoprene, *Proceedings of the National Academy of Sciences of the United States of America, 107*(15), 6640-6645.

Surratt, J. D., et al. (2008), Organosulfate formation in biogenic secondary organic aerosol, *Journal of Physical Chemistry A, 112*(36), 8345-8378.

Williams, B. J., et al. (2010), Major components of atmospheric organic aerosol in southern California as determined by hourly measurements of source marker compounds, *Atmospheric Chemistry and Physics, 10*(23), 11577-11603.

Wozniak, A. S., et al. (2008), Technical Note: Molecular characterization of aerosol-derived water soluble organic carbon using ultrahigh resolution electrospray ionization Fourier transform ion cyclotron resonance mass spectrometry, *Atmospheric Chemistry and Physics, 8*(17), 5099-5111.

Zhang, Q., C. Anastasio and M. Jimemez-Cruz (2002), Water-soluble organic nitrogen in atmospheric fine particles ($PM_{2.5}$) from northern California, *Journal of Geophysical Research-Atmospheres, 107*(D11), 4112, DOI: 10.1029/2001jd000870.

Zhang, Q., et al. (2007), Ubiquity and dominance of oxygenated species in organic aerosols in anthropogenically-influenced Northern Hemisphere midlatitudes, *Geophysical Research Letters, 34*(13), L13801 DOI:10.1029/2007GL029979.

## 3.5 Tables and Figures

**Table 3.1** Ensemble average, intensity weighted elemental ratios for each sample time. The nano-DESI data was collected in negative ion mode. These are four day averages. The ± after the values are the standard deviations of the four datasets.

| | | midnight-6am | 6am-noon | noon-6pm | 6pm-midnight |
|---|---|---|---|---|---|
| **nano-DESI HRMS** | **<O/C>** | 0.69 ± 0.02 | 0.71 ± 0.06 | 0.58 ± 0.03 | 0.59 ± 0.03 |
| | **<H/C>** | 1.5 ± 0.1 | 1.6 ± 0.1 | 1.5 ± 0.1 | 1.5 ± 0.1 |
| | **<N/C>** | 0.022 ± 0.01 | 0.018 ± 0.008 | 0.0056 ± 0.002 | 0.0063 ± 0.0008 |
| **AMS** | **<O/C>** | 0.33 ± 0.05 | 0.39 ± 0.04 | 0.42 ± 0.03 | 0.44 ± 0.03 |
| | **<H/C>** | 1.5 ± 0.07 | 1.4 ± 0.04 | 1.4 ± 0.02 | 1.4 ± 0.03 |
| | **<N/C>** | 0.0046 ± 0.001 | 0.0052 ± 0.001 | 0.0043 ± 0.003 | 0.0056 ± 0.001 |

**Table 3.2** The average elemental ratios for each compound group. The same time of day was averaged over four days (June 20th-June 23rd). The ± after the values are the standard deviations of the four datasets.

| | | Midnight-6am | 6am-noon | Noon-6pm | 6pm-midnight |
|---|---|---|---|---|---|
| <O/C> | CHO | 0.55 ± 0.02 | 0.55 ± 0.06 | 0.49 ± 0.02 | 0.50 ± 0.02 |
| | CHON | 0.78 ±0.08 | 0.73 ± 0.03 | 0.62 ± 0.01 | 0.64 ± 0.01 |
| | CHOS | 0.87 ± 0.09 | 0.93 ± 0.1 | 0.82 ± 0.09 | 0.88 ± 0.05 |
| | CHONS | 0.99 ± 0.02 | 1.0 ± 0.005 | 0.92 ± 0.03 | 0.89 ± 0.09 |
| <H/C> | CHO | 1.4 ± 0.0 | 1.4 ± 0.08 | 1.5 ± 0.05 | 1.5 ± 0.05 |
| | CHON | 1.5 ± 0.0 | 1.5 ± 0.05 | 1.5 ± 0.0 | 1.5 ± 0.05 |
| | CHOS | 1.7 ± 0.05 | 1.8 ± 0.1 | 1.8 ± 0.05 | 1.8 ± 0.0 |
| | CHONS | 1.7 ± 0.0 | 1.7 ± 0.0 | 1.7 ± 0.05 | 1.7 ± 0.05 |
| <N/C> | CHO | - | - | - | - |
| | CHON | 0.13 ± 0.01 | 0.13 ± 0.06 | 0.085 ± 0.003 | 0.089 ± 0.004 |
| | CHOS | - | - | - | - |
| | CHONS | 0.11 ± 0.008 | 0.12 ± 0.006 | 0.11 ± 0.02 | 0.10 ± 0.01 |

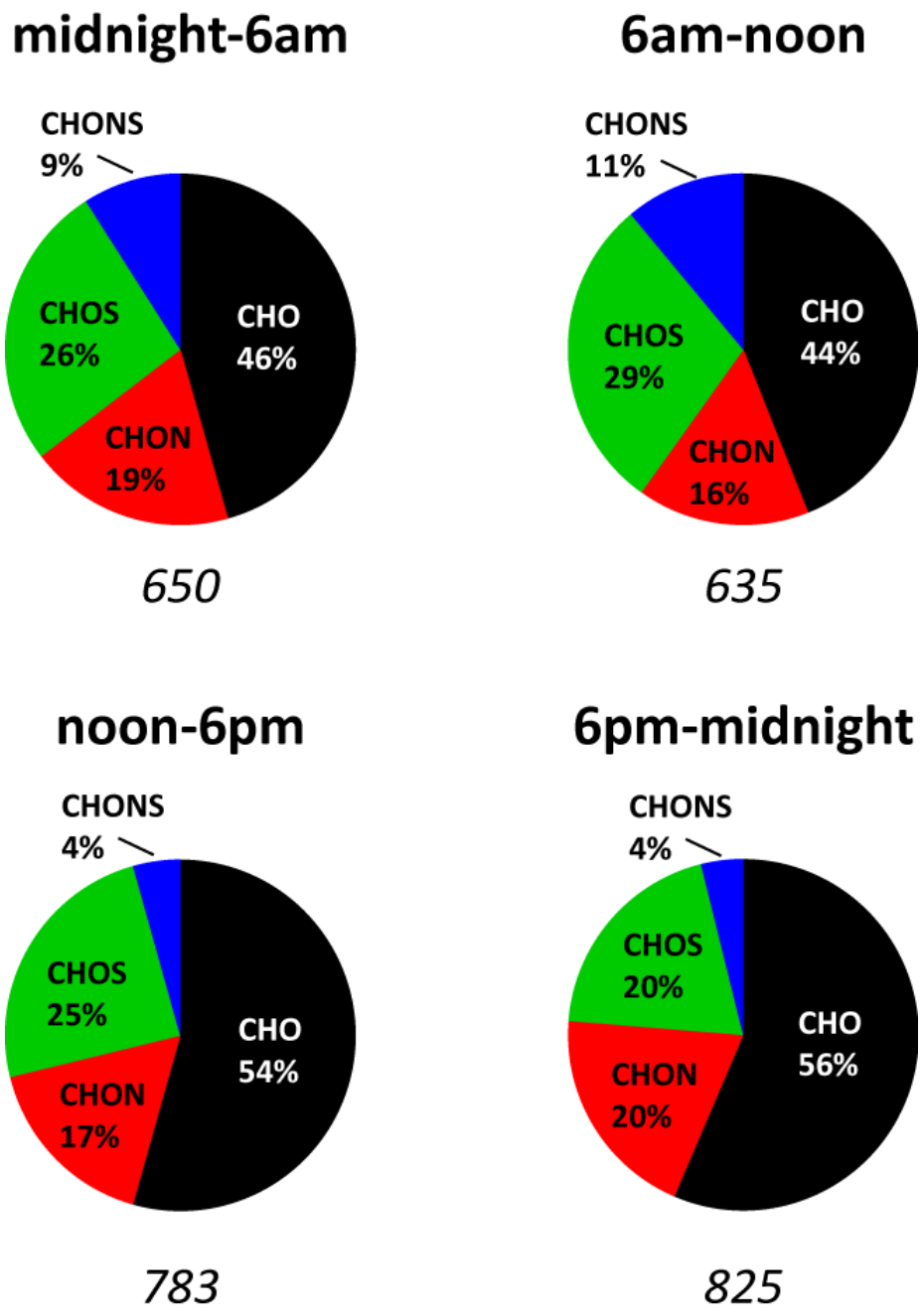


**Figure 3.1** Percentage of compounds in each class at different times of day averaged over four days. Average number of compounds observed in each sample period is given below the pie charts.

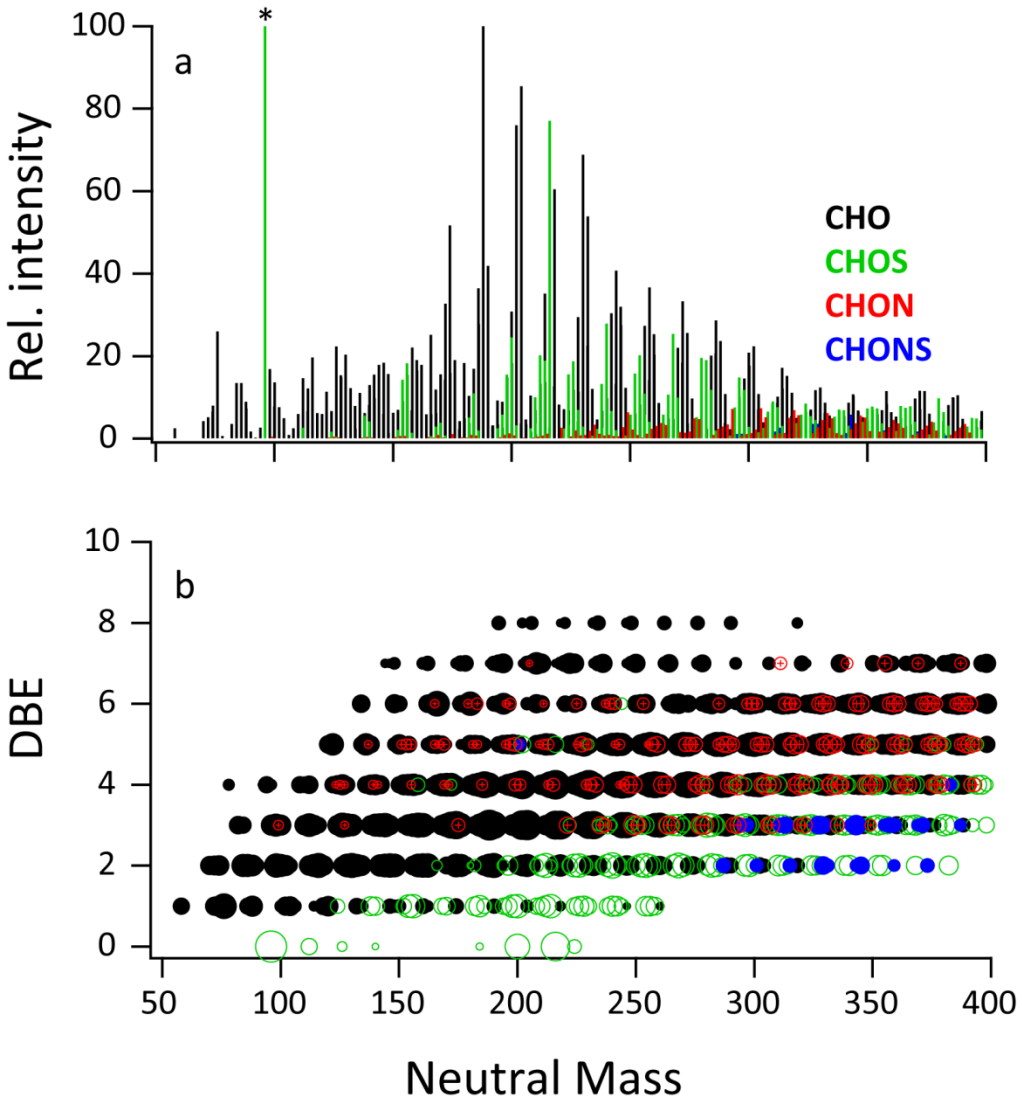


**Figure 3.2** Mass spectra and DBE plots for the sample collected on June 22nd noon-6pm. The starred peak in (a) has a relative intensity value of 137 on this scale. The size of the markers in (b) is proportional to the log of the relative intensity. The CHON (red) and CHOS (green) data points in (b) are shown as open circles.

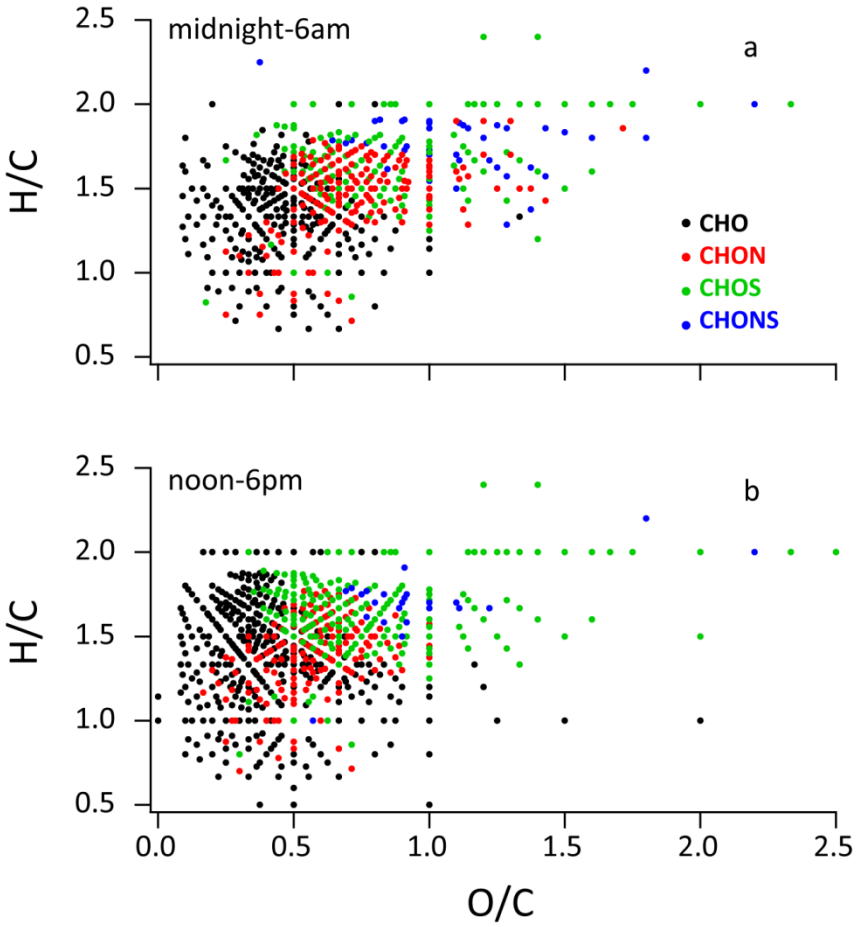


**Figure 3.3** Elemental ratios of the compounds in the June 23rd (a) midnight-6am sample and (b) noon-6pm sample.

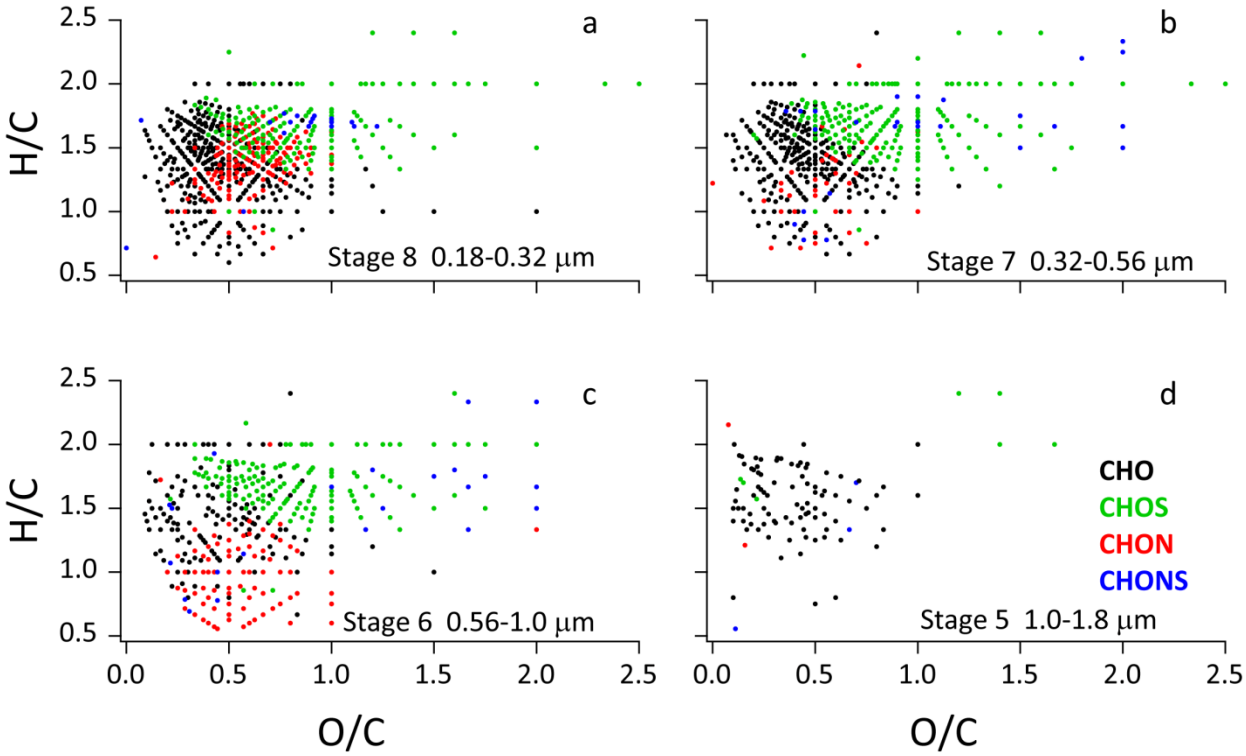


**Figure 3.4** Van Krevelen diagrams showing the elemental ratios for the samples from stages 8-5 (a-d) on the MOUDI ($0.18 < D_a < 1.8$ μm).

# Chapter 4

# Probing Molecular Associations of Field-Collected and Laboratory-Generated SOA with Nano-DESI High-Resolution Mass Spectrometry.

## 4.1 Introduction

Organic aerosols (OA), a major fraction of fine (< 2.5 μm) particulate matter, significantly affect visibility, climate, and human health (Charlson et al., 1992; Kanakidou et al., 2005; Pope and Dockery, 2006; Zhang, Q. et al., 2007). Secondary organic aerosols (SOA), a large fraction of OA, are formed from the gas-to-particle conversion of low-volatility organic compounds, and through aqueous chemistry (Seinfeld and Pankow, 2003; Williams et al., 2010; Ervens et al., 2011). SOA are complex mixtures resulting from the oxidation of biogenic and anthropogenic organic compounds and their composition can evolve further through heterogeneous and condensed phase reactions in the atmosphere (Goldstein and Galbally, 2007; Rudich et al., 2007; Donahue et al., 2009).

Although hundreds of organic compounds in SOA have been identified, a large fraction of the organic mass cannot be measured by traditional techniques, e.g., GC/MS, due to the large molecular mass and highly polar nature of many SOA compounds. Soft ionization methods, such as electrospray ionization (ESI) (Fenn et al., 1990), coupled to high resolution mass spectrometry (HR-MS) are well suited for the analysis of these compounds, allowing for the identification of the molecular composition of hundreds to thousands of individual organic molecules in each aerosol sample (Tolocka et al., 2004; Reemtsma et al., 2006; Reinhardt et al., 2007; Altieri et al., 2009; Nguyen et al., 2010; Schmitt-Kopplin et al., 2010; Hall and Johnston, 2011). We refer to these molecules as high molecular weight (high-MW) compounds or oligomers. The identities and abundances of observed high-MW species have been demonstrated to change based on the time of year (Kalberer et al., 2006) and the impact of intermittent sources such as biomass burning (Schmitt-Kopplin et al., 2010). Analyzing the chemical composition of high-MW compounds throughout the day can provide additional information on the sources and transformations of the aerosols.

Progress in identifying important chemical reactions and potential sources for high-MW species has been made using smog chamber experiments. The following citations are not meant to be comprehensive, but rather to be illustrative of the range of chamber studies that have been undertaken. Biogenic precursors such as isoprene (Dommen et al., 2006; Nguyen et al., 2011a; Zhang, H. et al., 2011), α-pinene (Gao et al., 2004; Iinuma et al., 2004; Tolocka et al., 2004; Reinhardt et al., 2007), limonene (Walser et al., 2008; Laskin et al., 2010), and anthropogenic precursors, such as 1,3,5-trimethylbenzene (Kalberer et al., 2004; Baltensperger et al., 2005), and cycloalkenes (Gao et al., 2004) have all been found to form high-MW SOA compounds in chamber studies. The mass spectra reported in these studies show differences in the molecular composition of SOA formed from different precursors, and under different experimental conditions. For example, the chemical composition of isoprene SOA changed when it was

formed under different relative humidity and $NO_x$ concentrations (Nguyen et al., 2011a; Zhang, H. et al., 2011). Kalberer et al. compared the composition of ambient SOA to that of chamber SOA generated using different precursors illustrating the potential for comparison studies to provide insights into the sources and chemistry of the SOA (Kalberer et al., 2006).

In ESI-MS studies, the aerosol sample is first extracted into an organic solvent and then electrosprayed into the mass spectrometer inlet. Potential solvent-analyte interactions introduced by the extraction step (Bateman et al., 2008) can be alleviated by quick dissolution and ionization of the sample directly from the substrate. A novel technique for this type of analysis is nano-desorption electrospray ionization (nano-DESI) mass spectrometry (Roach et al., 2010b). Laskin and coworkers have demonstrated the utility of nano-DESI for the soft ionization of complex mixtures on substrates with the preservation of some labile species and no sample preparation (Roach et al., 2010a; Eckert et al., 2012).

There have been numerous applications of HR-MS to chamber studies of SOA growth and the number of field-applications of HR-MS is also growing quickly. However, no systematic studies have been performed on the degree of overlap between molecular level composition of OA collected in the field and OA generated in lab studies. In this work, we present the molecular characterization of organic compounds inferred from nano-DESI/HR-MS analysis of aerosol samples collected in Bakersfield (BF) and Los Angeles (LA) California during the 2010 CalNex campaign. We compare the ambient chemical composition with SOA samples generated in a smog chamber under high $NO_x$ conditions with diesel fuel (DSL) and isoprene (ISO) precursors, and analyzed using the same nano-DESI/HR-MS approach. DSL and ISO SOA were chosen to represent potentially significant anthropogenic and biogenic influences, respectively, at the BF and LA site. The BF site is also characterized by elevated mixing ratios of ammonia ($NH_3$) (Markovic et al., manuscript in preparation, 2012) and additional chamber experiments were performed including the oxidation of DSL in the presence of $NH_3$. Hereinafter, the high-$NO_x$ photooxidation of DSL and ISO are referred to as "DSL-$NO_x$" and "ISO-$NO_x$," respectively, and the high-$NO_x$ photooxidation of diesel in the presence of $NH_3$ is referred to as "DSL-$NO_x$-$NH_3$." Composition differences in the ambient SOA samples throughout the day were inferred from the high resolution mass spectra. The contributions of DSL and ISO to SOA formation BF and LA were investigated and while both were found to be important SOA sources, contributions from other sources, such as gasoline (Bahreini et al., 2012; Hayes et al., submitted manuscript, 2012) and terpenes (Pandis et al., 1991; Griffin et al., 1999), were also indicated.

## 4.2 Experimental

### 4.2.1 Sampling and Instrumentation

The 2010 CalNex campaign had ground sites in BF and LA as well as aerial and ship-based measurements (NOAA, 2008). A summary of the field sites, the ambient sampling, and the chamber studies is provided in Section A of the Supporting Material. Briefly, the samples were collected at the BF (35.35°N, 118.97°W) and LA (34.14°N, 118.12°W) sampling sites. BF is located at the southern end of the San Joaquin Valley and is a city with agriculture, animal husbandry, and oil extraction/refining in the surrounding countryside. LA is a large urban area with a high population density and heavy vehicle traffic. June 23$^{rd}$ and June 5$^{th}$ were chosen for

in-depth analysis, in BF and LA respectively, because concurrent measurements indicated diurnal patterns in OA and high SOA loadings on those days (Hayes et al., submitted manuscript, 2012). Samples were collected on aluminum foil substrates using an 8 stage (BF) non-rotating and a 10-stage (LA) rotating Micro-Orifice Uniform Deposit Impactor (MOUDI, MSP Corp.) at ~30 standard liters per minute (SLM). BF samples were stored in a -20 ºC freezer at the site and a -80 ºC freezer at the lab, and LA samples were stored in a -20 ºC freezer. Samples on the eighth stage of the MOUDI, (size range of 0.18-0.32 μm aerodynamic diameter), showed the largest number of compounds in the MS of the BF samples and were chosen for intensive analysis. For consistency, the same stage was used for the LA samples, which corresponds to the middle of the accumulation mode mass distribution there (Hayes et al., submitted manuscript, 2012). All times discussed here are in local time (PDT).

On-line composition of the non-refractory components of the aerosol was measured using an Aerodyne High-Resolution Time-of-Flight Aerosol Mass Spectrometer (HR-ToF-AMS) at both sites (DeCarlo et al., 2006). In LA, the size resolved O/C was estimated from HR-ToF-AMS measurements using the relationship $O/C = 3.25(f_{44}) + 0.001$ where $f_{44}$ is the fraction of the total organic signal at m/z 44 (Hayes et al., submitted manuscript, 2012). A similar relationship of O/C and $f_{44}$ was found for Bakersfield: $O/C = 3.02\ (f_{44}) + 0.043$ (Appendix C4). The conversion between vacuum aerodynamic diameter ($D_{va}$) and aerodynamic diameter was determined assuming spherical particles and a density of 1.2 g/cm$^3$ (DeCarlo et al., 2004; Zhang, Q. et al., 2005). For Fourier transform infrared spectroscopy (FTIR) analysis, particles were collected on Teflon filters with 3-6 hour time resolution. Concentrations of organic functional groups, including alkane, carboxylic acid, organonitrate groups, etc. were quantified using automated algorithms described previously (Russell et al., 2009; Liu et al., 2011). Detailed sample collection and organic functional group analysis are presented in Liu et al. (submitted manuscript, 2012).

For the chamber experiments, SOA samples were generated from photooxidation reactions in a 5 m$^3$ Teflon chamber equipped with UV-B broadband lamps in the absence of inorganic seed particles (Nguyen et al., 2011b). The reaction was carried out at room temperature in the relative humidity (RH) range of 60-70%. DSL (diesel # 2 composite standard mixture, Restek, 0.5 g/mL in $CH_2Cl_2$) or ISO (Aldrich, purity 99%) were injected into the chamber in a clean glass bulb. An estimate of the initial mixing ratios of total DSL organics in the chamber was 100 ppb (assuming an average molecular weight of 230 g/mol (Wilson et al., 1990)) and the initial mixing ratio of ISO was 250 ppb. Nitric oxide (NO, injected from a cylinder containing 5000 ppm in $N_2$), nitrogen dioxide ($NO_2$), and ozone ($O_3$) were introduced into the chamber before the injection of DSL or ISO. The initial mixing ratios were [$NO + NO_2 = NO_x$]: 200 – 300 ppb and [$O_3$]: 50 – 90 ppb. For $NH_3$ experiments, ~ 150 ppb $NH_3$ (Fluka, 30% in water) was injected with dry air into the chamber before photooxidation. The UV photochemistry of $O_3$ initiated the photooxidation, similar to conditions in the atmosphere. The photooxidation time was approximately 5 h. The samples were collected through an activated charcoal denuder with a 30 SLM pump flow rate and humid make-up air onto aluminum substrates using the MOUDI. The collected SOA samples were vacuum sealed and frozen at – 20 °C for offline high-resolution nano-DESI-MS analyses.

Samples were analyzed at the Environmental Molecular Sciences Laboratory (Richland, Washington). Analysis was performed using a high resolution LTQ-Orbitrap™ MS (Thermo Fisher, Bremen, Germany) equipped with a recently developed nano-DESI source (Roach et al., 2010a, 2010b). The source is assembled from two fused-silica capillaries (193 μm o.d. /50 μm

i.d, Polymicro Technologies LLC, Phoenix, AZ). Acetonitrile was injected through the primary capillary forming a small droplet on the analyte surface. The dissolved analyte was transferred into the inlet of mass spectrometer through the nanospray capillary. The solvent was supplied at 1.5−2.5 μL/min flow rate to maintain a stable droplet on the surface. A voltage of ~6 kV was applied between the capillary end and the mass spectrometer inlet to obtain stable spray of charged droplets, and the system was operated in the positive ion mode with a resolution of 60,000 m/Δm (FWHM) at m/z 400. Positive mode data was used for this analysis. The instrument was externally mass calibrated using a standard ESI calibration mix of caffeine, MRFA, and Ultramark 1621 (calibration mix MSCAL 5, Sigma-Aldrich, Inc.).

### 4.2.2 Data Acquisition/ Analysis

Data analysis was performed in a similar manner to our previous work (Nguyen et al., 2011a; Nizkorodov et al., 2011). Briefly, background mass spectra acquired over the sample-free area were identified and removed from the mass spectra recorded when the probe was positioned over the sample area with deposited particulate matter (Roach et al., 2010a). Mass spectral features with a signal-to-noise ratio higher than 3 were extracted from raw spectra. Molecular assignments of the observed ions were performed using MIDAS molecular formula calculator (http://magnet.fsu.edu/~midas/) with the following constraints $C \leq 100$, $H \leq 200$, $O \leq 50$, $N \leq 3$, $S \leq 1$, $Na \leq 1$. Approximately 80-90% of the peaks could be assigned molecular formulas and assignments were aided by Kendrick analyses (Kendrick, 1963; Stenson et al., 2003) using O and $C_3H_4O_2$ as base units, and a second-order Kendrick analysis using a sequence of $CH_2$ and $H_2$ base units (Roach et al., 2011). The mass spectra were acquired over the mass range of m/z 100-1000. However, in this work we limit our discussion to peaks in the 100-400 Da range because they can be unambiguously assigned for $C_cH_hO_oN_n$ compounds given the mass accuracy and resolution used in this study.

In order to resolve and identify elemental compositions in complex mixtures such as aerosol, petroleum, and dissolved organic matter (DOM) samples both high mass resolution and high mass accuracy are required (Marshall et al., 2006; Reemtsma et al., 2006; Schmitt-Kopplin et al., 2010). High resolution enables the separation of closely-spaced peaks while high accuracy enables the determination of the elemental composition based on the exact mass. It has been demonstrated through mathematical modeling that ~0.1-0.5 mDa mass accuracy is necessary to determine unique elemental composition for typical organic compounds up to 500 Da (and higher when combined with Kendrick analysis) (Marshall et al., 2006]). In an analysis of extracted aerosol filter samples using negative mode ESI, Schmitt-Kopplin and co-workers showed that closely-spaced CHO and CHOS compounds ($C_3$ vs. $SH_4$) at ~400 Da were resolved with an instrument resolution of ~150,000 (Schmitt-Kopplin et al., 2010).

Compared to their study we used a relatively lower mass resolution of 60,000 m/Δm at m/z 400. However, we can still confidently identify peaks over a broad mass range based on the accurate mass measurements. Kendrick analysis aids identification by grouping higher mass peaks into families with lower mass peaks that can be unambiguously identified. The second-order transformation introduced recently (Roach et al., 2011), and used here, enables even more efficient grouping which facilitates identification of higher-mass peaks within each group that cannot be unambiguously identified using traditional first order Kendrick analysis. Mass accuracy can be affected by the presence of overlapping, unresolved peaks if the peaks have

similar abundance. For example, an unresolved CHO/CHOS doublet (e.g. $C_{16}H_{28}O_{10}S$ vs.$C_{19}H_{24}O_{10}$) with equivalent abundances would result in an error of ~1.7 mDa for either assignment. In contrast, when the relative abundance of one of the peaks in the unresolved doublet is low, the measured mass is very close to the exact mass of the more abundant peak. Under these conditions, while lower abundance species are unresolved and unassigned, the dominant species are accurately identified. In this study the majority (~75-80%) of our assignments had mass accuracy within ±0.35 mDa. While we do not necessarily resolve all of the peaks in the spectrum, the assignments are accurate as indicated by the absolute error.

The analyte molecules were observed as either protonated ($[M+H]^+$) or sodiated ($[M+Na]^+$) species. The assigned ionic formulas were converted to neutral formulas by subtracting either the exact mass of a proton or a sodium ion. Approximately 0-10% of the compounds in each sample were detected as both sodiated and protonated species. For these peaks, the average intensity was used. In this work, compounds containing zero, one, or two nitrogen atoms (0N, 1N, 2N, respectively) were compared. While analysis focused on positive mode spectra, elemental ratios from analysis of the negative mode spectra were included for comparison with AMS data.

There are many ways to look at the overlap between two measurements. We opted to use the percentage of peaks found in ambient samples that were also found in the chamber studies. The percentage of overlap between the ambient samples and the chamber studies was determined using equation 1.

% overlap = (number of matching peaks) / (number of peaks in ambient sample) x 100 (1)

where the 'matching peaks' are compounds that have the same observed molecular formulas in both the ambient and the chamber study samples. The relative intensities are not included in the overlap calculations due to the variability of ion intensities inherent in ESI. The number of conceivable molecular formulas of the type $C_cH_hO_oN_n$ that satisfy valence rules and weigh under 400 Da exceeds $10^4$, whereas the number of observed peaks in the field and lab samples was of order $10^3$. The probability of a random match between the samples at the overlap level observed in this work is small. A caveat to this approach is that the chemical formula may correspond to multiple isomers, thus percent overlaps include molecules having the same elemental composition regardless of their structure. The terms "molecules" and "compounds" in this study refer to all the possible isomers with a given molecular formula.

## 4.3 Results and Discussion

### 4.3.1 Comparing Ambient to Chamber Data

Figure 4.1 shows a comparison of the high resolution mass spectra from the ambient samples for each location exhibiting the best overlap with DSL-$NO_x$. The peaks in the mass spectra are color-coded as 0N, 1N, and 2N compounds with molecular formulas $C_cH_hO_o$, $C_cH_hO_oN_1$ and $C_cH_hO_oN_2$, respectively. Similar comparison mass spectra of all the BF and LA samples with DSL-$NO_x$, DSL-$NO_x$-$NH_3$, and ISO-$NO_x$ are provided in Appendices C6 through C11 in the Supporting Material. The measured peak intensities do not necessarily correlate to the absolute concentrations of the corresponding compounds in the sample. However, larger

concentrations generally result in larger relative peak intensities for structurally related compounds, and therefore, qualitative comparison of the peak intensity distributions (overall shapes) in mass spectra is still valuable. The relative intensities were calculated by dividing the measured intensity by the maximum intensity observed in that sample, except where noted.

Figure 4.1a shows that the intensity distributions of the BF sample collected from 6 am-noon and the DSL-$NO_x$ sample were similar, e.g., the maximum intensities occurred over roughly the same mass range and the mass ranges of the different subgroups (0N vs. 1N) correlated reasonably well. In contrast, Figure 4.1b shows that the LA sample collected from noon-6pm and the DSL-$NO_x$ sample appeared quite different in terms of the intensity distribution of mass spectral signals. In the LA sample, the intensity distribution was still increasing up to ~400 Da compared to a maximum at ~250 Da for the DSL-$NO_x$ sample. Additionally, there were significantly fewer 1N and 2N compounds compared to the DSL-$NO_x$ sample. A visual comparison of the BF 6am-noon with the LA noon-6pm sample (Figure 4.1a, b) shows a dramatically different intensity distribution, likely indicating different source composition/contributions and/or chemistry at the two sites.

Figure 4.2 shows how the distribution of 0N, 1N, and 2N compounds assigned for each sample changes with the measurement location and time. The total number of compounds in each sample is written above the corresponding column. The BF samples had a relatively consistent number of detected compounds in the night and early morning samples with a decrease in the afternoon (noon-6pm). In contrast, the LA data had lower numbers of compounds in the night samples and higher numbers of compounds during the day. In all cases, the majority of species were 0N or 1N compounds. The percentage of 2N compounds was below 10% in all samples, and averaged ~4%. The number of 1N or 2N compounds was significantly lower in the LA samples compared to both the BF and the chamber samples.

Figure 4.3 compares the overlap percentage (Equation 1) of the chamber and ambient sample data. The chamber experiment with the highest percent overlap with BF data was the DSL-$NO_x$ sample (Figure 4.3a) where 60 to 65% of the compounds identified in the BF sample were also observed in the laboratory SOA. The DSL-$NO_x$-$NH_3$ data had the second highest overlap and the ISO-$NO_x$ had the lowest overlap. Within the day in BF, the 6am-noon sample had the highest percent overlap with the DSL-$NO_x$ and DSL-NOx-$NH_3$ samples at 65% and 59% respectively. The overlap with ISO-NOx was relatively consistent throughout the day, between 37 and 40%. The BF noon-6pm sample had the lowest percent overlap with the DSL-$NO_x$ data, even though this sample had the lowest number of identified peaks and thus, would be expected to have the highest overlap if the samples were very similar since in the overlap comparison we divided by the number of peaks in the ambient sample. The total number of overlapping compounds was the lowest for this sample (Appendix C2) which suggests that either these sources, DSL and ISO, had the least impact on this sample or this sample was affected by different chemistry.

Generally, the BF samples showed more overlap with the DSL sample and there were small changes in the overlap with the DSL sample throughout the day. The small changes in overlap could be due to either variations in local sources such as gasoline, diesel, terpenes, etc., or to variations in atmospheric chemistry such as those due to changes in ozone and relative humidity. However, the extent to which variation in either sources or chemistry contributed to the observations cannot be determined from these data. The percent overlap of BF with ISO-$NO_x$ was slightly more constant throughout the day perhaps indicating a more distant, but

broadly arrayed, source resulting in a more stable signal, consistent with the high isoprene-emitting oak trees prevalent in the hills surrounding the San Joaquin Valley.

The LA data generally had less overlap with the chamber study data than BF (Figure 4.3b). The percent overlap between LA and the chamber studies followed the same trend with the highest overlap observed with DSL-$NO_x$ and the lowest overlap observed with ISO-$NO_x$. The percent overlap varied more within the day in LA, with the DSL-$NO_x$ sample matching ~31% of the compounds from 6am-noon and ~51% of the compounds from noon-6pm. The much higher percent overlap for the noon-6pm sample is consistent with the arrival of the afternoon SOA from both DSL and ISO influenced sources. The concentration of elemental carbon (EC) and the photochemical age both peaked during noon-6pm period also consistent with SOA influenced by DSL sources (Hayes et al., submitted manuscript, 2012). The percent overlap of the LA noon-6pm sample with the chamber samples was lower than any of the BF data. This difference was likely due to the presence (or the increased concentrations) of other sources in LA, including gasoline SOA which has been asserted to be a dominant source there (Bahreini et al., 2012; Hayes et al., submitted manuscript, 2012), and/or a potentially shorter photochemical processing time relative to both BF and the chamber studies.

The bulk H/C, O/C, and N/C elemental ratios are commonly used to characterize SOA, and the corresponding averaged values for all samples, weighted by relative intensities (Bateman et al., 2009; Nguyen et al., 2010), are listed in Table 4.1. Collocated HR-ToF-AMS were used in both field studies to measure the composition of the aerosol in real time and the uncertainties listed for the AMS data in Table 4.1 follow those suggested by Aiken et al. (2008). The H/C ratio measured by the nano-DESI method was fairly consistent throughout all of the field and laboratory samples ranging from 1.7 to 1.5 in the LA and BF afternoon (6pm-midnight) samples, respectively. The H/C ratio measured by the AMS was somewhat lower, ranging from 1.3-1.5 (Table 4.1).

The O/C ratios measured with the nano-DESI analysis had a slightly larger range with the lowest values measured in the LA samples, between 0.13 and 0.24, and the highest value, 0.46, observed in the ISO-$NO_x$ sample. A comparison of the O/C and N/C values to AMS data must be considered with caution because selective ionization in ESI may lead, depending on the sample and ionization mode, to either an overestimation or an underestimation of the <O/C> value. In addition, we analyzed only the 0.18-0.32 μm size fraction in the ambient samples which is smaller than the size range sampled by AMS (0.05–1.0 μm). In BF, no dependence of the <O/C> on the aerosol size was found from an analysis of the AMS data so the AMS <O/C> for the ensemble submicron particles is used to represent the <O/C> in the 0.18-0.32 μm size range. The BF <O/C> values of 0.32 -0.35 for the positive mode data and 0.56-0.76 for the negative mode data were comparable to the <O/C> values of 0.28-0.44 measured by the AMS on the same day (Tables 4.1, Appendix C3). In contrast, AMS measurements showed that the <O/C> values in LA were lower and depended on the size of the aerosol (Appendix C4). The LA data for the nano-DESI-MS analysis had <O/C> values ranging from 0.13-0.24 in the positive mode and 0.27-0.63 in the negative mode (Tables 4.1, Appendix C3). These two ranges bracket the AMS <O/C> values of 0.31-0.39 for the same aerosol size range (Table 4.1).

For the positive mode data, the <N/C> values from BF were about 4 to 14 times higher than average N/C values measured with AMS. In LA, the AMS values were about 0.5 to 9 times higher than the nano-DESI values (Table 4.1). The AMS N/C values are not size resolved which could explain some but likely not all of the differences. More work comparing the responses of the two different techniques to nitrogen containing compounds is necessary to fully understand

these observations. The much lower <N/C> values measured in the LA samples with nano-DESI-MS further indicate differences in chemistry between the two sites. Since both the LA and BF regions have plenty of $NO_x$ and VOC's this difference in the <N/C> is likely indicative of both different aerosol ages and different chemistry leading to nitrogen containing species, as we discuss below.

### 4.3.2 Comparing LA to BF

Significant differences were observed in the mass spectral overlap and the <O/C> and <N/C> ratios between the LA and BF samples. The degree of overlap between LA and BF was calculated using equation 2.

% overlap = (number of matching peaks)/ (number of peaks detected in LA sample) x 100 (2)

where 'matching peaks' were those identified in both samples. Similar trends were observed with either BF or LA sample placed in the denominator, for brevity only comparisons against LA are discussed. The LA samples with the highest percent overlap with BF data were the two afternoon samples (noon-midnight) and the percent overlap of the four LA samples with each of the BF samples followed a similar pattern as observed in the overlap between LA and the chamber data (Figure 4.3 and Appendix C15).

Insights into the differences in SOA composition characteristic for the two locations can be gained from examining the compounds unique to each sample. The double bond equivalence (DBE), which represents the sum of all rings and double bonds in the molecule, is calculated using equation 3.

$$DBE = 1 + c - (h/2) + (n/2) \quad (3)$$

where c, h, and n refer to the number of carbon, hydrogen, and nitrogen atoms in the identified species, respectively. This equation assumes a valence of 3 for nitrogen; the calculated DBE will be slightly higher if most of the nitrogen-containing compounds have valence of 5. The percent of unsaturation was calculated by dividing the DBE values for each compound by the number of single bonds in a saturated hydrocarbon with the same number of carbon atoms (Smith et al., 2009). Figure 4.4 shows a comparison of the percent unsaturation of the BF and LA noon-6pm samples which ranged from 0 to around 25% and generally decreased with increasing mass. The unique compounds in BF were more unsaturated (average 11%) and had higher O/C values than the unique compounds in LA (average 8%). The aromaticity index (AI) (Koch and Dittmar, 2006), an estimation of the number of C=C double bonds, was calculated for the unique BF data. Approximately 62% of the compounds above 200 Da had AI values of zero, suggesting that many of the double bonds were carbonyls and nitrogen-oxygen functional groups. The higher percent unsaturation for the BF sample in this region is thus largely driven by the increased number of oxygen atoms.

The lower oxidation level of the compounds in LA (Figure 4.4) suggests this SOA was younger and had undergone less heterogeneous, homogenous, and/or photolytic (Bateman et al., 2011) processing. This is consistent with the AMS results showing that the average O/C value increased with increasing aerosol size (Appendix C4). The aerosol sample measured here, in the

0.18-0.32 μm range, was less oxidized than the more processed aerosols found in larger size fractions, although a caveat is that primary aerosols are generally concentrated in the smaller size fractions (Hayes et al., submitted manuscript, 2012). The compounds with low O/C values unique to the LA samples may also indicate different sources between the two sites. The younger age of the aerosol can also explain the very low number of nitrogen containing compounds observed in the LA samples despite high $NO_x$ levels. If the aerosol sample in the 0.18-0.32 μm range in LA was only a few hours old then there was less time for organonitrates to form and partition into the particle phase. It should be noted that lower measured numbers of nitrogen containing compounds in LA could also be a caused by increased degradation reactions such as hydrolysis (Hu et al, 2011).

AMS measurements in LA suggested low concentrations of organonitrates over the whole size range (0.05 –1.0 μm) (Hayes et al., submitted manuscript 2012). Lower concentrations of organonitrates ($PM_{2.5}$) in LA vs. BF were also observed with FTIR analysis. In BF on June 23rd, the organonitrate group concentration from FTIR was 0.2 $\mu g/m^3$ compared to 0.09 $\mu g/m^3$ in LA on June 5th. Thus, the amount of organonitrates was lower overall in LA compared to BF. Also, the much higher nitrogen content in BF could have been driven by the high ammonia levels there (average value of 20 ppb with an hourly maximum of 65 ppb) (Markovic et al., manuscript in preparation, 2012) which can result in production of reduced nitrogen compounds (Laskin et al., 2010; Wang et al., 2010).

### 4.3.3 Comparing Unique Species Observed in Chamber and Ambient Samples

A comparison of the unique compounds between the chamber experiments can help elucidate their relative contributions to the ambient samples. The hypothesis is that each type of chamber-generated SOA may have a set of unique and reproducible "signature" peaks, which could be used for source apportionment of the field data. An analysis of the overlap between the ISO-$NO_x$ sample (504 total peaks) and the DSL-$NO_x$ sample (732 total peaks) resulted in 401 (55% with respect to the total number of peaks in this sample) unique DSL-$NO_x$ compounds, 173 (34%) unique ISO-$NO_x$ compounds, and 331 compounds that were common to both DSL-$NO_x$ and ISO-$NO_x$ samples. Approximately 25-30% of the unique DSL-$NO_x$ compounds and approximately 3-5% of the unique ISO-$NO_x$ compounds overlapped (Equation 1) with BF (Appendix C17). Since the majority of the overlap between ISO-$NO_x$ and BF consisted of compounds that are common to both ISO-$NO_x$ and DSL-$NO_x$, we cannot separate the relative contributions of the two sources well. However, given the greater overlap with unique compounds in DSL, it is likely that BF was more influenced by anthropogenic diesel-like sources than by biogenic isoprene-like sources. Part of the difficulty in separating ISO and DSL sources is that many molecular formulas, such as $C_3H_4O_2$ (methylglyoxal), are common to the oxidation of both isoprene and aromatic compounds.

An analysis of the overlap between the DSL-$NO_x$-$NH_3$ sample (595 total peaks) and the DSL-$NO_x$ sample (732 total peaks) resulted in 223 (31%) unique DSL-$NO_x$ compounds and 86 (14%) unique DLS-$NO_x$-$NH_3$ compounds. Figure 4.5 shows the percent overlap (Equation 1) of the BF and LA noon-6pm samples with the unique DSL-$NO_x$ and unique DSL-$NO_x$-$NH_3$. Similar trends in the data were observed for the other samples (Appendices C18 and C19). The data are separated by the number of nitrogen atoms in the molecular formulas. In BF, the percent overlap with the unique DSL-$NO_x$-$NH_3$ was higher for the 2N compounds, suggesting

$NH_3$-mediated chemistry is responsible for the formation of some of the organic nitrogen in BF. In LA, the percent overlap for the unique DSL-$NO_x$-$NH_3$ was slightly higher for 1N compounds than for 0N; however, there was no overlap with the 2N compounds. The unique DSL-$NO_x$-$NH_3$ overlap was always lower than the unique DSL-$NO_x$ in LA, suggesting that oxidized nitrogen (e.g., nitric acid esters) played a bigger role in producing SOA in LA than reduced nitrogen (e.g., amines, imines, heterocyclic N-containing compounds). The results obtained from our comparison are consistent with the expectation that urban sites like LA have much lower influence of $NH_3$ relative to rural/urban sites like BF (Hughes et al., 2000). In the San Joaquin Valley major sources for ammonia include agriculture and animal husbandry (Markovic et al., manuscript in preparation 2012). Based on other concurrent measurements at the two sites, the mixing ratios of $NH_3$ in BF were on average ~ 10 times higher than in LA (Markovic et al., manuscript in preparation 2012; Ellis et al, manuscript in preparation 2012). The higher overlap with the 2N compounds for the unique DSL-$NO_x$-$NH_3$ with BF data suggests that some of the 2N compounds observed in BF were formed through reactions of organic compounds with gaseous $NH_3$ (Laskin et al., 2010; Wang et al., 2010).

## 4.4 Conclusions

The molecular composition of aerosol samples collected from chamber studies and in BF and LA during CalNex were investigated using high resolution mass spectrometry. Between 100 and 800 unique compounds were identified in each sample (Figure 4.2). The percent overlap of the ambient samples with the three chamber experiments each showed the same trend: DSL-$NO_x$ had the highest overlap followed by DSL-$NO_x$-$NH_3$ and ISO-$NO_x$ (Figure 4.3). The number of peaks identified for the LA night samples was lower than the number identified for the LA day samples. The highest overlaps with the chamber experiments were observed for the noon-6pm sample, consistent with the SOA plume arriving from downtown LA.

There were significant differences in the mass spectra measured for the LA and BF samples (Figures 4.1 and Appendices C6-C11). A comparison of the molecular compositions in LA and BF showed compounds with higher O/C values and higher percent unsaturation for BF. The higher oxidation level of the BF samples may indicate a fresher LA sample and/or different sources at the two sites. The DSL-$NO_x$-$NH_3$ sample had significantly more overlap with the 2N compounds in each BF sample than the DSL-$NO_x$ sample. This suggests that some of the nitrogen containing compounds in BF were formed by $NH_3$ chemistry. There were significantly more nitrogen containing compounds in the BF samples than in the LA samples consistent with AMS and FTIR results showing low levels of organonitrates in LA. Additionally, the higher number of CHON compounds in BF could have been driven by the higher concentrations of $NH_3$ in BF.

Combining all the compounds observed in chamber experiments with diesel and isoprene oxidation results in overlap with 70% or less of the ambient compounds. The inherent differences between ambient and chamber experiments, including the increased time for oxidation available in an ambient environment, could explain some of these differences. However, it is evident that diesel and isoprene do not cover the full range of sources contributing to SOA in either BF or LA. The utility of this comparative approach indicates that a more complete assessment of expected sources to the high-MW fraction of the aerosol, including chamber experiments with other SOA precursors such as gasoline (Bahreini et al., 2012; Hayes

et al., submitted manuscript, 2012), terpenes (Pandis et al., 1991; Griffin et al., 1999), and petroleum and cooking emissions (Liu et al., submitted manuscript, 2012) could be useful in the source apportionment of ambient aerosols.

## 4.5 References


Aiken, A. C., et al. (2008), O/C and OM/OC ratios of primary, secondary, and ambient organic aerosols with high-resolution time-of-flight aerosol mass spectrometry, *Environ. Sci. Technol.*, *42*(12), 4478-4485.

Altieri, K. E., B. J. Turpin and S. P. Seitzinger (2009), Oligomers, organosulfates, and nitrooxy organosulfates in rainwater identified by ultra-high resolution electrospray ionization FT-ICR mass spectrometry, *Atmos. Chem. Phys.*, *9*(7), 2533-2542.

Bahreini, R., et al. (2012), Gasoline emissions dominate over diesel in formation of secondary organic aerosol mass, *Geophys. Res. Lett.*, *39* (6), L06805.

Baltensperger, U., et al. (2005), Secondary organic aerosols from anthropogenic and biogenic precursors, *Faraday Discuss.*, *130*, 265-278.

Bateman, A. P., et al. (2008), The effect of solvent on the analysis of secondary organic aerosol using electrospray ionization mass spectrometry, *Environ. Sci. Technol.*, *42*(19), 7341-7346.

Bateman, A. P., S. A. Nizkorodov, J. Laskin and A. Laskin (2009), Time-resolved molecular characterization of limonene/ozone aerosol using high-resolution electrospray ionization mass spectrometry, *Phys. Chem. Chem. Phys.*, *11*(36), 7931-7942.

Bateman, A. P., S. A. Nizkorodov, J. Laskin and A. Laskin (2011), Photolytic processing of secondary organic aerosols dissolved in cloud droplets, *Phys. Chem. Chem. Phys.*, *13*(26), 12199-12212.

Charlson, R. J., et al. (1992), Climate Forcing by Anthropogenic Aerosols, *Science*, *255*(5043), 423-430.

DeCarlo, P. F., et al. (2006), Field-deployable, high-resolution, time-of-flight aerosol mass spectrometer, *Anal. Chem.*, *78*(24), 8281-8289.

DeCarlo, P. F., et al. (2004), Particle morphology and density characterization by combined mobility and aerodynamic diameter measurements. Part 1: Theory, *Aerosol Sci. Technol.*, *38*(12), 1185-1205.

Dommen, J., et al. (2006), Laboratory observation of oligomers in the aerosol from isoprene/NO(x) photooxidation, *Geophys. Res. Lett.*, *33*(13), L13805.

Donahue, N. M., A. L. Robinson and S. N. Pandis (2009), Atmospheric organic particulate matter: From smoke to secondary organic aerosol, *Atmos. Environ.*, *43*(1), 94-106.

Eckert, P. A., P. J. Roach, A. Laskin and J. Laskin (2012), Chemical characterization of crude petroleum using nanospray desorption electrospray ionization coupled with high-resolution mass spectrometry, *Anal. Chem.*, *84*(3), 1517-1525.

Ervens, B., B. J. Turpin and R. J. Weber (2011), Secondary organic aerosol formation in cloud droplets and aqueous particles (aqSOA): a review of laboratory, field and model studies, *Atmos. Chem. Phys.*, *11*(21), 11069-11102.

Fenn, J. B., et al. (1990), Electrospray ionization-principles and practice, *Mass Spectrom. Rev.*, *9*(1), 37-70.

Gao, S., et al. (2004), Particle phase acidity and oligomer formation in secondary organic aerosol, *Environ. Sci. Technol.*, *38*(24), 6582-6589.

Goldstein, A. H. and I. E. Galbally (2007), Known and unexplored organic constituents in the earth's atmosphere, *Environ. Sci. Technol.*, *41*(5), 1514-1521.

Griffin, R. J., D. R. Cocker, R. C. Flagan and J. H. Seinfeld (1999), Organic aerosol formation from the oxidation of biogenic hydrocarbons, *J. Geophys. Res.-Atmos.*, *104*(D3), 3555-3567.

Hall, W. A. and M. V. Johnston (2011), Oligomer content of alpha-pinene secondary organic aerosol, *Aerosol Sci. Technol.*, *45*(1), 37-45.

Hu, K. S.; A. I. Darer and M. J. Elrod (2011), Thermodynamics and kinetics of the hydrolysis of atmospherically relevant organonitrates and organosulfates, *Atmos. Chem. Phys.*, *11*(16), 8307-8320.

Hughes, L. S., et al. (2000), Evolution of atmospheric particles along trajectories crossing the Los Angeles basin, *Environ. Sci. Technol.*, *34*(15), 3058-3068.

Iinuma, Y., O. Boge, T. Gnauk and H. Herrmann (2004), Aerosol-chamber study of the alpha-pinene/O-3 reaction: influence of particle acidity on aerosol yields and products, *Atmos. Environ.*, *38*(5), 761-773.

Kalberer, M., et al. (2004), Identification of polymers as major components of atmospheric organic aerosols, *Science*, *303*(5664), 1659-1662.

Kalberer, M., M. Sax and V. Samburova (2006), Molecular size evolution of oligomers in organic aerosols collected in urban atmospheres and generated in a smog chamber, *Environ. Sci. Technol.*, *40*(19), 5917-5922.

Kanakidou, M., et al. (2005), Organic aerosol and global climate modelling: a review, *Atmos. Chem. Phys.*, *5*, 1053-1123.

Kendrick, E. (1963), A mass scale based on ch2=14.0000 for high resolution mass spectrometry of organic compounds, *Anal. Chem.*, *35*(13), 2146-2154.

Koch, B. P. and T. Dittmar (2006), From mass to structure: an aromaticity index for high-resolution mass data of natural organic matter, *Rapid Commun. Mass Spectrom.*, *20*(5), 926-932.

Laskin, J., et al. (2010), High-resolution desorption electrospray ionization mass spectrometry for chemical characterization of organic aerosols, *Anal. Chem.*, *82*(5), 2048-2058.

Liu, S., D. A. Day, J. E. Shields and L. M. Russell (2011), Ozone-driven daytime formation of secondary organic aerosol containing carboxylic acid groups and alkane groups, *Atmos. Chem. Phys.*, *11*(16), 8321-8341.

Marshall, A. G., K. Sunghwan and R. P. Rodgers (2006), Truly "exact" mass: Elemental composition can be determined uniquely from molecular mass measurement at ~0.1mDa accuracy for molecules up to ~500Da, *Int. J. Mass Spectrom. (Netherlands)*, *251*(2-3), 260-265265.

NOAA: National Oceanic and Atmospheric Administration (2008), 2010 CalNex White Paper: Research at the Nexus of Air Quality and Climate Change, *Available at:* http://www.esrl.noaa.gov/csd/projects/calnex/whitepaper.pdf

Nguyen, T. B., et al. (2010), High-resolution mass spectrometry analysis of secondary organic aerosol generated by ozonolysis of isoprene, *Atmos. Environ.*, *44*(8), 1032-1042.

Nguyen, T. B., J. Laskin, A. Laskin and S. A. Nizkorodov (2011a), Nitrogen-containing organic compounds and oligomers in secondary organic aerosol formed by photooxidation of isoprene, *Environ. Sci. Technol.*, *45*(16), 6908-6918.

Nguyen, T. B., et al. (2011b), Effect of humidity on the composition of isoprene photooxidation secondary organic aerosol, *Atmos. Chem. Phys.*, *11*(14), 6931-6944.

Nizkorodov, S. A., J. Laskin and A. Laskin (2011), Molecular chemistry of organic aerosols through the application of high resolution mass spectrometry, *Phys. Chem. Chem. Phys.*, *13*(9), 3612-3629.

Pandis, S. N., S. E. Paulson, J. H. Seinfeld and R. C. Flagan (1991), Aerosol formation in the photooxidation of isoprene and beta-pinene, *Atmospheric Environment Part a-General Topics*, *25*(5-6), 997-1008.

Pope, C. A. and D. W. Dockery (2006), Health effects of fine particulate air pollution: Lines that connect, *J. Air Waste Manage. Assoc.*, *56*(6), 709-742.

Reemtsma, T., et al. (2006), Identification of fulvic acids and sulfated and nitrated analogues in atmospheric aerosol by electrospray ionization Fourier transform ion cyclotron resonance mass spectrometry, *Anal. Chem.*, *78*(24), 8299-8304.

Reinhardt, A., et al. (2007), Ultrahigh mass resolution and accurate mass measurements as a tool to characterize oligomers in secondary organic aerosols, *Anal. Chem.*, *79*(11), 4074-4082.

Roach, P. J., J. Laskin and A. Laskin (2010a), Molecular characterization of organic aerosols using nanospray-desorption/electrospray ionization-mass spectrometry, *Anal. Chem.*, *82*(19), 7979-7986.

Roach, P. J., J. Laskin and A. Laskin (2010b), Nanospray desorption electrospray ionization: an ambient method for liquid-extraction surface sampling in mass spectrometry, *Analyst*, *135*(9), 2233-2236.

Roach, P. J., J. Laskin and A. Laskin (2011), Higher-order mass defect analysis for mass spectra of complex organic mixtures, *Anal. Chem.*, *83*(12), 4924-4929.

Rudich, Y., N. M. Donahue and T. F. Mentel (2007). Aging of organic aerosol: Bridging the gap between laboratory and field studies, *Annu. Rev. Phys. Chem.*, *58***,** 321-352.

Russell, L. M., et al. (2009), Oxygenated fraction and mass of organic aerosol from direct emission and atmospheric processing measured on the R/V Ronald Brown during TEXAQS/GoMACCS 2006, *J. Geophys. Res.-Atmos.*, *114*, D00F05, doi: 10.1029/2008JD011275.

Schmitt-Kopplin, P., et al. (2010), Analysis of the unresolved organic fraction in atmospheric aerosols with ultrahigh-resolution mass spectrometry and nuclear magnetic resonance spectroscopy: organosulfates as photochemical smog constituents, *Anal. Chem.*, *82*(19), 8017-8026.

Seinfeld, J. H. and J. F. Pankow (2003), Organic atmospheric particulate material, *Annu. Rev. Phys. Chem.*, *54*, 121-140.

Smith, J. S., A. Laskin and J. Laskin (2009), Molecular characterization of biomass burning aerosols using high-resolution mass spectrometry, *Anal. Chem.*, *81*(4), 1512-1521.

Stenson, A. C., A. G. Marshall and W. T. Cooper (2003), Exact masses and chemical formulas of individual Suwannee River fulvic acids from ultrahigh resolution electrospray ionization Fourier transform ion cyclotron resonance mass spectra, *Anal. Chem.*, *75*(6), 1275-1284.

Tolocka, M. P., et al. (2004), Formation of oligomers in secondary organic aerosol, *Environ. Sci. Technol.*, *38*(5), 1428-1434.

Walser, M. L., et al. (2008), High-resolution mass spectrometric analysis of secondary organic aerosol produced by ozonation of limonene, *Phys. Chem. Chem. Phys.*, *10*(7), 1009-1022.

Wang, X. F., et al. (2010), Evidence for high molecular weight nitrogen-containing organic salts in urban aerosols, *Environ. Sci. Technol.*, *44*(12), 4441-4446.

Williams, B. J., et al. (2010), Major components of atmospheric organic aerosol in southern California as determined by hourly measurements of source marker compounds, *Atmos. Chem. Phys.*, *10*(23), 11577-11603.

Wilson, J. L., et al. (1990), Laboratory investigation of residual liquid organics in United States Environmental Protection Agency: 1990; Vol. EPA 600/6-90/004

Zhang, H., et al. (2011), Effect of relative humidity on SOA formation from isoprene/NO photooxidation: enhancement of 2-methylglyceric acid and its corresponding oligoesters under dry conditions, *Atmos. Chem. Phys.*, *11*(13), 6411-6424.

Zhang, Q., et al. (2005), Time- and size-resolved chemical composition of submicron particles in Pittsburgh: Implications for aerosol sources and processes, *J. Geophys. Res.-Atmos.*, *110*, D07S09, doi: 10.1029/2004JD004649.

Zhang, Q., et al. (2007), Ubiquity and dominance of oxygenated species in organic aerosols in anthropogenically-influenced Northern Hemisphere midlatitudes, *Geophys. Res. Lett.*, *34*, L13801, doi:10.1029/2007GL029979.

## 4.6 Tables and Figures

**Table 4.1** Ensemble average, intensity weighted H/C, O/C, and N/C values of the compounds observed for each sample and the AMS values averaged over the same sample time periods. Only the LA AMS O/C values are size resolved.

| | Nano-DESI | | | AMS | | |
|---|---|---|---|---|---|---|
| **Sample** | **H/C** | **O/C** | **N/C ($x10^{-3}$)** | **H/C** | **O/C** | **N/C ($x10^{-3}$)** |
| **Diesel-$NO_x$** | 1.7 | 0.28 | 28 | - | - | - |
| **Diesel-NOx-$NH_3$** | 1.6 | 0.32 | 39 | - | - | - |
| **Isoprene-$NO_x$** | 1.7 | 0.46 | 44 | - | - | - |
| **BF midnight-6am** | 1.6 | 0.33 | 42 | 1.5 ± 0.2 | 0.28 ± 0.09 | 3.1 ± 0.7 |
| **BF 6am-noon** | 1.6 | 0.32 | 33 | 1.4 ± 0.1 | 0.40 ± 0.1 | 4.2 ± 0.9 |
| **BF noon-6pm** | 1.5 | 0.35 | 18 | 1.4 ± 0.1 | 0.43 ± 0.1 | 4.1 ± 0.9 |
| **BF 6pm-midnight** | 1.5 | 0.35 | 30 | 1.3 ± 0.1 | 0.44 ± 0.1 | 4.6 ± 1 |
| **LA midnight-6am** | 1.4 | 0.19 | 2.4 | 1.5 ± 0.2 | 0.35 ± 0.1 | 22 ± 5 |
| **LA 6am-noon** | 1.5 | 0.13 | 21 | 1.4 ± 0.1 | 0.31 ± 0.1 | 14 ± 3 |
| **LA noon-6pm** | 1.7 | 0.24 | 19 | 1.4 ± 0.1 | 0.39 ± 0.1 | 6.9 ± 2 |
| **LA 6pm-midnight** | 1.7 | 0.23 | 13 | 1.5 ± 0.2 | 0.37 ± 0.1 | 11 ±2 |

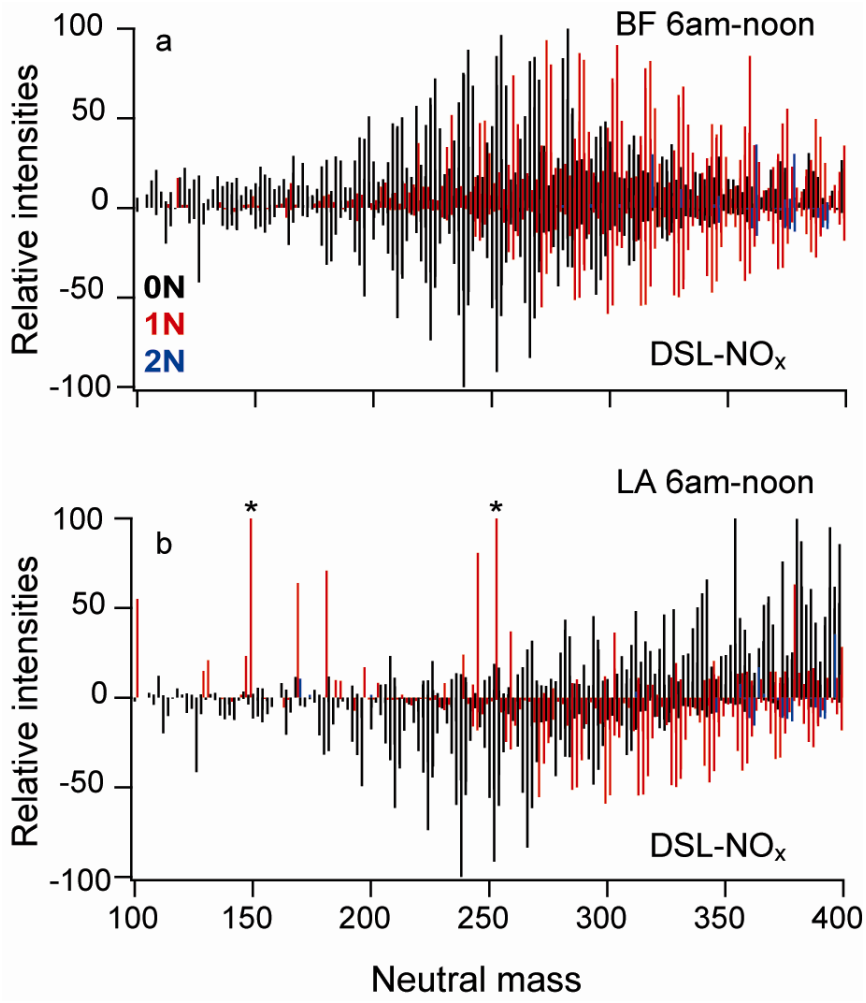


**Figure 4.1** Comparison of the mass spectra of the ambient samples from each site with the best DSL-$NO_x$ overlap: (a) BF 6 am-noon and (b) LA noon-6 pm. The DSL-$NO_x$ mass spectra are plotted with negative relative intensities to aid comparison. The colors correspond to the number of N atoms in the chemical formula with black = 0N, red = 1N, blue = 2N. The two starred peaks in the LA noon-6pm sample have intensities of 260 and 250 on this scale.

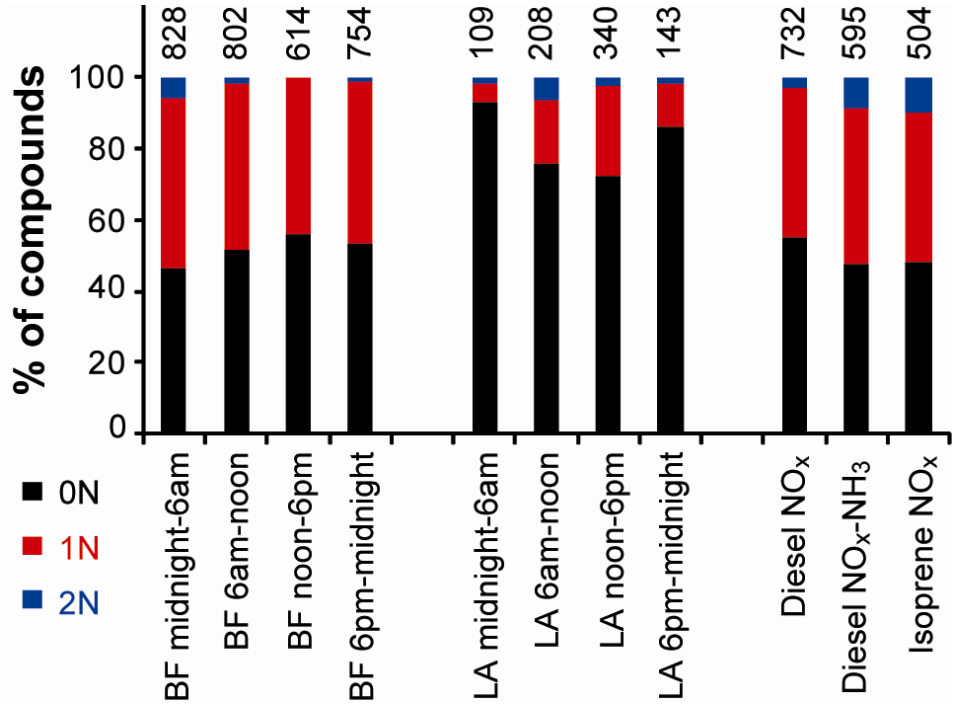


**Figure 4.2** Percentage of formulas assigned 0N, 1N, and 2N for each sample. The 0N, 1N, and 2N compounds correspond to molecular formulas $C_xH_yO_z$, $C_xH_yO_zN$ and $C_xH_yO_zN_2$, respectively. The total number of identified peaks in each sample is shown above each column.

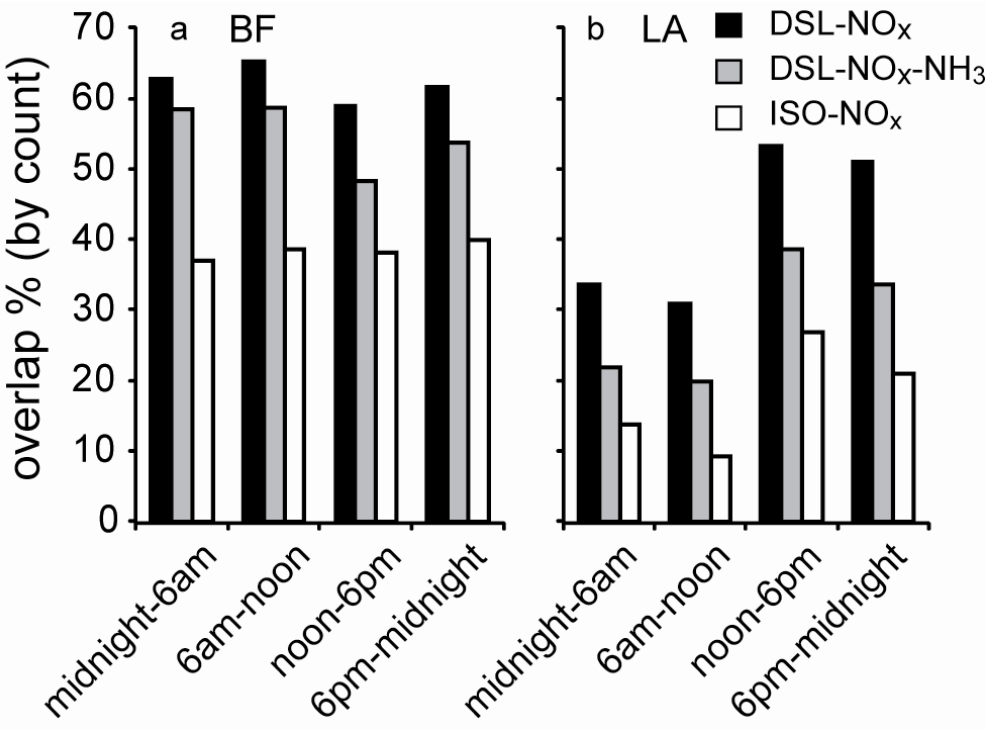


**Figure 4.3** Percent overlap calculated from Eq. (1) for (a) BF and (b) LA samples with respect to the three chamber studies, DSL-$NO_x$ (black), DSL-$NO_x$-$NH_3$ (grey), and ISO-$NO_x$ (white).

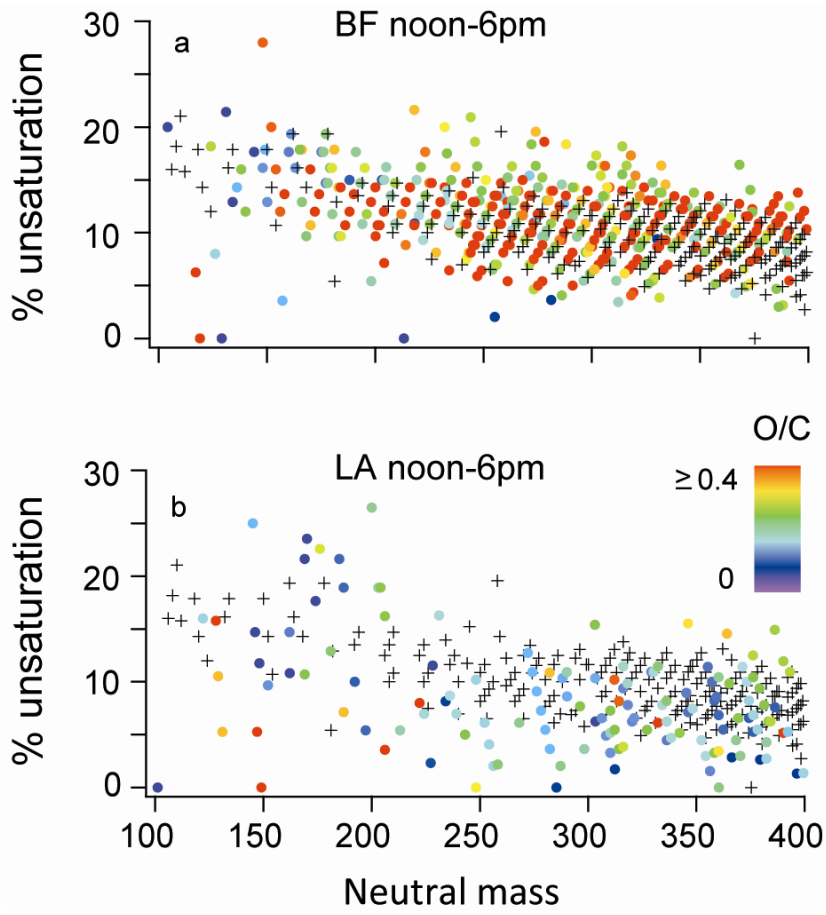


**Figure 4.4** The percent unsaturation of each unique compound plotted vs. the neutral mass for (a) the BF noon-6pm sample and (b) the LA noon-6pm sample. The data are color-coded by the O/C value of the compound as indicated in the legend. The grey pluses are the common peaks for comparison.

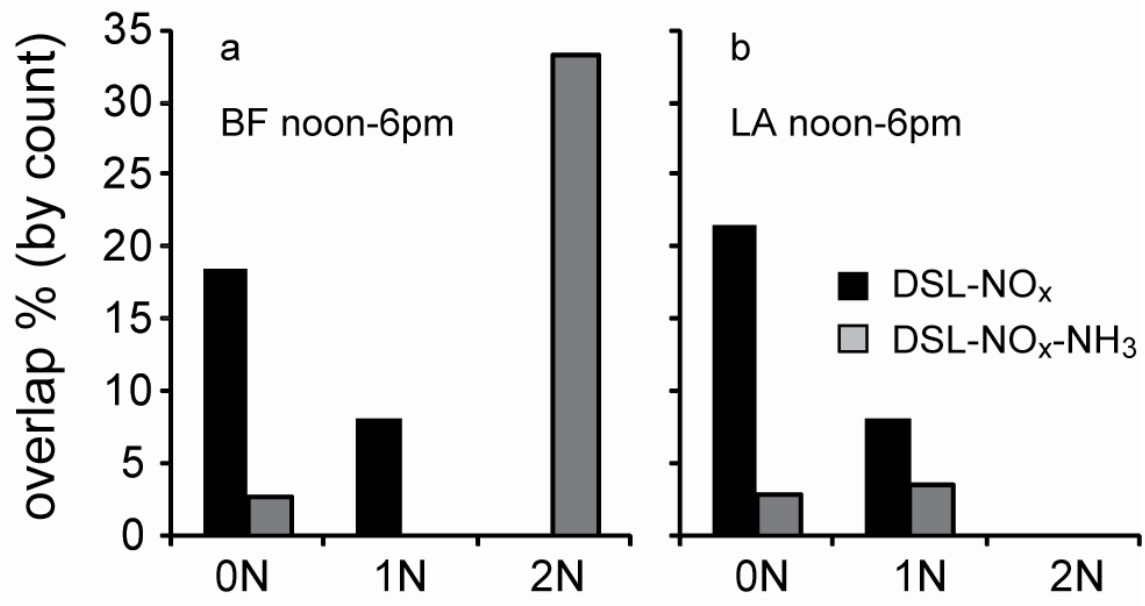


**Figure 4.5** Percent overlap of the unique DSL-$NO_x$ and unique DSL-$NO_x$-$NH_3$ peaks with (a) BF noon-6pm and (b) LA noon-6pm samples. The data are broken down by the number of nitrogen atoms in the chemical formula. The high overlap between 2N compounds and DSL-$NO_x$-$NH_3$ peaks implies an important role of ammonia in forming nitrogen containing compounds in BF.

# Chapter 5

# Summary and Future Work

Organic aerosols are a major fraction of fine particulate matter and they affect visibility, climate, and human health. SOA is a large fraction of OA and is a complex mixture of organic molecules resulting from the oxidation of biogenic and anthropogenic organic compounds. This dissertation presents work on the analysis of the chemical composition of the oligomeric fraction of SOA in the fine mode of ambient aerosols. The samples investigated in this dissertation were collected during CalNex 2010 and were analyzed using nano-DESI and high resolution mass spectrometry. Four six-hour samples, starting at midnight, were collected per day allowing for the analysis of changes in the composition throughout the day. The sample time resolution allowed insights to be made into the chemical transformations and sources for these oligomeric compounds. Size resolved samples were also analyzed to determine how the composition of this fraction of SOA varied with aerosol size. Finally, comparisons with chamber study samples were made to provide information on the types of sources and the source strengths in the ambient environments.

In Chapter 2, the chemical compositions of eight samples collected over two days in Bakersfield and measured with positive mode nano-DESI were investigated. There were three groups of compounds identified: compounds containing no nitrogen atoms and compounds containing one and two nitrogen atoms (0N, 1N, and 2N respectively). The compounds containing no nitrogen atoms had higher numbers of compounds and higher relative intensities in the afternoon samples. This correlated with the highest levels of ozone and sunlight, indicating that photochemistry and/or ozonolysis were likely producing these compounds. The nitrogen containing compounds (1N and 2N) had higher numbers and relative intensities in the night samples. A large fraction of these compounds likely contain reduced nitrogen groups such as amines or imines which are more easily ionized with positive mode ESI. Additionally, these compounds had lower O/C values than the majority of the nitrogen containing compounds measured in the negative mode which are more likely to be oxidized organic nitrogen compounds. Over 50% of the 1N and 2N compounds had precursor-product pairs that matched imine formation reactions involving ammonia and carbonyl groups in the precursors. Thus, photochemistry/ozonolysis during the day and heterogeneous reactions with ammonia at night likely played important roles in the formation of the oligomeric fraction that was measured with positive mode ESI in Bakersfield.

In Chapter 3, the chemical composition of four consecutive days worth of samples collected in Bakersfield measured with negative mode nano-DESI were investigated. Four groups of samples were identified: compounds containing only carbon hydrogen and oxygen (CHO), compounds containing sulfur (CHOS), compounds containing nitrogen (CHON) and compounds containing both nitrogen and sulfur (CHONS). Based on the elemental compositions and the O/S and O/N ratios necessary for sulfate and nitrate groups, the majority of these compounds were likely to be organosulfates, organonitrates, and nitroxy organosulfates. The number of compounds in each time period (e.g., midnight-6am) was averaged over the four days. There were more CHO compounds in the afternoon, consistent with results from the positive mode. The CHOS had the smallest average differences throughout the day, suggesting a more

remote source for the majority of the compounds. The source(s) could be either terrestrial or marine or both and more work is necessary to determine where and how these compounds formed. In addition, there were more CHON and CHONS compounds at night, consistent with a large nitrate radical source for the organonitrates. A fraction of the CHOS and CHONS compounds had molecular formulas that matched biogenically derived organosulfates and nitroxy organosulfates that were measured at the same site using other methods. These results indicate the presence of both biogenic and anthropogenic sources for these aerosols. Size resolved samples for the bottom four stages of the MOUDI were also analyzed. The number of CHO compounds decreased gradually with increasing aerosol size, and the CHO, CHOS, and CHONS compounds were all primarily found in aerosol sizes below 1.0 μm. The CHON compounds had a bimodal size distribution, and a large fraction of the compounds in the second mode had elemental ratios consistent with aromatic compounds.

In Chapter 4, the chemical composition of an entire days worth of samples (four six hour samples) collected in Bakersfield and in Los Angeles were compared with chamber studies under high $NO_x$ conditions using diesel fuel and isoprene as precursors. Diesel and isoprene were chosen to represent anthropogenic and biogenic sources thought to be major SOA precursors. The overlap in the chemical composition was used to indicate to what extent the chamber samples matched what was found in the ambient samples. For all of the ambient samples, the diesel overlap was higher than for isoprene. The overlaps with the chamber studies were higher for Bakersfield than for LA samples. These results indicate that diesel was likely a larger source for these oligomeric compounds than isoprene and that LA likely was dominated by either different sources or different chemistry/formation reactions than what was observed in the chambers and in Bakersfield. In Bakersfield the diesel could be from both on-road and off-road vehicles while in LA the majority of the diesel should be due to on road vehicles. This difference could be another cause for the differences in overlap with the chamber diesel between Bakersfield and LA. Comparing the two sets of ambient samples from Bakersfield and LA, the Bakersfield sample was more oxidized, had significantly more compounds, and more nitrogen containing compounds. The higher nitrogen content was consistent with FTIR results, from the Russell group at UCSD, showing more organonitrates in Bakersfield. Also, the ammonia concentrations were higher in Bakersfield which could cause increased formation of reduced nitrogen compounds. Major sources for ammonia near Bakersfield include agriculture and animal husbandry operations. The role of ammonia in Bakersfield is supported by the result that the addition of ammonia to a chamber study with diesel was necessary to form many of the 2N compounds observed in Bakersfield. The overlaps observed are consistent with both diesel and isoprene being important sources for SOA in Bakersfield and in LA; however, the lack of complete overlap indicated that additional sources were likely present at both sites.

This dissertation has demonstrated the capabilities of nano-DESI, a direct surface sampling soft ionization technique, coupled to a high resolution mass spectrometer, to investigate the chemical composition of the oligomeric fraction of SOA. Analysis with nano-DESI can be more sensitive than analysis via solvent extraction. This increased sensitivity has enabled the analysis of samples with six hour time resolution compared to the usual day to week long integrated sampling times. Future work in this area should focus on answering three main questions: (1) What is the composition of ambient samples in different locations/environments? (2) What are the sources for these compounds? (3) What impacts do these compounds have on the physical properties of aerosol samples?

To make progress on the first question, more studies of the chemical composition of the oligomeric fraction of the aerosol in different ambient environments are needed. So far, only a few studies on the east coast (including NY and VA) and a few in California have been conducted. Expanding the range of environments and conditions is necessary to characterize the full range of compounds that form in the atmosphere. In this dissertation, samples from Bakersfield and Los Angeles were analyzed. Both of these sites have strong anthropogenic sources mixed with biogenic sources. Future ambient studies should examine environments with different types of sources (e.g., terpenes vs. isoprene) and environmental conditions (e.g., high and low NOx). The type of solvent used for extraction can affect the types of compounds observed. In this dissertation acetonitrile was used as the nano-DESI solvent because previous work by the Laskin group showed that acetonitrile as a solvent made it possible to extract and ionize a large number of compounds. Future work with other solvents such as water, methanol, toluene, etc. may allow additional compounds to be measured that are not ionized well with acetonitrile.

This dissertation presents, for the first time, analysis of the chemical composition of four consecutive samples per day. Thus, analysis of aerosol samples at other locations with this time resolution will also be novel. The time resolution used in this study was possible, however, because both Bakersfield and LA had relatively high OA loadings which may not be the case in other locations. The sampling was done with a MOUDI, which uses 30 SLM flow rates and so aerosol samplers with higher flow rates (such as high volume filters) may resolve this latter issue, although information on the composition as a function of size would then be lost. Another possibility would be to include an aerosol preconcentrator upstream of the sampler. A preconcentrator may increase the volume of atmosphere sampled (perhaps by an order of magnitude or more!) while keeping the flow rates low enough for size-resolved sampling. With improvements in this area, it may also be possible to increase the time resolution further, which could be useful in a study with very dynamic conditions, such as downwind of a forest fire.

The analysis of samples from new locations with high time resolution could greatly increase our understanding of the formation pathways and the types of compounds formed. Additionally, studies looking at the composition throughout the year are also necessary because the sources and environmental conditions can be very different in the summer vs. the winter, for example. A study analyzing samples taken periodically throughout the year at one site could be used to answer questions about the impacts of different sources and environmental conditions (e.g., humidity levels, ozone levels, etc.). Additionally, it has been shown that there are changes in the level of emissions of anthropogenic sources such as diesel throughout the week. Research that looks at the composition of the oligomeric fraction as a function of the day of the week could provide additional insight into the role of different source concentrations and different atmospheric conditions (e.g., $NO_x$ and ozone levels) on the formation of the oligomeric fraction of SOA. In brief, there are very few data sets of the type presented in this dissertation and more are greatly needed to answer the question of what types of compounds are found in ambient samples.

The second question regarding the sources of these compounds is an important issue to resolve because the nature of sources will ultimately affect climate model predictions and development of control strategies. In smog chambers, controlled experiments on potential sources for these oligomeric compounds can be done. Experiments with these chambers have shown that many different VOC's can form these high-MW compounds under many different conditions (e.g. high/low NOx, acidic seeds vs. no seeds, etc.). These studies have also

elucidated many of the different types of heterogeneous and particle phase reactions that can form the compounds. What we cannot currently do is exclusively link compounds observed in laboratory samples to compounds observed in the ambient atmosphere. In other words, we have no marker compounds for different sources for these types of compounds. A marker type of analysis may never be possible due to the huge complexity of the types of compounds that can form and the multitude of different reaction pathways. In Chapter 4, an analysis was presented that examines the overlap between ambient samples and chamber samples formed with expected VOC precursors. This analysis covered diesel fuel and isoprene, but there are many different potential sources and studies expanding this analysis to VOC's from terpenes and gasoline, for example, would be valuable next steps.

Additionally, the smog chamber experiments used here looked at formation from isoprene alone; no other VOC's were introduced. However, the atmosphere is not a single component system, so chamber experiments employing different mixtures of VOC's could more closely approximate ambient samples. This may be especially important when analyzing the composition of the oligomers since the monomer units of an oligomer could be formed from many different VOC precursors. For the chamber experiments with diesel, raw diesel fuel, a complex mixture of compounds, was injected into the chamber and future work to determine which specific compounds had the most impact on the formation of these oligomers would be useful for control strategies. Furthermore, work to look at the differences between raw diesel vs. burned diesel, by sampling of the end of a tail pipe for example, is another area to expand chamber studies of the sources. The VOC's found in fugitive emissions vs. tail pipe emissions can vary, which may have an effect on the types and amount of aerosols that are formed.

The research in this dissertation was done using ESI with no prior separation of the samples. ESI is not uniformly efficient in charging molecules, which can make it a non-quantitative technique. Different VOC precursors may produce different amounts of either a compound or a class of compounds. The quantification of the compounds could thus be used as an additional degree of comparison between samples that could also give further insight into sources. If marker compounds or classes/types of compounds are found for a given source, quantification could also be used to estimate source strengths. Currently, the best technique of quantification for these compounds is separation with liquid chromatography (LC) and then calibration of the concentration with a compound of similar structure. A good way to utilize this technique would be a research campaign that includes two (or more) collectors in parallel, followed by analysis using nano-DESI on one sample and LC/ESI/MS on the other sample. This would combine the characterization of the full mass range that is available via nano-DESI with the compound structure identification and quantification available via LC/MS.

The final question that future work should address concerns tying research already underway on the physical properties of aerosols (hygroscopicity, CCN activity, etc.) with the chemical composition of the oligomeric fraction of the aerosols. This work is important because many of these high-MW oligomeric compounds have high O/C values, which make them more water soluble, and, as they form, can change the CCN activity of the aerosols. Additionally, some of the compounds are likely chromophores which, when formed, can change the radiative absorption properties of the aerosol. Future work combining an analysis of the changing physical properties with a simultaneous analysis of the chemical composition could advance our understanding of the relationships between the two (physical and chemical) properties. The nano-DESI analysis presented here would be particularly useful for this type of work because of the small sample sizes necessary and the avoidance of potential modifications introduced during

a solvent extraction. The data sets presented in this dissertation show the utility of this type of analysis both for expanding the range of ambient environments studied and for analyzing possible sources and formation mechanisms. Future work in this area, as outlined above, could enhance our understanding of the compositions, the sources, and the physical properties of ambient aerosols.

# Appendix A: Supplemental Information for Chapter 2

## Appendix A1
## Additional information on the field site, meteorology, and sampling

### Field collected samples

The 2010 CalNex campaign had ground sites in Los Angeles and Bakersfield, CA, as well as aerial and ship-based measurements (NOAA, 2008). The samples discussed in this paper were collected at the Bakersfield site along with a suite of other measurements including meteorological data, aerosol mass spectrometry (AMS), and ion chromatography. The ion chromatography data discussed was not reported over June 22$^{nd}$ and 23$^{rd}$. It was reported from 5/21/2010 to 6/20/2010 and thus an average diurnal pattern is compared. The Bakersfield field site was located at the Kern County Cooperative Extension property in the southeastern part of the city. Bakersfield is located (35.35°N, 118.97°W ) in the southern end of the San Joaquin Valley (SJV), which is bordered by the Sierra Nevada Mountains on the east, the Tehachapi Mountains to the south, and the Coastal Ranges to the west.

The days of June 22 and 23 were selected for the in-depth molecular characterization of OA samples based on the real-time measurements by AMS and Thermal Desorption Aerosol GC/MS (TAG) instruments that showed high ambient concentrations of SOA during that time. The trends in the meteorological data for these two days are typical of the trends seen throughout the campaign. The following meteorological parameters were measured: Wind speed and direction with an R.M. Young 5103 wind monitor; RH and temperature with a Vaisala HMP-45 RH/T sensor with radiation shield; $O_3$ with a Dasibi 1008-PC ozone analyzer. The local wind direction was primarily from the northwest during the daytime and from the south or east during the night due to downslope flows from the surrounding mountains.

All meteorological data reported here are averaged over six hours to coincide with the length of the sample collection and times are given in local time (PDT). Appendix A2 shows relative humidity (RH) and ozone records from the sampling site on June 22$^{nd}$ and 23$^{rd}$. The maximum average wind speed was ~3 m/s occurring between noon and 6 pm on both days and the minimum was between 1-2 m/s from midnight to noon. The maximum average temperature occurred from noon to 6 pm and was ~33°C on June 22$^{nd}$ and ~36°C on June 23$^{rd}$. This corresponded to minimum relative humidity of 18-19% and maximum ozone concentrations of 73 ppb on June 22$^{nd}$ and 85 ppb on June 23$^{rd}$ (Appendix A2c and A1c'). The minimum average temperature occurred from midnight to 6 am and was ~18°C on June 22$^{nd}$ and ~21°C on June 23$^{rd}$ corresponding to maximum relative humidity of 43% and 52% and minimums in ozone of 8 ppb and 17 ppb respectively. Within the six hours from midnight to 6 am, the relative humidity never exceeded 70%, indicating that conditions were relatively dry.

Samples were collected on aluminum foils using a Micro-Orifice Uniform Deposit Impactor (MOUDI) model 100R (MSP, Inc.) without rotation. The sampling inlet was located approximately five meters above the ground attached to the top of an air conditioned trailer housing the MOUDI. A PM 2.5 cyclone was placed upstream of the MOUDI. Samples were collected at 31 L/min for 5 hours and 50 minutes per sample for a total sample volume of 10.9 $m^3$. Samples were stored in a -20 ºC freezer at the site and a -80 ºC freezer at the lab pending

analysis. Samples on the eighth stage of the MOUDI, (size range of 0.32 -0.18 μm), had the highest loadings of the compounds of interest so samples from this stage were chosen for intensive study.

Organic mass and O/C for nonrefractory submicron particles ($PM_1$) were quantified using a high-resolution time-of-flight aerosol mass spectrometer (HR-ToF-AMS, Aerodyne, Billerica, MA) (DeCarlo et al., 2006). The high signal-to-noise ratio V mode measurements were used for quantification. A collection efficiency of 0.8 was applied to each of the 5-min ensemble mass and size-resolved measurements throughout the study (Ahlm et al., 2012). Size-resolved O/C was evaluated by organic mass fraction of m/z 44 ($f_{44}$), as $f_{44}$ correlated to O/C with an r of 0.93 during June 22-23. Such high correlation of $f_{44}$ and O/C was frequently observed in ambient measurements and was suggested for O/C estimation when only unit mass measurements are available (Aiken et al., 2008). That $f_{44}$ did not change with size suggested that O/C was independent of particle size. Size-resolved O/C was also evaluated from size distributions of the 27 fragments with largest mass, which accounted for 80% of the total oxygen and carbon in $PM_1$. The ratios of these mass fragments also showed no size dependence, supporting the conclusion that O/C was independent of particle size. Therefore, the measured $PM_1$ O/C was used to represent the O/C in the 0.18-0.32μm fraction for this study.

**Data Acquisition/ Analysis**

Kendrick analysis renormalizes experimental *m/z* values to the nominal mass of a chemical group selected as the basis (e.g., O, $C_3H_4O_2$, $CH_2$ etc.). The Kendrick mass ($KM_{basis}$) specific to the selected basis is calculated by re-normalizing the IUPAC mass scale to the exact mass of the basis group (i.e. O – 15.9949 Da, $C_3H_4O_2$ – 72.02113 Da, $CH_2$ – 14.01565 Da). For instance, values of $KM_{C3H4O2}$ are calculated using the following equation:

$$KM_{C3H4O2} = \text{experimental mass} \times (72/72.02113) \quad (1)$$

The Kendrick mass defect ($KMD_{C3H4O2}$) is then defined as the difference between nominal mass (NM) and $KM_{C3H4O2}$, whereas NM is the nearest integer of $KM_{C3H4O2}$:

$$KMD_{C3H4O2} = NM - KM_{C3H4O2} \quad (2)$$

Homologous compounds differing only by the number of base units have identical KMD values. The second-order Kendrick transformation renormalizes the KMD values to the mass defect of a second base. Compounds that differ only by the two bases ($CH_2$ and $H_2$ were used here), have equivalent values of $KMD^2_{CH2,H2}$ and can be grouped into larger two-dimensional homologous sets (Roach et al., 2011). Once one member of a homologous series or a set has been identified, the rest of the homologous species are immediately identified.

Both high mass resolution and high mass accuracy are necessary to resolve and identify molecules in complex mixtures such as aerosol, dissolve organic matter (DOM), and petroleum samples (Marshall et al., 2006; Schmitt-Kopplin et al., 2010). High accuracy enables the determination of the elemental composition based on the exact mass while high resolution enables separation of closely-spaced peaks. Marshall and co-workers (2006) have demonstrated that ~0.1-0.5 mDa mass accuracy provides unique elemental composition for typical organic compounds up to 500 Da (and higher when combined with Kendrick analysis). Schmitt-Kopplin and co-workers (2010) showed that resolution of ~150,000 is necessary to resolve closely spaced CHO and CHOS peaks at ~400 Da. Compared to that study, we used relatively low resolving power of 60,000 at m/z 412. However we can still confidently identify peaks over a broad mass range based on the accurate mass measurement. The second-order mass defect transformation

introduced recently by Roach et al. (2011) and used in this study enables more efficient grouping and identification of higher-mass peaks as compared to the traditionally used Kendrick analysis. The efficient grouping facilitates identification of higher-mass peaks within each group that cannot be unambiguously identified using Kendrick analysis. The presence of overlapping, unresolved peaks can affect mass accuracy if the peaks are of similar abundance. For example, an unresolved CHO/CHOS doublet (e.g. $C_{16}H_{28}O_{10}S$ vs.$C_{19}H_{24}O_{10}$) with equivalent abundances would result in an error of ~1.7 mDa for either peak assignment. In contrast, when the relative abundance of one of the peaks in the unresolved doublet is low, the measured mass is very close to the exact mass of the more abundant peak. The mass accuracy for the majority of our assignments is within ±0.3 mDa. Even though we do not necessarily resolve all of the peaks in the spectrum, the assignments are accurate as indicated by the absolute error.

**References**


Ahlm, L., et al. (2012), Formation and growth of ultrafine particles from secondary sources in Bakersfield, California, *J. Geophys. Res.-Atmos.*, *117*, D00V08 DOI: 10.1029/2011JD017144.

Aiken, A. C., et al. (2008), O/C and OM/OC ratios of primary, secondary, and ambient organic aerosols with high-resolution time-of-flight aerosol mass spectrometry, *Environ. Sci. Technol.*, *42*(12), 4478-4485.

DeCarlo, P. F., et al. (2006), Field-deployable, high-resolution, time-of-flight aerosol mass spectrometer, *Anal. Chem.*, *78*(24), 8281-8289.

Marshall, A. G., K. Sunghwan and R. P. Rodgers (2006), Truly "exact" mass: Elemental composition can be determined uniquely from molecular mass measurement at ~0.1mDa accuracy for molecules up to ~500Da, *Int. J. Mass Spectrom. (Netherlands)*, *251*(2-3), 260-265265.

NOAA: National Oceanic and Atmospheric Administration (2008), 2010 CalNex White Paper: Research at the Nexus of Air Quality and Climate Change, *Available at* http://www.esrl.noaa.gov/csd/projects/calnex/whitepaper.pdf

Roach, P. J., J. Laskin and A. Laskin (2011), Higher-order mass defect analysis for mass spectra of complex organic mixtures, *Anal. Chem.*, *83*(12), 4924-4929.

Schmitt-Kopplin, P., et al. (2010), Analysis of the unresolved organic fraction in atmospheric aerosols with ultrahigh-resolution mass spectrometry and nuclear magnetic resonance spectroscopy: Organosulfates as photochemical smog constituents, *Anal. Chem.*, *82*(19), 8017-8026.

# Appendix A2
# Relative Humidity and Ozone

Relative humidity (purple) and ozone (green) for the sampling period in local time (PDT). The highest ozone levels were in the afternoon (c and c') and highest relative humidity was in the early morning (a and a'). The values discussed in the text are averaged over six hours to coincide with the length of time for the sample collection.

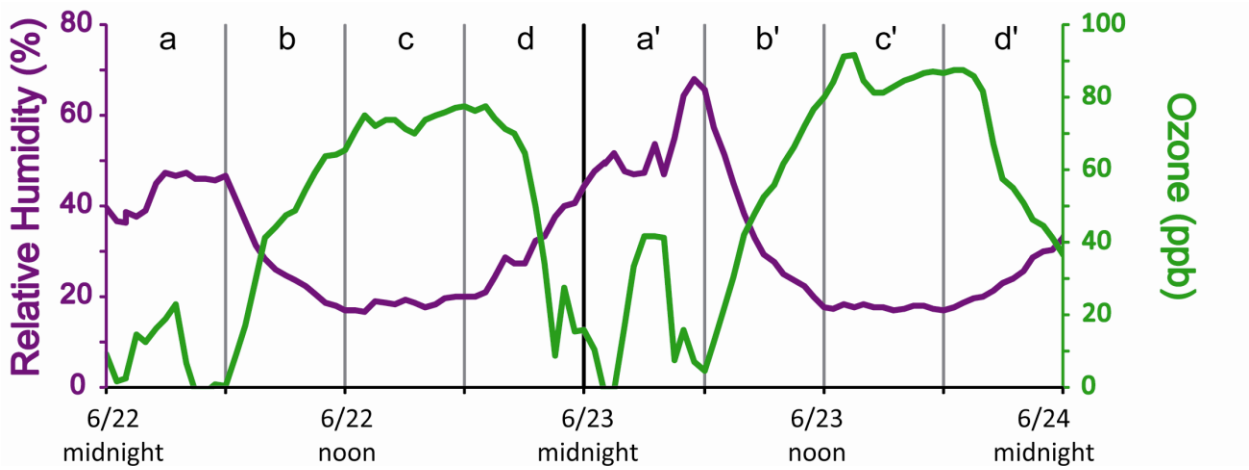

# Appendix A3
# Mass spectra for samples collected on June 22nd

Mass spectra of the identified peaks in each of the four samples collected on June 22nd. The pie charts show the percentage of compounds by number that fall in each group. The starred peak in (b), at 99.105 Da has relative intensity of 460 on this scale.

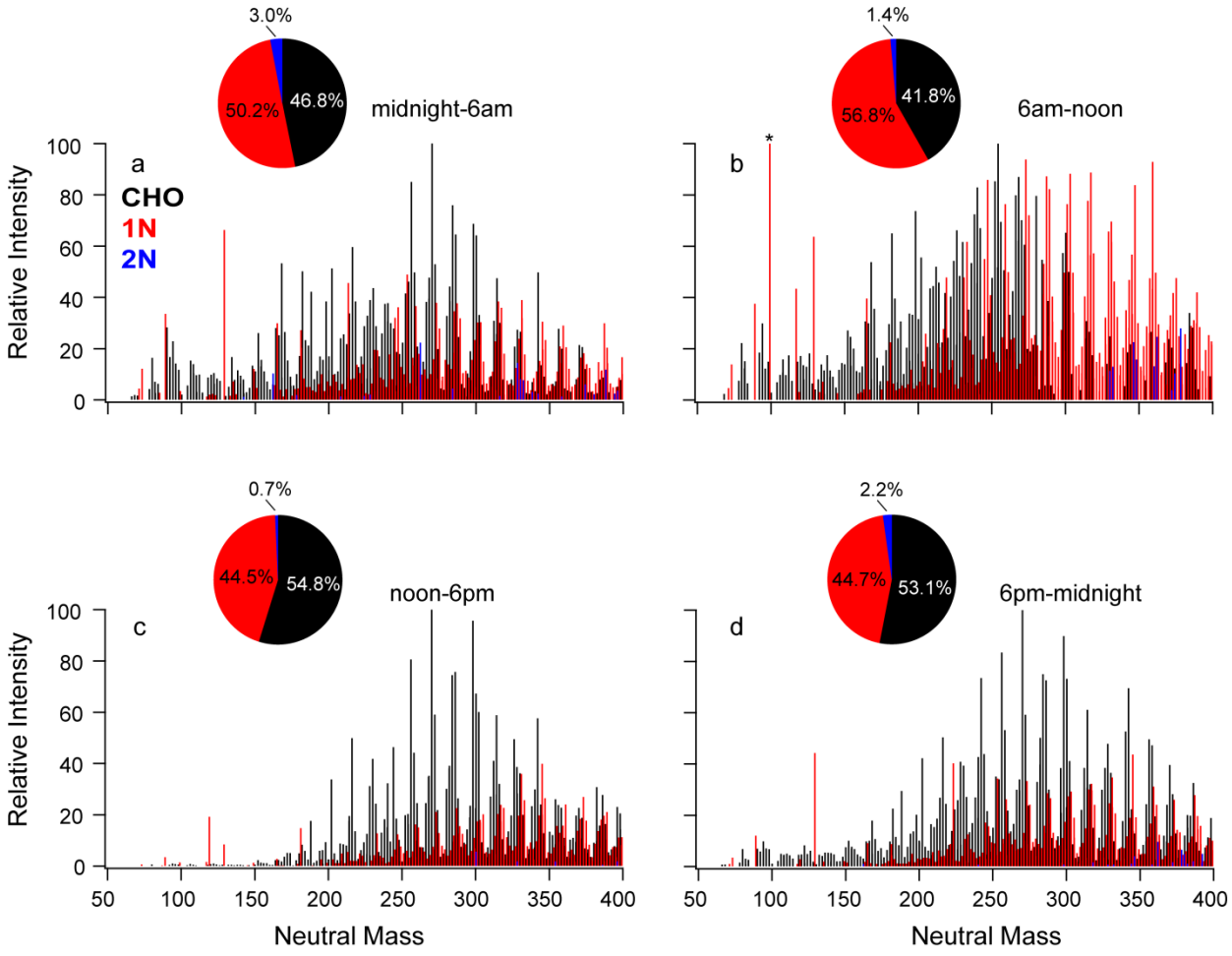

# Appendix A4
# Van Krevelen diagrams for samples collected on June 23rd

Van Krevelen diagrams for the four samples collected on June 23rd. (a) midnight-6am, (b) 6am-noon, (c) noon-6pm, (d) 6pm-midnight. The H/C versus the O/C values for each identified compound are shown broken down by the number of nitrogen atoms in the chemical formula. Black markers are 0N and red and blue correspond to compounds with one and two nitrogen atoms respectively. The green diamond corresponds to AMS data averaged over the same sample time.

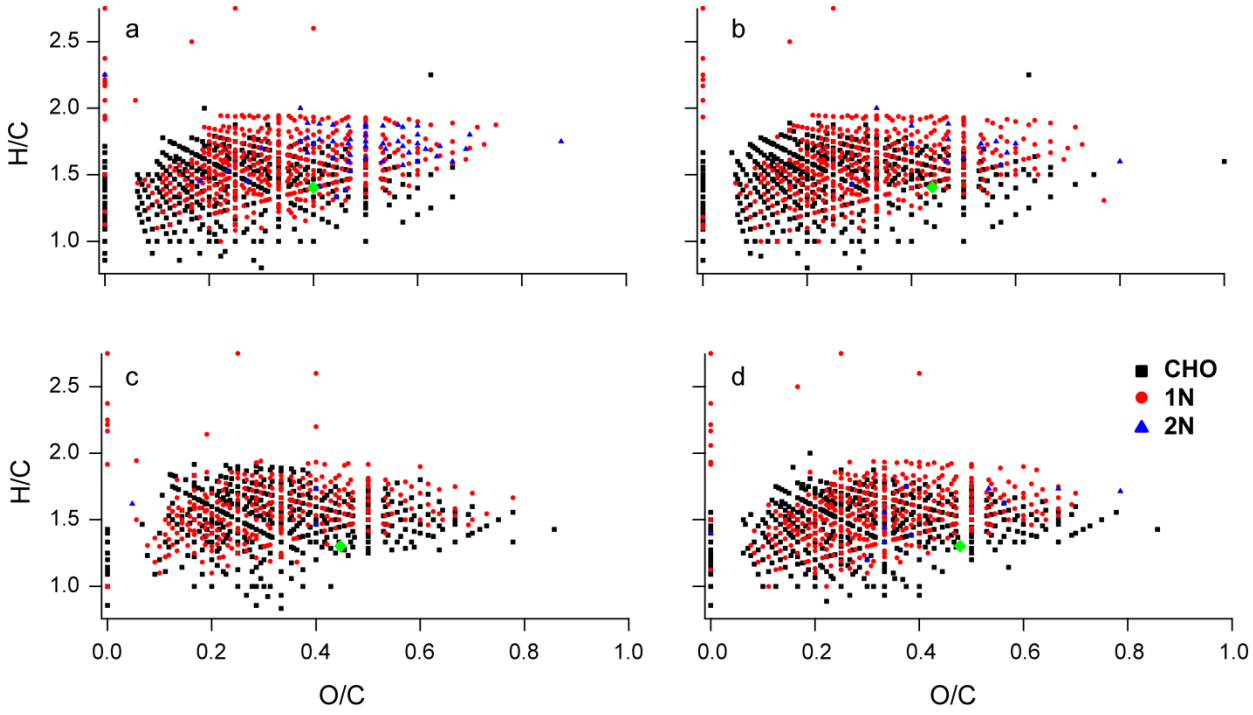

# Appendix A5
# Van Krevelen comparison of $NOC^+$ and $NOC^-$

Van Krevelen diagram for NOC from the sample collected on June 23rd. (a) midnight-6am, (b) 6am-noon, (c) noon-6pm, (d) 6pm-midnight. Blue markers are compounds measured in both negative and positive mode, and red and black are compounds measured in only the positive and negative mode respectively.

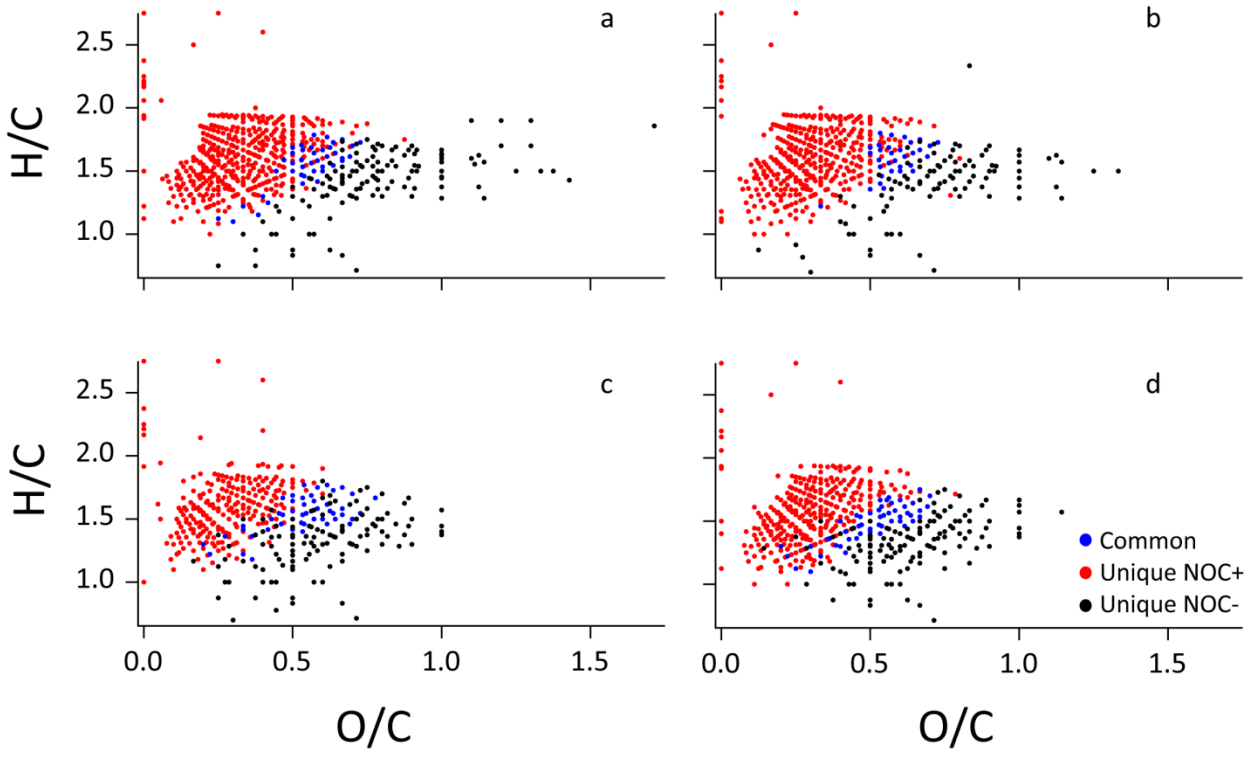

# Appendix A6
# Sulfur and 3N containing compounds

Compounds identified with one sulfur atom or three nitrogen atoms on June 23rd. The samples in which they were observed and their relative intensities in that sample are also given.

| Neutral Mass | Molecular formula | Relative Intensity (%) | Sample observed |
|---|---|---|---|
| 120.0721 | $C_4H_{12}N_2S$ | 6.3 | 6pm-midnight |
| 135.0796 | $C_7H_9N_3$ | 1.6 | Noon-6pm |
| 166.0412 | $C_4H_{10}N_2O_3S$ | 2.1 | Midnight-6am |
| 203.1059 | $C_{11}H_{13}N_3O$ | 1.2 | Noonn-6pm |
| 222.1038 | $C_8H_{18}N_2O_3S$ | 4.0 | Midnight-6am |
| 301.1579 | $C_{20}H_{19}N_3$ | 14.8 | 6pm-midnight |
| 327.1735 | $C_{22}H_{21}N_3$ | 9.2 | 6pm-midnight |

# Appendix A7
# Compounds that fail the tests for ammonium adducts

Compounds that disappear with 30V CID and fail all three tests for possible ammonium adducts listed in the text. (a) 6/23/2010 midnight-6am, (b) 6/23/2010 6am-noon, (c) 6/23/2010 noon-6pm, (d) 6/23/2010 6pm- midnight.

| Chemical formula | Exact mass | Relative intensity | Sample |
|---|---|---|---|
| $C_{10}H_{20}N_1O_6^+$ | 250.1285 | 0.2245, 0.0765 | a, d |
| $C_{12}H_{22}N_1O_6^+$ | 276.1442 | 0.5080, 0.2995 | a, d |
| $C_{15}H_{30}N_1O_6^+$ | 320.2068 | 0.2716, 0.0553 | b, d |
| $C_{15}H_{27}N_2O_6^+$ | 331.1864 | 0.1829, 0.1035 | a, b |
| $C_{18}H_{32}N_1O_5^+$ | 342.2275 | 0.2767, 0.0893 | b, d |
| $C_{19}H_{34}N_1O_7^+$ | 388.233 | 0.3127, 0.1269 | b, d |
| $C_{22}H_{40}N_1O_5^+$ | 398.2901 | 0.0893, 0.2017 | a, b |
| $C_{10}H_{13}N_2O_3^+$ | 209.0921 | 0.06420 | d |
| $C_8H_{15}N_2O_7^+$ | 251.0874 | 0.08899 | a |
| $C_{10}H_{19}N_2O_6^+$ | 263.1238 | 0.33446 | a |
| $C_{18}H_{36}N_1O_1^+$ | 282.2791 | 0.05990 | c |
| $C_{14}H_{25}N_2O_7^+$ | 333.1656 | 0.10537 | a |
| $C_{15}H_{29}N_2O_6^+$ | 333.202 | 0.18552 | b |
| $C_{13}H_{23}N_2O_8^+$ | 335.1449 | 0.06362 | a |
| $C_{14}H_{27}N_2O_7^+$ | 335.1813 | 0.19479 | a |
| $C_{15}H_{27}N_2O_7^+$ | 347.1813 | 0.17974 | a |
| $C_{15}H_{29}N_2O_7^+$ | 349.1969 | 0.21559 | a |
| $C_{16}H_{33}N_2O_6^+$ | 349.2333 | 0.09493 | a |
| $C_{16}H_{27}N_2O_7^+$ | 359.1813 | 0.08068 | a |
| $C_{15}H_{25}N_2O_8^+$ | 361.1605 | 0.07247 | a |
| $C_{16}H_{29}N_2O_7^+$ | 361.1969 | 0.09556 | a |
| $C_{16}H_{31}N_2O_7^+$ | 363.2126 | 0.18632 | a |
| $C_{17}H_{31}N_2O_7^+$ | 375.2126 | 0.12773 | a |
| $C_{15}H_{25}N_2O_9^+$ | 377.1554 | 0.05784 | a |
| $C_{16}H_{29}N_2O_8^+$ | 377.1918 | 0.16071 | a |
| $C_{17}H_{33}N_2O_7^+$ | 377.2282 | 0.07709 | a |
| $C_{15}H_{29}N_2O_9^+$ | 381.1867 | 0.16578 | a |
| $C_{18}H_{31}N_2O_7^+$ | 387.2126 | 0.05147 | a |
| $C_{18}H_{33}N_2O_7^+$ | 389.2282 | 0.05512 | a |
| $C_{18}H_{35}N_2O_7^+$ | 391.2439 | 0.06413 | a |
| $C_{15}H_{27}N_2O_{10}^+$ | 395.166 | 0.14823 | d |
| $C_{16}H_{31}N_2O_9^+$ | 395.2024 | 0.11287 | a |

# Appendix A8
# Average elemental ratios

**Table S3**. Ensemble average, intensity weighted elemental ratios for the positive and negative mode nano-DESI analysis of the eight samples collected on June 22nd and 23rd with the average O/C, H/C, and N/C values from AMS over the same time periods.

| | Positive mode (n-DESI) | | | Negative mode (n-DESI) | | | AMS | | |
|---|---|---|---|---|---|---|---|---|---|
| **Sample** | **H/C** | **O/C** | **N/C** | **H/C** | **O/C** | **N/C** | **H/C** | **O/C** | **N/C** |
| **6/22 midnight-6am** | 1.6 | 0.34 | 0.033 | 1.5 | 0.69 | 0.010 | 1.5 | 0.28 | 0.0031 |
| **6/22 6am-noon** | 1.6 | 0.34 | 0.043 | 1.6 | 0.74 | 0.017 | 1.4 | 0.40 | 0.0042 |
| **6/22 noon-6pm** | 1.6 | 0.35 | 0.021 | 1.5 | 0.56 | 0.0057 | 1.4 | 0.43 | 0.0041 |
| **6/22 6pm-midnight** | 1.6 | 0.35 | 0.024 | 1.5 | 0.55 | 0.0070 | 1.3 | 0.44 | 0.0046 |
| **6/23 midnight-6am** | 1.6 | 0.33 | 0.041 | 1.5 | 0.71 | 0.036 | 1.4 | 0.40 | 0.0041 |
| **6/23 6am-noon** | 1.6 | 0.33 | 0.029 | 1.5 | 0.70 | 0.018 | 1.4 | 0.44 | 0.0042 |
| **6/23 noon-6pm** | 1.6 | 0.36 | 0.012 | 1.5 | 0.57 | 0.0041 | 1.3 | 0.45 | 0.0041 |
| **6/23 6pm-midnight** | 1.6 | 0.37 | 0.023 | 1.5 | 0.60 | 0.0053 | 1.3 | 0.48 | 0.0061 |

# Appendix B: Supplemental Information for Chapter 3

## Appendix B1
## Additional information on the field site, analysis, and MS/MS

### Field collected samples

The samples discussed in this paper were collected at the CalNex Bakersfield site along with a suite of other measurements including meteorological data, aerosol mass spectrometry (AMS), and filter analysis using liquid chromatography mass spectrometry (LC-MS). The Bakersfield field site was located in the southeastern part of the city at the Kern County Cooperative Extension property. Bakersfield is located (35.35°N, 118.97°W ) in the southern end of the San Joaquin Valley (SJV), which is bordered by the Sierra Nevada Mountains on the east, the Tehachapi Mountains to the south, and the Coastal Ranges to the west.

The days of June 20$^{th}$ through 24$^{th}$ were selected for the in-depth molecular characterization of OA samples based on the concurrent real-time measurements by other researchers using an Aerosol Mass Spectrometer (AMS) and a Thermal Desorption Aerosol GC/MS (TAG) instrument that showed high ambient concentrations of SOA during that time. The trends in the meteorological data for these two days are typical of the trends seen throughout the campaign. The following meteorological parameters were measured: Wind speed and direction with an R.M. Young 5103 wind monitor; RH and temperature with a Vaisala HMP-45 RH/T sensor with radiation shield; $O_3$ with a Dasibi 1008-PC ozone analyzer. Appendix B2 shows meteorology data from the sampling site on June 20$^{th}$ through the 24$^{th}$. Samples were collected on aluminum foils using a Micro-Orifice Uniform Deposit Impactor (MOUDI) model 100R (MSP, Inc.) without rotation. The sampling inlet was attached to the top of an air conditioned trailer housing the MOUDI located approximately five meters above the ground. A PM 2.5 cyclone was placed upstream of the MOUDI. Samples were collected at 31 L/min for 5 hours and 50 minutes per sample for a total sample volume of 10.9 m$^3$. Samples were stored in a -20 ºC freezer at the site and a -80 ºC freezer at the lab pending analysis.

Organic mass and O/C for nonrefractory submicron particles ($PM_1$) were quantified using a high-resolution time-of-flight aerosol mass spectrometer (HR-ToF-AMS, Aerodyne, Billerica, MA) (DeCarlo et al., 2006). The high signal-to-noise ratio V mode measurements were used for quantification. A collection efficiency of 0.8 was applied to each of the 5-min ensemble mass and size-resolved measurements throughout the study (Ahlm et al., 2012). Size-resolved O/C was evaluated by organic mass fraction of *m/z* 44 ($f_{44}$); for samples collected on June 22$^{nd}$ and 23$^{rd}$ the $f_{44}$ correlated to O/C with an r of 0.93. Such high correlation of $f_{44}$ and O/C was frequently observed in ambient measurements and was suggested for O/C estimation when only unit mass measurements are available (Aiken et al., 2008). On June 23$^{rd}$, $f_{44}$ did not change with size suggesting that O/C was independent of particle size. Size-resolved O/C was also evaluated from size distributions of the 27 fragments with largest mass, which accounted for 80% of the total oxygen and carbon in $PM_1$. The ratios of these mass fragments also showed no size dependence, supporting the conclusion that O/C was independent of particle size. Therefore, the measured $PM_1$ O/C was used to represent the O/C for this study.

A high volume filter sampler operating at 226 L/min with a $PM_{2.5}$ cyclone was used to collect aerosol samples. The samples were stored in a freezer at -18°C until analysis. Field

blanks were collected weekly by placing prebaked quartz fiber filters into the samplers for 15 min. and then removing them and storing them in the same manner as the field samples. Extraction was performed using methanol and ultrasonication for 45 min. The extracts were cleaned by passing them through a 25 mm Acrodisc syringe filter with a 0.2 μm PTFE membrane (Pall Life Sciences). Extracts were dried under a gentle $N_2$ gas stream at ambient temperature and then reconstituted with 250 mL of a 1:1 (v/v) solvent mixture of 0.1% acetic acid in water (LC-MS Chromasolv grade, Sigma-Aldrich) and 0.1% acetic acid in methanol (LC-MS Chromasolv grade, Sigma-Aldrich). Samples were shaken and sonicated for 5 min and stored at -20°C until chemical analysis. The field and lab blanks were treated similarly and none of the compounds discussed here were observed in the blanks.

A mass range of 63-1000 *m/z* was collected and chromatographic separations were carried out using a Waters Acquity UPLC HSS (high-strength silica) column (2.1 x 100 mm, 1.8 μm particle size) at 45°C. The mobile phases consisted of eluent (A) 0.1% acetic acid in water (LC-MS Chromasolv grade, Sigma-Aldrich) and eluent (B) 0.1% acetic acid in methanol (LC-MS Chromasolv grade, Sigma-Aldrich). Calibration was conducted throughout with a constant infusion into the ESI source of a reference mixture consisting of purine (*m/z* 119.044), leucine-enkephalin (*m/z* 554.269), and HP-0921 acetate adduct (*m/z* 980.016) (Agilent Technologies) covering the entire mass range of compounds considered. Mass resolution was maintained at ~9000 m/Δm, which allows for accurate mass measurements and subsequent elemental compositions of observed ions to be determined. None of the organosulfates detected in the $PM_{2.5}$ samples have commercially available standards for quantification. As a result, calibration curves of propyl sulfate (City Chemical, 98% purity), octyl sulfate (Sigma, 99% purity), and decyl sulfate (Fluka, 99% purity) were generated for use as surrogate standards. Extraction efficiency as determined by analyzing blank filters spiked with the surrogate standards ranged from 73-76% and a constant correction factor of 75% was applied. Corrections for the quantity of filter extracted were made, and all concentrations and abundances reported are for the entire 86-$cm^2$ quartz filter.

**Data Analysis**

Both high mass accuracy and high mass resolution are necessary in order to resolve and identify elemental compositions in complex mixtures such as aerosol, petroleum, and dissolved organic matter (DOM) samples (Marshall et al., 2006; Reemtsma et al., 2006; Schmitt-Kopplin et al., 2010). High accuracy enables the determination of the elemental composition based on the exact mass while high resolution enables the separation of closely-spaced peaks. Marshall et al. (2006) have demonstrated through mathematical modeling that ~0.1-0.5 mDa mass accuracy is necessary to determine unique elemental composition for typical organic compounds up to 500 Da (and higher when combined with Kendrick analysis). Schmitt-Kopplin and co-workers (2010) showed that closely spaced CHO and CHOS compounds ($C_3$ vs. $SH_4$) at ~400 Da were resolved with an instrument resolution of ~150,000 in an analysis of extracted aerosol filter samples using negative mode ESI. Compared to their study we used a relatively lower mass resolution of 60,000 m/Δm at *m/z* 400 (FWHM). However, in this work, based on accurate mass measurements, we can still confidently identify peaks over a wide mass range. One identification technique, Kendrick analysis, aids identification by grouping higher mass peaks into families with lower mass peaks that can be unambiguously identified. The second order

transformation used here enables even more efficient grouping which further aids identification of higher-mass peaks within each group that cannot be unambiguously identified using traditional 1D Kendrick analysis (Roach et al., 2011). If the peaks have a similar abundance, mass accuracy can be affected by the presence of overlapping, unresolved peaks. For example, an unresolved CHO/CHOS doublet (e.g. $C_{16}H_{28}O_{10}S$ vs.$C_{19}H_{24}O_{10}$) with equal abundances would result in an error of ~1.7 mDa for either assignment. However, the measured mass is very close to the exact mass of the more abundant peak when the relative abundance of one of the peaks in the unresolved doublet is low. Under these conditions, while lower abundance species are unresolved and unassigned, the dominant species are accurately identified. In this study the majority (~75-80%) of our assignments had mass accuracy within ± 0.3 mDa. While we do not necessarily resolve all of the peaks in the spectrum, the assignments are accurate as indicated by the absolute error.

**MS/MS**

The Orbitrap mass spectrometer has three mass spectrometers in series: a linear quadrupole, a C-trap, and the Orbitrap itself. Ions were isolated and collision induced dissociation was performed in the linear quadrupole (LTQ) and the fragment ions were measured in the Orbitrap MS. Since the optimum collision energy has been shown to have a positive correlation with mass, a normalized collision energy (NCE) is used that compensates for the mass dependency with selectable values between 0-100%. In this study, we found values of 15-25% were optimal to produce fragment ions while still maintaining some of the parent peak intensity.

The smallest window for isolation is 0.1 *m/z* which is too large to isolate a single peak out of the multiple peaks at each nominal mass. For example, in Appendix 7b the 0.1 m/z window isolated one primary ion at 253.0390 and two other minor ions at 253.0028 and 253.0754. The identities of all three are: $C_8H_{13}O_7S_1$, $C_7H_9O_8S_1$, and $C_9H_{17}O_6S_1$ respectively. After applying the NCE at 18% the fragments of all three are observed at 173 which correspond to losses of $SO_3$ from all three sulfur containing compounds. This type of analysis was possible because the intensity of the primary peak was much higher than the other isobaric ions and the fragment ions followed the same intensity pattern. In this work we are looking primarily for the loss of $SO_3$ and the appearance of $HSO_4^-$ which have been shown to be indicative of organosulfates (Reemtsma et al., 2006). Since all three ions in Appendix 7 contain sulfur, the bisulfate ion can be a fragment of one, two, or all of the ions.

## References


Ahlm, L., et al. (2012), Formation and growth of ultrafine particles from secondary sources in Bakersfield, California, *J. Geophys. Res.-Atmos.*, *117*, D00V08 DOI: 10.1029/2011JD017144.

Aiken, A. C., et al. (2008), O/C and OM/OC ratios of primary, secondary, and ambient organic aerosols with high-resolution time-of-flight aerosol mass spectrometry, *Environ. Sci. Technol.*, *42*(12), 4478-4485.

DeCarlo, P. F., et al. (2006), Field-deployable, high-resolution, time-of-flight aerosol mass spectrometer, *Analytical Chemistry*, *78*(24), 8281-8289.

Marshall, A. G., K. Sunghwan and R. P. Rodgers (2006), Truly "exact" mass: Elemental composition can be determined uniquely from molecular mass measurement at ~0.1mDa accuracy for molecules up to ~500Da, *International Journal of Mass Spectrometry*, *251*(2-3), 260-265265.

Reemtsma, T., et al. (2006), Identification of fulvic acids and sulfated and nitrated analogues in atmospheric aerosol by electrospray ionization Fourier transform ion cyclotron resonance mass spectrometry, *Analytical Chemistry*, *78*(24), 8299-8304.

Roach, P. J., J. Laskin and A. Laskin (2011), Higher-order mass defect analysis for mass spectra of complex organic mixtures, *Analytical Chemistry*, *83*(12), 4924-4929.

Schmitt-Kopplin, P., et al. (2010), Analysis of the unresolved organic fraction in atmospheric aerosols with ultrahigh-resolution mass spectrometry and nuclear magnetic resonance spectroscopy: organosulfates as photochemical smog constituents, *Analytical Chemistry*, *82*(19), 8017-8026.

# Appendix B2
# Meteorological data

Meteorological data for the five days discussed in the paper (June 20th-June 24th).

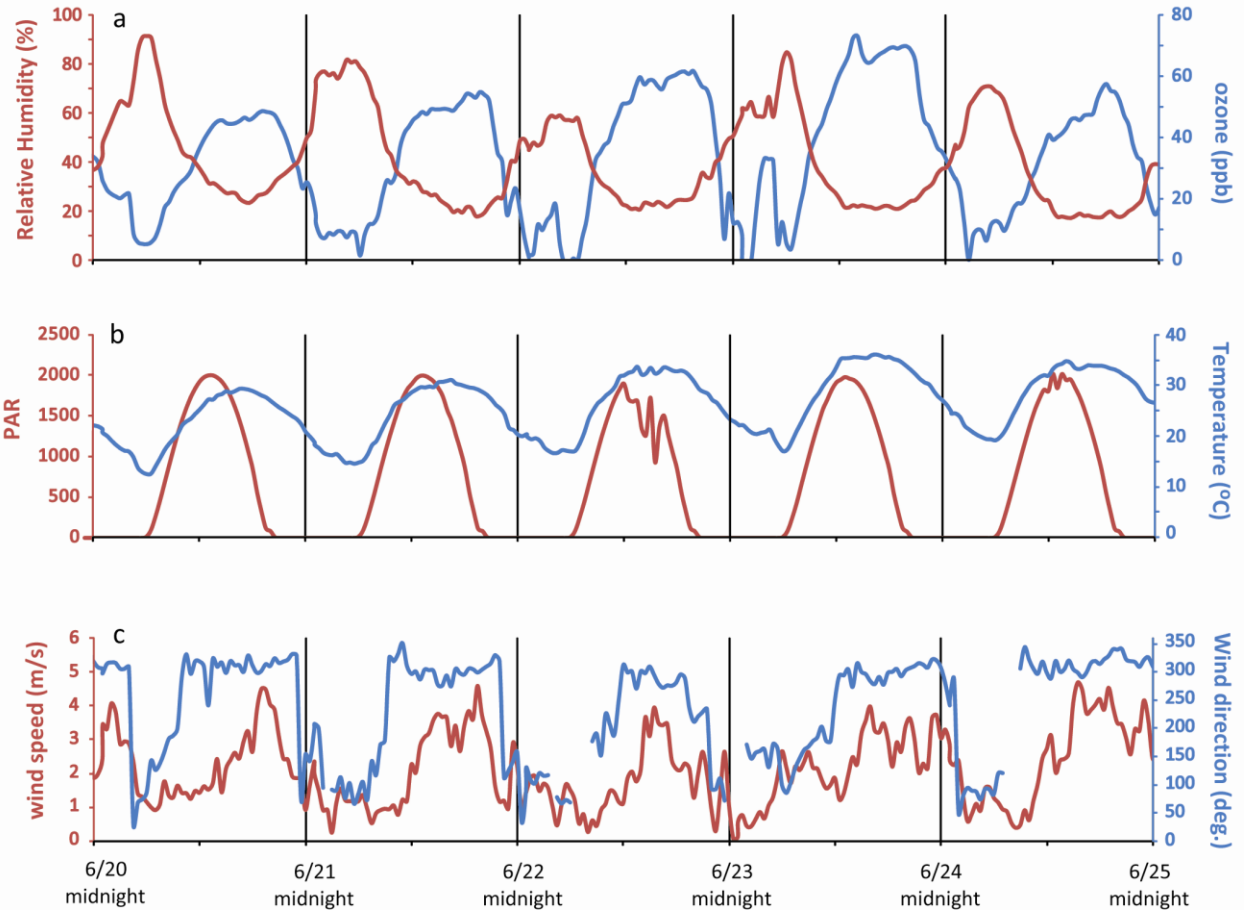

# Appendix B3
# Van Krevelen diagrams for the four samples collected on June 20th

Van Krevelen diagrams for the four samples collected on June 20th. (a) midnight-6am, (b) 6am-noon, (c) noon-6pm, (d) 6pm-midnight. The H/C versus the O/C values for each identified compound are shown broken down by group.

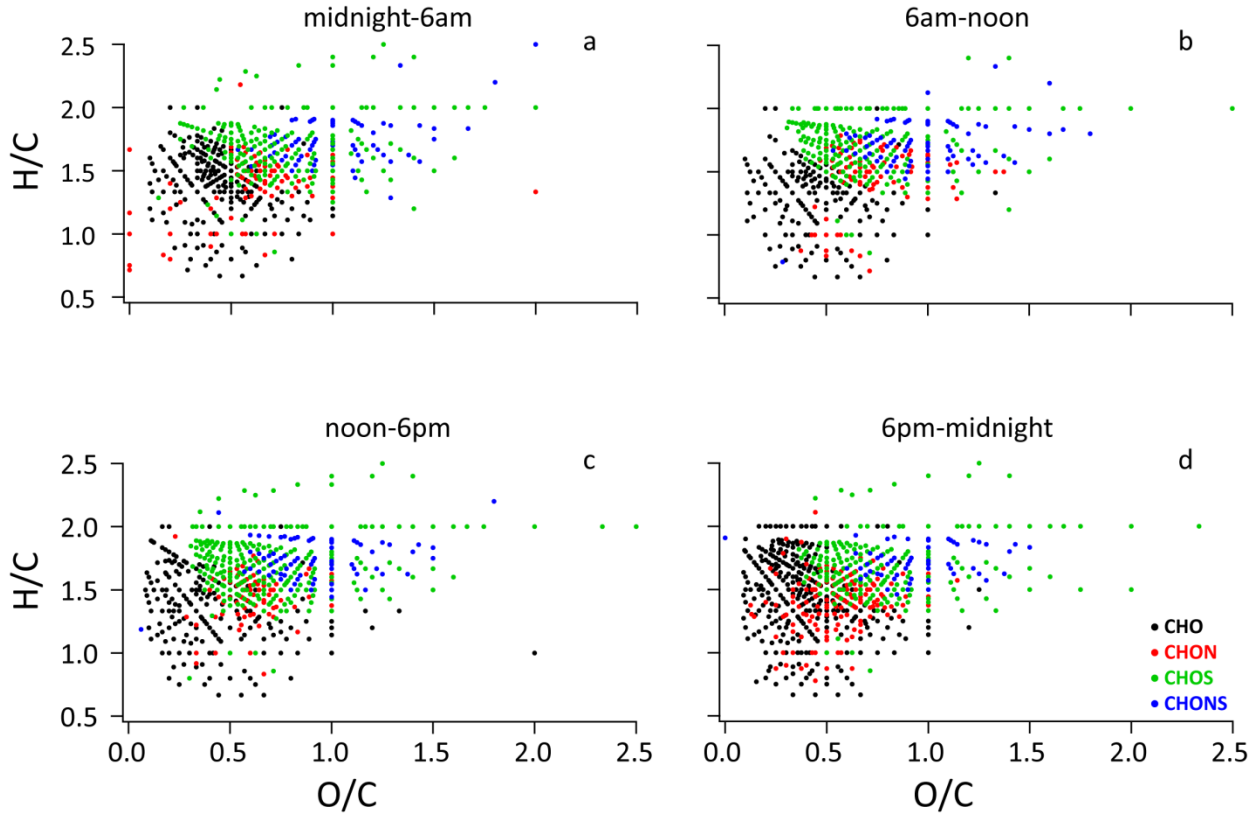

## Appendix B4
## Van Krevelen diagrams for the four samples collected on June 21st

Van Krevelen diagrams for the four samples collected on June 21st. (a) midnight-6am, (b) 6am-noon, (c) noon-6pm, (d) 6pm-midnight. The H/C versus the O/C values for each identified compound are shown broken down by group.

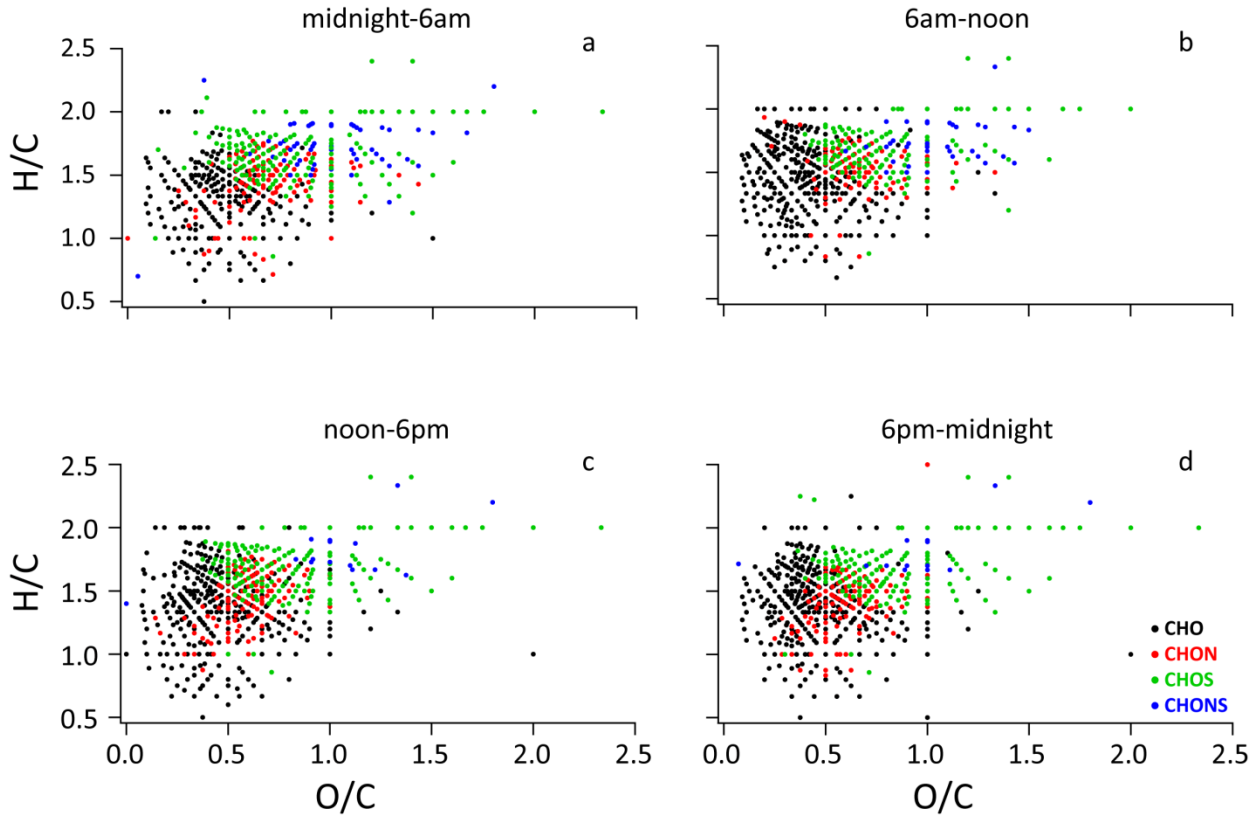

# Appendix B5
# Van Krevelen diagrams for the four samples collected on June 22nd

Van Krevelen diagrams for the four samples collected on June 22nd. (a) midnight-6am, (b) 6am-noon, (c) noon-6pm, (d) 6pm-midnight. The H/C versus the O/C values for each identified compound are shown broken down by group.

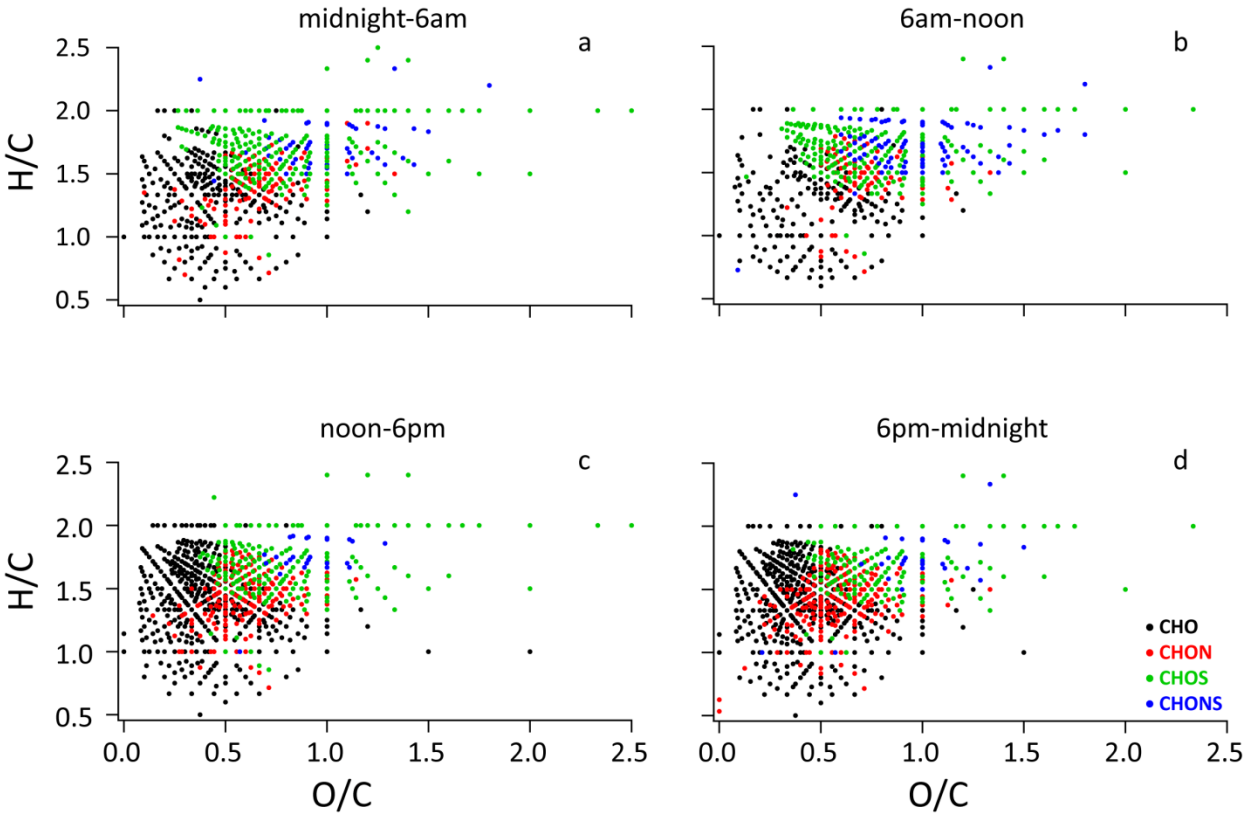

## Appendix B6
## Van Krevelen diagrams for the four samples collected on June 23rd

Van Krevelen diagrams for the four samples collected on June 23rd. (a) midnight-6am, (b) 6am-noon, (c) noon-6pm, (d) 6pm-midnight. The H/C versus the O/C values for each identified compound are shown broken down by group.

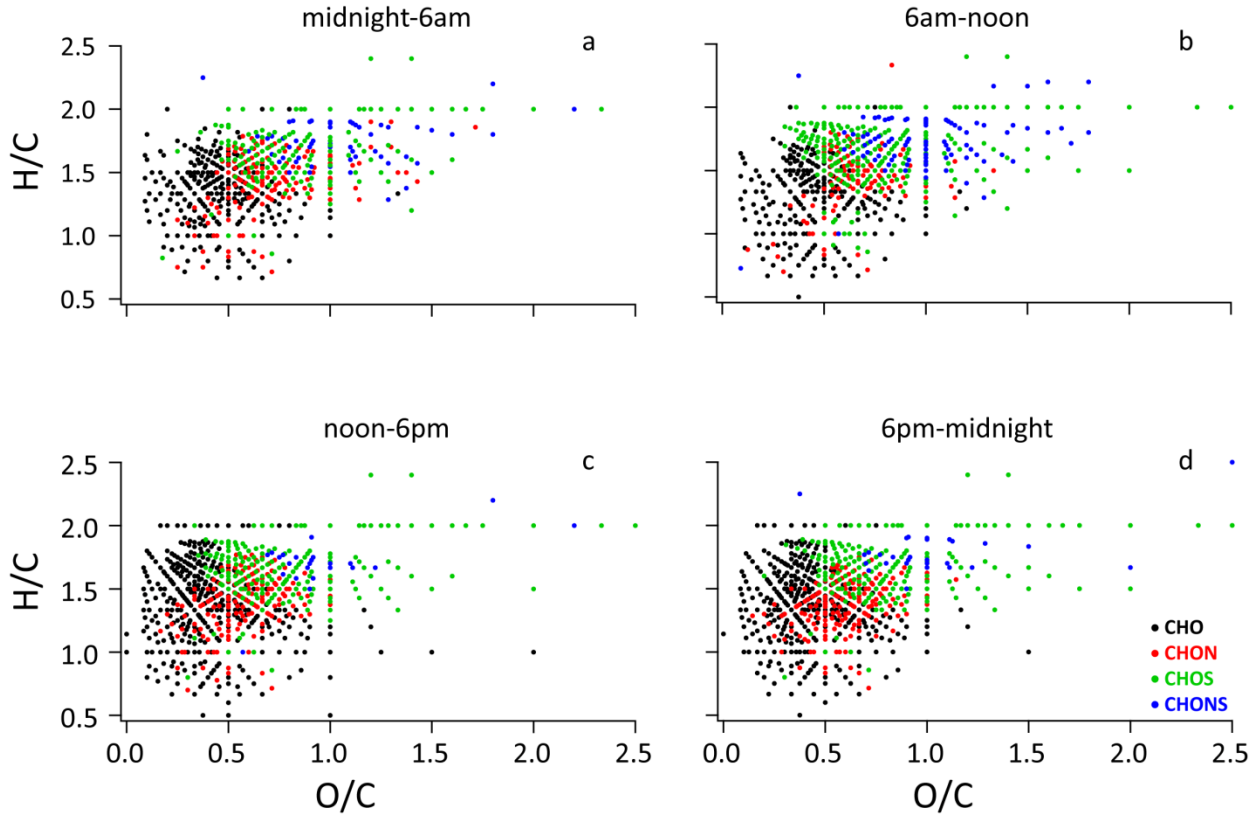

# Appendix B7
# Isolation and product MS/MS of CHOS compounds

MS/MS of CHOS compounds from the June 21st midnight-6am sample. (a) product ion mass spectra (b) precursor mass spectra with ionization window 0.1 Da.

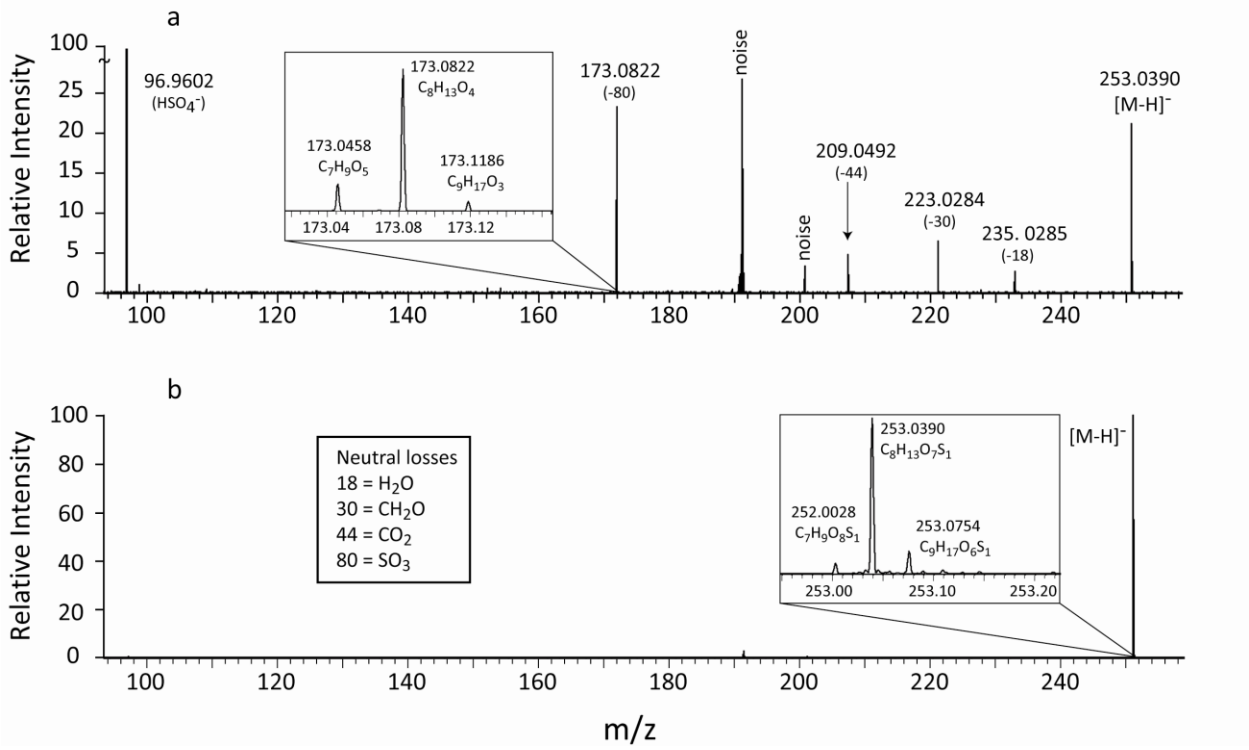

# Appendix B8
# Number of compounds of each class for size resolved samples

Number of compounds identified in each class by aerodynamic diameter ($D_a$). The bottom four stages of a MOUDI were analyzed ($0.18 < D_a < 1.8$ μm)

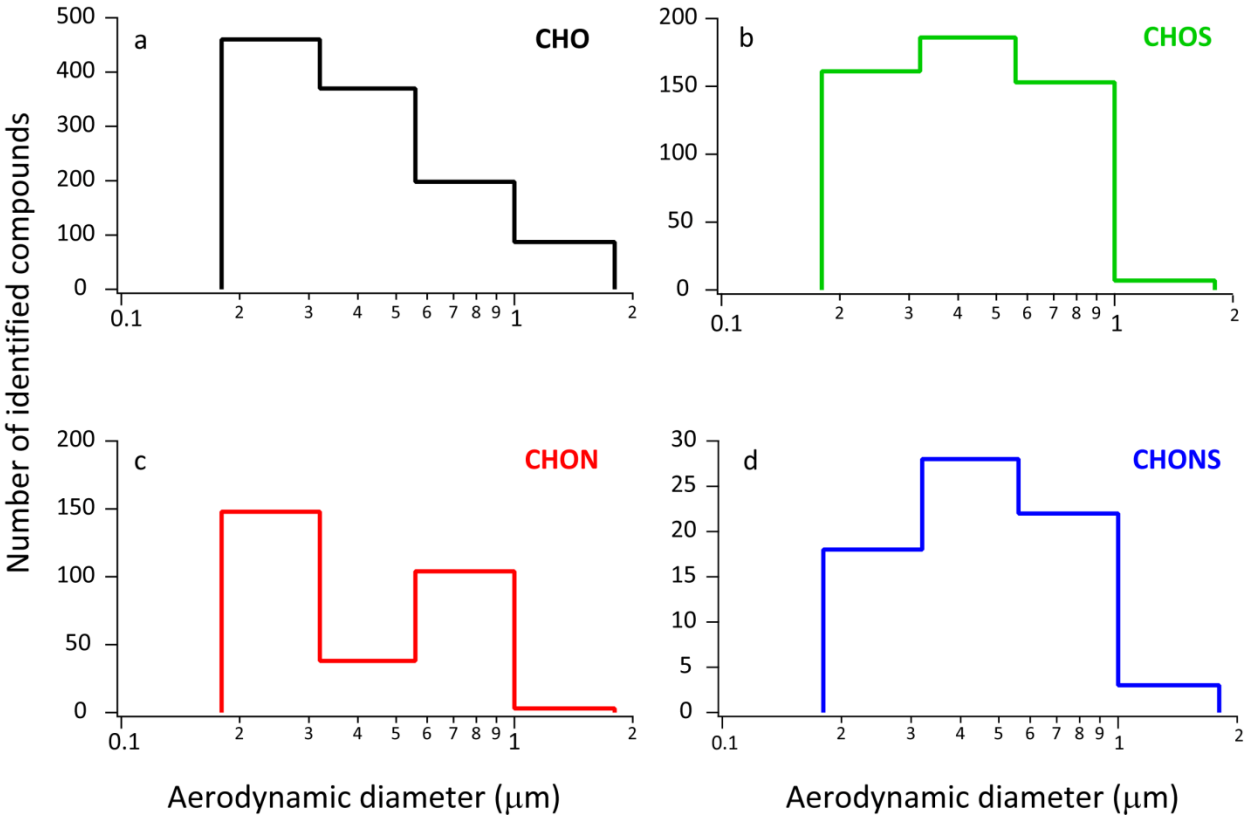

# Appendix B9
# Number of compounds, by group, observed in each sample

Number of compounds observed in each sample. The data are separated by compound group.

| | | CHO | CHOS | CHON | CHONS | Total |
|---|---|---|---|---|---|---|
| **June 20th** | **midnight-6am** | 291 | 188 | 92 | 69 | 640 |
| | **6am-noon** | 208 | 195 | 98 | 76 | 577 |
| | **Noon-6pm** | 270 | 253 | 93 | 72 | 688 |
| | **6pm-midnight** | 447 | 197 | 163 | 57 | 864 |
| **June 21st** | **midnight-6am** | 251 | 150 | 125 | 53 | 579 |
| | **6am-noon** | 353 | 126 | 90 | 35 | 604 |
| | **Noon-6pm** | 368 | 147 | 110 | 15 | 640 |
| | **6pm-midnight** | 390 | 135 | 111 | 13 | 649 |
| **June 22nd** | **midnight-6am** | 335 | 206 | 112 | 52 | 705 |
| | **6am-noon** | 230 | 197 | 90 | 83 | 600 |
| | **Noon-6pm** | 542 | 179 | 163 | 25 | 909 |
| | **6pm-midnight** | 537 | 135 | 206 | 28 | 906 |
| **June 23rd** | **midnight-6am** | 310 | 143 | 163 | 60 | 676 |
| | **6am-noon** | 327 | 222 | 125 | 86 | 760 |
| | **Noon-6pm** | 521 | 188 | 161 | 23 | 893 |
| | **6pm-midnight** | 488 | 188 | 176 | 29 | 881 |

# Appendix B10
# Results of the 30V CID test

Results from a test with collision induced dissociation (CID). Number of compounds found in the June 23rd midnight-6am sample that were still observed despite a 30 V field gradient in the source. The data is further separated by the relative intensity (RI) of the peak in the June 23rd sample without the CID.

| | % kept (out of x # of peaks) | | | |
|---|---|---|---|---|
| | **Total** | **≥ 5% RI** | **≥ 3% RI** | **≥ 2% RI** |
| **CHO** | 95% (310) | 100% (63) | 100% (119) | 100% (155) |
| **CHOS** | 94% (143) | 97% (30) | 96% (56) | 97% (78) |
| **$CHON_x$** | 62% (163) | 89% (9) | 85% (27) | 82% (61) |
| **Only $CHON_1$** | 73% (129) | 100% (6) | 100% (16) | 96% (45) |
| **Only $CHON_2$** | 18% (28) | 100% (1) | 63% (8) | 38% (13) |
| **Only $CHON_3$** | 33% (6) | 100% (1) | 67% (3) | 67% (3) |
| **CHONS** | 82% (60) | 92% (12) | 96% (23) | 97% (30) |

# Appendix B11
# Intensity weighted elemental ratios compared with AMS

Ensemble average, intensity weighted elemental ratios of all compounds in each sample. The values AMS measurements averaged over the same time periods are given in the right columns. The uncertainties for the AMS values follow those suggested by Aiken et al. 2008.[3] Further experiments are necessary to determine the uncertainties of the elemental ratios in the nano-DESI analysis. The times are given in 24 hours (e.g. 0 = midnight, 18 = 6pm, etc.).

| | | Nano-DESI HRMS | | | AMS | | |
|---|---|---|---|---|---|---|---|
| | | **<O/C>** | **<H/C>** | **<N/C>** | **<O/C>** | **<H/C>** | **<N/C>** |
| **June 20th** | **0-6** | 0.65 | 1.6 | 0.019 | 0.33 ± 0.1 | 1.5 ± 0.1 | 0.0055 ±0.001 |
| | **6-12** | 0.75 | 1.7 | 0.030 | 0.35 ± 0.1 | 1.5 ± 0.1 | 0.0070 ± 0.002 |
| | **12-18** | 0.61 | 1.6 | 0.0088 | 0.38 ± 0.1 | 1.4 ± 0.1 | 0.0046 ± 0.001 |
| | **18-0** | 0.60 | 1.6 | 0.0075 | 0.41 ± 0.1 | 1.4 ± 0.1 | 0.0069 ± 0.002 |
| **June 21st** | **0-6** | 0.69 | 2.5 | 0.030 | 0.30 ± 0.1 | 1.5 ± 0.2 | 0.0058 ± 0.001 |
| | **6-12** | 0.62 | 1.6 | 0.0082 | 0.36 ± 0.1 | 1.4 ± 0.1 | 0.0054 ± 0.001 |
| | **12-18** | 0.57 | 1.5 | 0.0038 | 0.43 ± 0.1 | 1.4 ± 0.1 | 0.0043 ± 0.001 |
| | **18-0** | 0.57 | 1.5 | 0.0059 | 0.43 ± 0.1 | 1.4 ± 0.1 | 0.0048 ± 0.001 |
| **June 22nd** | **0-6** | 0.67 | 1.5 | 0.012 | 0.28 ± 0.09 | 1.5 ± 0.2 | 0.0031 ± 0.0007 |
| | **6-12** | 0.72 | 1.6 | 0.018 | 0.40 ± 0.1 | 1.4 ± 0.1 | 0.0042 ±0.0009 |
| | **12-18** | 0.55 | 1.5 | 0.0058 | 0.43 ± 0.1 | 1.4 ± 0.1 | 0.0041 ±0.0009 |
| | **18-0** | 0.54 | 1.5 | 0.0075 | 0.44 ± 0.1 | 1.3 ± 0.1 | 0.0047 ± 0.001 |
| **June 23rd** | **0-6** | 0.69 | 1.5 | 0.049 | 0.40 ± 0.1 | 1.4 ± 0.1 | 0.0041 ± 0.0009 |
| | **6-12** | 0.68 | 1.5 | 0.018 | 0.44 ± 0.1 | 1.4 ± 0.1 | 0.0042 ± 0.0009 |
| | **12-18** | 0.56 | 1.5 | 0.0042 | 0.45 ± 0.1 | 1.3 ± 0.1 | 0.0041 ± 0.0009 |
| | **18-0** | 0.59 | 1.5 | 0.0052 | 0.48 ± 0.1 | 1.3 ± 0.1 | 0.0061 ± 0.001 |

# Appendix B12
# Number of compounds in each sample above given AI values

Number of compounds in each sample with Aromaticity Index (AI) values: 0.5 >AI >0.67 and ones with AI ≥0.67. Compounds in the first group are likely to have an aromatic ring; those in the second group may be condensed aromatic compounds. The sum of the two columns is the total number of compounds in each sample with aromatic characteristics.

| | | CHO | | CHOS | | CHON | | CHONS | |
|---|---|---|---|---|---|---|---|---|---|
| | | **> 0.5** | **≥ 0.67** | **> 0.5** | **≥ 0.67** | **> 0.5** | **≥ 0.67** | **> 0.5** | **≥ 0.67** |
| **June 20th** | **midnight-6am** | 5 | 0 | - | - | 0 | 12 | 0 | 0 |
| | **6am-noon** | 4 | 1 | - | - | 1 | 2 | 1 | 0 |
| | **noon-6pm** | 5 | 1 | - | - | 0 | 1 | 0 | 0 |
| | **6pm-midnight** | 7 | 2 | - | - | 4 | 1 | 0 | 0 |
| **June 21st** | **midnight-6am** | 3 | 3 | - | - | 1 | 1 | 0 | 1 |
| | **6am-noon** | 3 | 1 | - | - | 0 | 1 | 0 | 0 |
| | **noon-6pm** | 11 | 6 | - | - | 3 | 0 | 0 | 0 |
| | **6pm-midnight** | 5 | 3 | - | - | 2 | 1 | 0 | 0 |
| **June 22nd** | **midnight-6am** | 10 | 9 | - | - | 1 | 1 | 0 | 0 |
| | **6am-noon** | 11 | 5 | - | - | 0 | 1 | 0 | 1 |
| | **noon-6pm** | 14 | 8 | - | - | 2 | 0 | 0 | 0 |
| | **6pm-midnight** | 13 | 8 | - | - | 2 | 4 | 0 | 0 |
| **June 23rd** | **midnight-6am** | 7 | 1 | - | - | 1 | 3 | 0 | 0 |
| | **6am-noon** | 7 | 5 | - | - | 3 | 2 | 0 | 1 |
| | **noon-6pm** | 16 | 10 | - | - | 4 | 4 | 0 | 0 |
| | **6pm-midnight** | 13 | 5 | - | - | 2 | 1 | 0 | 0 |

# Appendix B13
# Compounds outside the ranges of the van Krevelen diagrams

Compounds outside of the range of O/C and H/C values plotted in the van Krevelen diagrams. a-d correspond to the sample time when an elemental formula was observed (a= midnight-6am, b= 6am-noon, c= noon-6pm, d= 6pm-midnight). In the last column the size resolved data is included; the numbers 8, 7, and 6 refer to the MODI stages on which that elemental formula was observed.

| | | | | **Time of day when the formula was found** | | | | **Size fraction** |
|---|---|---|---|---|---|---|---|---|
| **mass** | **formula** | **O/C** | **H/C** | **June 20th** | **June 21st** | **June 22nd** | **June 23rd** | **June 24th** |
| 64.0160 | $CH_4O_3$ | 3.0 | 4.0 | a | | | | |
| 95.9881 | $CH_4O_3S$ | 3.0 | 4.0 | b, d | b | a, c, d | a, b, c, d | 8, 7, 6 |
| 111.983 | $CH_4O_4S$ | 4.0 | 4.0 | a, b, c, d | | a, c, d | a, b, c, d | 8, 7 |
| 124.978 | $CH_3NO_4S$ | 4.0 | 3.0 | a | | b | a, d | 8, 7 |
| 125.999 | $C_2H_6O_4S$ | 2.0 | 3.0 | | | a, c | a, d | 7 |
| 140.014 | $C_3H_8O_4S$ | 1.3 | 2.7 | a | | a, c | a | 7 |
| 141.994 | $C_2H_6O_5S$ | 2.5 | 3.0 | | | a | | |
| 155.973 | $C_2H_4O_6S$ | 3.0 | 2.0 | a, b, c, d | a, b, c, d | a, b, c, d | a, b, c, d | 7, 6 |
| 156.009 | $C_3H_8O_5S$ | 1.7 | 2.7 | a, c | | | | 7, 6 |
| 172.004 | $C_3H_8O_6S$ | 2.0 | 2.7 | c | | | b | 7, 6 |
| 186.049 | $C_3H_{10}N_2O_7$ | 2.3 | 3.3 | a | | | | |
| 192.006 | $C_9H_4O_5$ | 0.56 | 0.44 | | a, c, d | a, c ,d | b, c, d | |
| 193.012 | $C_7H_3N_3O_4$ | 0.57 | 0.43 | | | | | |
| 202.974 | $C_3H_5NO_8S$ | 4.0 | 2.5 | | a | a | | |
| 203.010 | $C_3H_9NO_7S$ | 2.3 | 3.0 | | a | a | | |
| 214.974 | $C_3H_5NO_8S$ | 2.7 | 1.7 | a | | | | |
| 320.0433 | $C_{17}H_8N_2O_5$ | 0.29 | 0.47 | | | | | 6 |
| 336.0382 | $C_{17}H_8N_2O_6$ | 0.35 | 0.47 | | | | | 6 |

# Appendix B14
# Average elemental ratios separated by compound class

Intensity weighted average elemental ratios for each sample separated by compound class.

| | | <O/C> | | | | <H/C> | | | | <N/C> | | | |
|---|---|---|---|---|---|---|---|---|---|---|---|---|---|
| | | CHO | CHOS | CHON | CHONS | CHO | CHOS | CHON | CHONS | CHO | CHOS | CHON | CHONS |
| June 20th | 0-6 | 0.52 | 0.78 | 0.69 | 0.97 | 1.4 | 1.7 | 1.5 | 1.7 | - | - | 0.12 | 0.10 |
| | 6-12 | 0.55 | 0.81 | 0.76 | 0.99 | 1.4 | 1.8 | 1.5 | 1.7 | - | - | 0.11 | 0.12 |
| | 12-18 | 0.47 | 0.71 | 0.62 | 0.91 | 1.4 | 1.7 | 1.5 | 1.7 | - | - | 0.088 | 0.10 |
| | 18-0 | 0.49 | 0.82 | 0.63 | 0.93 | 1.5 | 1.8 | 1.5 | 1.7 | - | - | 0.091 | 0.098 |
| June 21st | 0-6 | 0.56 | 0.83 | 0.81 | 1.0 | 1.4 | 1.7 | 1.5 | 1.7 | - | - | 0.13 | 0.11 |
| | 6-12 | 0.47 | 1.1 | 0.69 | 1.0 | 1.5 | 2.0 | 1.6 | 1.7 | - | - | 0.096 | 0.11 |
| | 12-18 | 0.51 | 0.80 | 0.62 | 0.88 | 1.5 | 1.8 | 1.5 | 1.7 | - | - | 0.084 | 0.14 |
| | 18-0 | 0.50 | 0.87 | 0.65 | 0.75 | 1.5 | 1.8 | 1.5 | 1.7 | - | - | 0.092 | 0.12 |
| June 22nd | 0-6 | 0.55 | 0.87 | 0.74 | 1.0 | 1.4 | 1.8 | 1.5 | 1.7 | - | - | 0.11 | 0.11 |
| | 6-12 | 0.61 | 0.81 | 0.73 | 1.0 | 1.3 | 1.7 | 1.5 | 1.7 | - | - | 0.087 | 0.11 |
| | 12-18 | 0.49 | 0.83 | 0.65 | 0.93 | 1.5 | 1.8 | 1.5 | 1.8 | - | - | 0.081 | 0.10 |
| | 18-0 | 0.49 | 0.87 | 0.63 | 0.93 | 1.5 | 1.8 | 1.5 | 1.7 | - | - | 0.083 | 0.10 |
| June 23rd | 0-6 | 0.55 | 0.88 | 0.86 | 1.0 | 1.4 | 1.7 | 1.5 | 1.7 | - | - | 0.14 | 0.12 |
| | 6-12 | 0.56 | 0.84 | 0.74 | 1.0 | 1.4 | 1.8 | 1.5 | 1.7 | - | - | 0.10 | 0.12 |
| | 12-18 | 0.50 | 0.86 | 0.63 | 0.94 | 1.5 | 1.8 | 1.5 | 1.7 | - | - | 0.087 | 0.10 |
| | 18-0 | 0.53 | 0.89 | 0.63 | 0.95 | 1.4 | 1.8 | 1.4 | 1.8 | - | - | 0.088 | 0.10 |

# Appendix B15
# Organosulfates also found with LC/ESI/MS by Surratt et al.

Organosulfate compounds detected with both LC/ESI/MS analysis of 24 hour filters and nano-DESI analysis of MOUDI substrates. These organosulfates were also reported in (Surratt et al., 2008) as being formed from biogenic precursors. The first number given is the concentration in ng/m$^3$ found with LC/ESI/MS and the letters in parenthesis correspond to the time of day the elemental formula was observed in the nano-DESI analysis (a= midnight-6am, b= 6am-noon, c= noon-6pm, d= 6pm-midnight). The data in red are the only two samples where the compound was observed with LC/ESI/MS but not with nano-DESI.

| | | **Concentration in ng/m$^3$ with LC/ESI/MS (fractions of day the formula was found in nano-DESI analysis)** | | | |
|---|---|---|---|---|---|
| **Neutral mass** | **formula** | **June 20$^{th}$** | **June 21$^{st}$** | **June 22$^{nd}$** | **June 23$^{rd}$** |
| 224.0355 | $C_7H_{11}O_6S_1$ | 0.000 (-) | 0.314 (-) | 0.273 (c, d) | 0.391 (a-d) |
| 227.994 | $C_5H_7O_8S_1$ | 0.000 (a-d) | 0.140 (a-d) | 0.000 (a-d) | 0.165 (a-d) |
| 238.0511 | $C_8H_{13}O_6S_1$ | 0.121 (a-d) | 0.036 (b-d) | 0.109 (a-d) | 0.036 (a-d) |
| 250.0511 | $C_9H_{13}O_6S_1$ | 0.034 (a-d) | 0.012 (a-d) | 0.000 (a-d) | 0.000 (b-d) |
| 250.0875 | $C_{10}H_{17}O_5S_1$ | 0.020 (a-d) | 0.025 (a, c, d) | 0.000 (a, c) | 0.040 (c) |
| 252.0668 | $C_9H_{15}O_6S_1$ | 0.058 (a, b, d) | 0.084 (d) | 0.147 (a-d) | 0.110 (a-d) |
| 254.046 | $C_8H_{13}O_7S_1$ | 0.064 (a-d) | 0.095 (a-d) | 0.000 (a-d) | 0.000 (a-d) |
| 266.0824 | $C_{10}H_{17}O_6S_1$ | 0.000 (a-d) | 0.000 (a-d) | 0.000 (a-d) | 0.000 (a-d) |
| 268.0617 | $C_9H_{15}O_7S_1$ | 0.092 (a-d) | 0.137 (a-d) | 0.071 (a-d) | 0.152 (a-d) |
| 280.0617 | $C_{10}H_{15}O_7S_1$ | 0.106 (a-d) | 0.126 (a, b, d) | 0.076 (a-d) | 0.122 (a-d) |
| 282.0773 | $C_{10}H_{17}O_7S_1$ | 0.032 (a-d) | 0.043 (a, b, d) | 0.036 (a-d) | 0.067 (a-d) |
| 284.0566 | $C_9H_{15}O_8S_1$ | 0.007 (a-d) | 0.000 (a-d) | 0.000 (a-d) | 0.000 (a-d) |
| 284.093 | $C_{10}H_{19}O_7S_1$ | 0.000 (a-d) | 0.013 (-) | 0.000 (a, b) | 0.000 (-) |
| 298.0722 | $C_{10}H_{17}O_8S_1$ | 0.012 (a-d) | 0.000 (a-d) | 0.108 (a-d) | 0.022 (a-d) |
| 139.9779 | $C_2H_3O_5S_1$ | 0.069 (b, c) | 0.000 (-) | 0.000 (a, c) | 0.000 (b-d) |
| 153.9936 | $C_3H_5O_5S_1$ | 0.064 (a-d) | 0.144 (a-d) | 0.081 (a-d) | 0.15 (a-d) |
| 155.9729 | $C_2H_3O_6S_1$ | 0.019 (a-d) | 0.039 (a-d) | 0.019 (a-d) | 0.085 (a-d) |
| 169.9885 | $C_3H_5O_6S_1$ | 0.045 (a-d) | 0.107 (a, c, d) | 0.056 (a-c) | 0.118 (a-d) |
| 199.9991 | $C_4H_7O_7S_1$ | 0.129 (a-d) | 0.301 (a, c, d) | 0.319 (a-d) | 0.528 (a-d) |
| 211.9991 | $C_5H_7O_7S_1$ | 0.067 (a-d) | 0.000 (a, c, d) | 0.125 (a-d) | 0.000 (a-d) |
| 214.0147 | $C_5H_9O_7S_1$ | 0.048 (a-d) | 0.114 (a, c, d) | 0.118 (a-d) | 0.104 (a-d) |
| 216.0304 | $C_5H_{11}O_7S_1$ | 0.387 (a-d) | 1.104 (a, c, d) | 1.157 (a-d) | 1.691 (a-d) |

# Appendix B16
# Nitroxy organosulfates also found with LC/ESI/MS by Surratt et al

Nitroxy organosulfate compounds detected with both LC/ESI/MS analysis of 24 hour filters and nano-DESI analysis of MOUDI substrates. These nitroxy organosulfates were also reported in (Surratt et al., 2008) as being formed from biogenic precursors. The first number given is the concentration in ng/m$^3$ found with LC/ESI/MS and the letters in parenthesis correspond to the time of day the elemental formula was observed in the nano-DESI analysis (a= midnight-6am, b= 6am-noon, c= noon-6pm, d= 6pm-midnight). The data in red are samples where the compound was observed with LC/ESI/MS but not with nano-DESI.

| | | **Concentration in ng/m$^3$ with LC/ESI/MS (fractions of day the formula was found with nano-DESI analysis)** | | | |
|---|---|---|---|---|---|
| **Neutral mass** | **formula** | **June 20$^{th}$** | **June 21$^{st}$** | **June 22$^{nd}$** | **June 23$^{rd}$** |
| 295.0726 | $C_{10}H_{16}N_1O_7S_1$ | 0.000 (a-d) | 1.225 (b, d) | 0.000 (a, c, d) | 0.000 (b, d) |
| 297.0518 | $C_9H_{14}N_1O_8S_1$ | 2.560 (a, b, d) | 7.306 (d) | 3.313 (c) | 1.880 (c) |
| 311.0675 | $C_{10}H_{16}N_1O_8S_1$ | 0.023 (a-d) | 0.044 (a, b, d) | 0.009 (a-d) | 0.000 (a-d) |
| 313.0468 | $C_9H_{14}N_1O_9S_1$ | 0.011 (a-d) | 0.019 (a, b, d) | 0.022 (a-d) | 0.055 (a-d) |
| 327.0624 | $C_{10}H_{16}N_1O_9S_1$ | 0.186 (a-d) | 0.532 (a, b, d) | 0.090 (a-d) | 0.000 (a-d) |
| 329.078 | $C_{10}H_{18}N_1O_9S_1$ | 0.008 (a-d) | 0.025 (a, b, d) | 0.000 (a-d) | 0.000 (a, b, d) |
| 331.0573 | $C_9H_{16}N_1O_{10}S_1$ | 0.005 (a-d) | 0.004 (a, b) | 0.000 (a-d) | 0.000 (a, b, d) |
| 343.0573 | $C_{10}H_{16}N_1O_{10}S_1$ | 0.141 (a-d) | 0.203 (a, b, d) | 0.081 (a-d) | 0.380 (a-d) |
| 374.0631 | $C_{10}H_{17}N_2O_{11}S_1$ | 0.685 (-) | 0.274 (-) | 0.076 (-) | 0.377 (-) |
| 390.058 | $C_{10}H_{17}N_2O_{12}S_1$ | 0.685 (b) | 0.274 (-) | 0.076 (-) | 0.377 (a, b) |
| 261.0155 | $C_5H_{10}N_1O_9S_1$ | 0.000 (a, c) | 0.027 (a, c, d) | 0.064 (a, b) | 0.021 (a-c) |
| 306.0005 | $C_5H_9N_2O_{11}S_1$ | 0.141 (-) | 0.169 (-) | 0.100 (-) | 0.198 (1, c) |

# Appendix B17
# Average elemental ratios for size resolved samples

Aerosol, size resolved, intensity weighted, average elemental ratios for each compound class. The results for the 12 hour samples collected on June 24th from noon-midnight are shown; stages 5-8 of the MOUDI were analyzed.

| | Stage: | 8 (0.18-0.32 μm) | 7 (0.32-0.56 μm) | 6 (0.56-1.0 μm) | 5 (1.0-1.8 μm) |
|---|---|---|---|---|---|
| <O/C> | all | 0.60 | 0.67 | 0.92 | 0.30 |
| | CHO | 0.53 | 0.54 | 0.54 | 0.32 |
| | CHON | 0.65 | 0.58 | 0.53 | 0.26 |
| | CHOS | 1.0 | 0.99 | 1.3 | 0.30 |
| | CHONS | 0.86 | 0.94 | 0.99 | 0.19 |
| <H/C> | all | 1.5 | 1.6 | 1.7 | 1.6 |
| | CHO | 1.5 | 1.5 | 1.4 | 1.6 |
| | CHON | 1.5 | 1.4 | 0.94 | 1.2 |
| | CHOS | 1.9 | 1.9 | 2.2 | 1.8 |
| | CHONS | 1.7 | 1.7 | 1.5 | 0.68 |
| <N/C> | all | 0.0047 | 0.0016 | 0.030 | 0.016 |
| | CHO | - | - | - | - |
| | CHON | 0.084 | 0.11 | 0.30 | 0.19 |
| | CHOS | - | - | - | - |
| | CHONS | 0.10 | 0.13 | 0.22 | 0.15 |

# Appendix C: Supplemental Information for Chapter 4

## Appendix C1
## Additional information on the sampling and instrumentation

### Sampling and Instrumentation

The Bakersfield field site (35.35°N, 118.97°W) was located at the Kern County Cooperative Extension property in the southeastern part of the city. Data collected on June 23, 2010 was chosen for in-depth analysis because concurrent measurements indicated high SOA loadings on that day. The sampling inlet was located approximately five meters above the ground attached to the top of an air conditioned trailer housing the MOUDI. A PM 2.5 cyclone was placed upstream of the MOUDI. Samples were collected at 31 L/min for 5 hours and 50 minutes per sample for a total sample volume of 10.9 $m^3$ and a total of four samples per day.

The Los Angeles field site (34.14°N, 118.12°W) was located on the Caltech campus and sampling was done from the roof of the Keck building. Data collected on June 5, 2010 was chosen for in-depth analysis because concurrent AMS measurements showed a clean diurnal pattern for OA and high SOA loadings on that day. Los Angeles samples were collected on aluminum foil substrates using two ten stage MOUDIs with rotation (model 110-R) operated in a time-staggered fashion (6 hours per each set of samples). To coincide with the Bakersfield analysis, stage eight was used for intensive study.

The chamber at UC Irvine was thoroughly flushed with dry purge air (Parker Model 75-62) and humidified with a Nafion multi-channel humidifier (Perma Pure FC125). VOC used for the photooxidation were Diesel # 2 composite standard mixture (DSL, Restek 0.5 g/mL in $CH_2Cl_2$) and isoprene (ISO, Aldrich, purity 99%). DSL is a mixture of > 70% alkanes, ~ 20 % aromatics, and trace polar compounds [*Irwin et al.*, 1997]. Ozone was monitored by a commercial photometer (Thermo Model 49i) and NO and $NO_y$ were measured with a chemiluminescence analyzer (Thermo Model 42i). No additional precursors for the hydroxyl (OH) radicals were added.

The oxidants were generated via the standard $NO/NO_2/O_3$ photochemistry. SOA formation was observed 10-20 min after the lamps were turned on and the particle mass concentrations were monitored with a scanning mobility particle sizer (TSI Model 3080) by assuming 1.2 g/mL average density. Particle concentrations for DSL-$NO_x$, ISO-$NO_x$ and DSL-$NO_x$-$NH_3$ samples reached approximately 80, 70, and 50 $\mu g/m^3$, respectively, at the beginning of SOA collection. The photooxidation time was approximately 5 h.

Results from ammonia measurements, by the Murphy group from U. Toronto, are cited in this paper. In LA, $NH_3$ was measured with a Quantum Cascade laser based Tunable Infrared Differential Absorption Spectroscopy (QC-TIDLAS) instrument and in BF an Ambient Ion Monitor/Ion Chromatograph (AIM-IC) was used.

### References

Irwin, R. J.; et al. (1997), Environmental contaminants encyclopedia Diesel Oil #2 entry. In Division, W. R., Ed. National Park Service: Fort Collins, CO, 1997, 76-84.

# Appendix C2
# Number of common peaks between samples

Number of common peaks between samples. The times are given in 24 hours (e.g. 0 = midnight, 18 = 6pm, etc.). The DSL-$NO_x$-$NH_3$ sample is labeled DSL-$NH_3$ for brevity.

| | **DSL $NO_x$** | **DSL $NH_3$** | **ISO $NO_x$** | **BF 0-6** | **BF 6-12** | **BF 12-18** | **BF 18-24** | **LA 0-6** | **LA 6-12** | **LA 12-18** | **LA 18-24** |
|---|---|---|---|---|---|---|---|---|---|---|---|
| **DSL-$NO_x$** | 732 | | | | | | | | | | |
| **DSL -$NH_3$** | 509 | 595 | | | | | | | | | |
| **ISO-$NO_x$** | 331 | 303 | 504 | | | | | | | | |
| **BF 0-6** | 519 | 483 | 306 | 828 | | | | | | | |
| **BF 6-12** | 523 | 471 | 309 | 692 | 802 | | | | | | |
| **BF 12-18** | 362 | 297 | 234 | 431 | 440 | 614 | | | | | |
| **BF 18-24** | 465 | 404 | 301 | 607 | 608 | 504 | 754 | | | | |
| **LA 0-6** | 37 | 24 | 15 | 42 | 48 | 42 | 47 | 109 | | | |
| **LA 6-12** | 64 | 41 | 19 | 77 | 79 | 77 | 78 | 40 | 208 | | |
| **LA 12-18** | 181 | 131 | 91 | 196 | 205 | 202 | 204 | 41 | 92 | 340 | |
| **LA 18-24** | 73 | 48 | 30 | 80 | 87 | 92 | 83 | 42 | 69 | 97 | 143 |

# Appendix C3
# Average elemental ratios: positive and negative mode ESI

Average elemental ratios for the nano-DESI analysis. The times are given in 24 hours (e.g. 0 = midnight, 18 = 6pm, etc.). The DSL-$NO_x$-$NH_3$ sample is labeled DSL-$NH_3$ for brevity.

| | **Positive Mode nano-DESI** | | | | | | **Negative Mode nano-DESI** | | | | | |
|---|---|---|---|---|---|---|---|---|---|---|---|---|
| | **Intensity weighted** | | | **Not Intensity weighted** | | | **Intensity weighted** | | | **Not Intensity weighted** | | |
| | **H/C** | **O/C** | **N/C** | **H/C** | **O/C** | **N/C** | **H/C** | **O/C** | **N/C** | **H/C** | **O/C** | **N/C** |
| **DSL-$NO_x$** | 1.7 | 0.28 | 0.028 | 1.6 | 0.32 | 0.031 | - | - | - | - | - | - |
| **DSL-$NH_3$** | 1.6 | 0.32 | 0.039 | 1.6 | 0.35 | 0.041 | - | - | - | - | - | - |
| **ISO-$NO_x$** | 1.7 | 0.46 | 0.044 | 1.6 | 0.49 | 0.046 | - | - | - | - | - | - |
| **BF 0-6** | 1.6 | 0.33 | 0.042 | 1.5 | 0.31 | 0.043 | 1.5 | 0.76 | 0.057 | 1.5 | 0.72 | 0.050 |
| **BF 6-12** | 1.6 | 0.32 | 0.033 | 1.5 | 0.30 | 0.035 | 1.6 | 0.75 | 0.027 | 1.5 | 0.73 | 0.038 |
| **BF 12-18** | 1.5 | 0.35 | 0.018 | 1.5 | 0.33 | 0.031 | 1.5 | 0.56 | 0.014 | 1.4 | 0.59 | 0.036 |
| **BF 18-0** | 1.5 | 0.35 | 0.030 | 1.5 | 0.32 | 0.034 | 1.5 | 0.62 | 0.012 | 1.4 | 0.64 | 0.038 |
| **LA 0-6** | 1.4 | 0.19 | 0.0024 | 1.4 | 0.21 | 0.0057 | 1.7 | 0.27 | 0.016 | 1.6 | 0.36 | 0.023 |
| **LA 6-12** | 1.5 | 0.13 | 0.021 | 1.6 | 0.18 | 0.020 | 1.7 | 0.63 | 0.033 | 1.6 | 0.62 | 0.025 |
| **LA 12-18** | 1.7 | 0.24 | 0.019 | 1.6 | 0.24 | 0.020 | 1.6 | 0.56 | 0.005 | 1.5 | 0.49 | 0.011 |
| **LA 18-0** | 1.7 | 0.23 | 0.013 | 1.6 | 0.25 | 0.011 | 1.7 | 0.52 | 0.012 | 1.6 | 0.52 | 0.014 |

# Appendix C4
# Average O/C values for AMS data collected in LA

Average O/C values from AMS data collected in LA on June 5th over the size ranges available to MOUDI. For the aerosols, the 0.19-0.34 μm (vacuum aerodynamic diameter) size range corresponds to the 0.18-0.32 μm (aerodynamic diameter) collected with MOUDI and these values are discussed in the paper. The uncertainties shown are ± 31%.

| | **Average O/C from AMS in LA** | | | |
|---|---|---|---|---|
| **Size range (μm)** | **Midnight-6am** | **6am-noon** | **Noon-6pm** | **6pm-midnight** |
| 0.11-0.17 | 0.33 ± 0.1 | 0.32 ± 0.1 | 0.31 ± 0.1 | 0.31 ± 0.1 |
| ***0.19-0.33*** | ***0.35 ± 0.1*** | ***0.31 ± 0.1*** | ***0.39 ± 0.1*** | ***0.37 ± 0.1*** |
| 0.35-0.57 | 0.38 ± 0.1 | 0.49 ± 0.1 | 0.43 ± 0.1 | 0.44 ± 0.1 |
| 0.59-1.0 | 0.52 ± 0.2 | 0.63 ± 0.2 | 0.52 ± 0.2 | 0.49 ± 0.1 |

## Appendix C5
## Correlation of O/C to $f_{44}$ for Bakersfield AMS data

Scatter plot of $f_{44}$ vs. O/C calculated from HR-TOF-AMS data collected in Bakersfield. The solid line is a linear fit of the data. The data is one hour averages; data for June 23rd is shown in red.

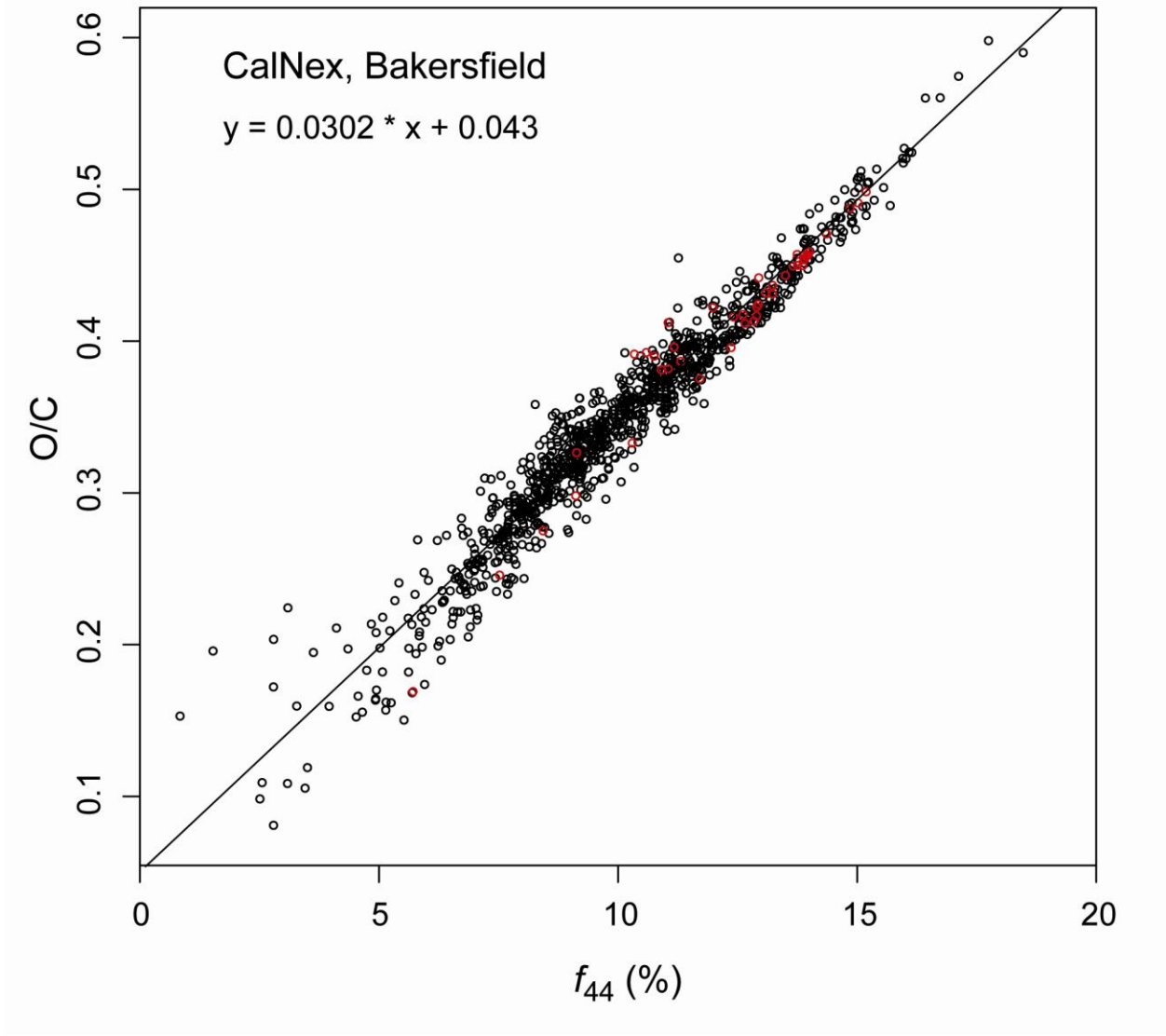

# Appendix C6
# Comparison MS BF to DSL-$NO_x$ chamber

Comparison of the mass spectra for the BF ambient samples to the DSL-$NO_x$ chamber experiment. The ambient mass spectra are on top and the diesel mass spectra are plotted with negative relative intensities to aid comparison. The colors correspond to the number of nitrogen atoms in the chemical formula with black = 0N, red = 1N, blue = 2N. The 6am-noon panel (b) is shown in Figure 1 (a) of the main text. The starred peaks in (c) and (d) have intensities of 160 and 200 respectively on this scale.

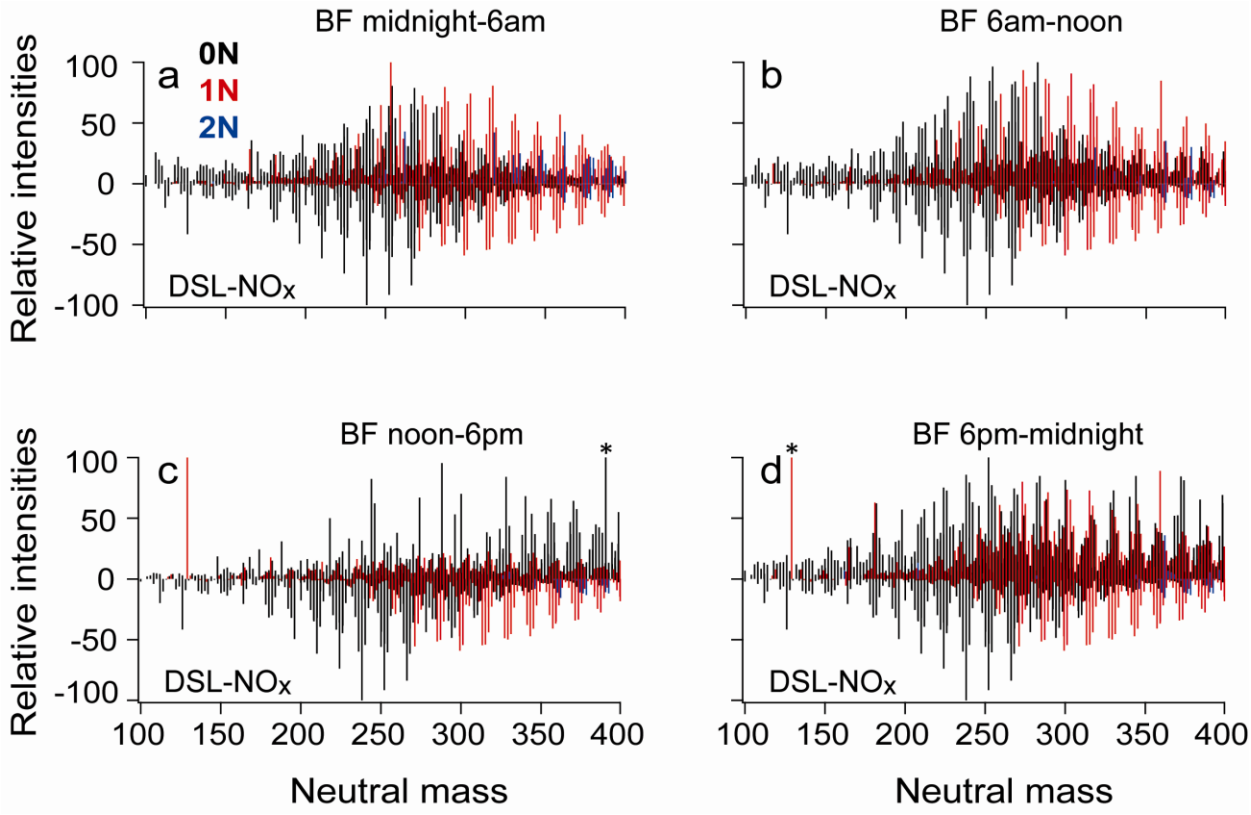

# Appendix C7
# Comparison MS LA to DSL-$NO_x$ chamber

Comparison of the mass spectra for the LA ambient samples to the DSL-$NO_x$ chamber experiment. The ambient mass spectra are on top and the diesel mass spectra are plotted with negative relative intensities to aid comparison. The colors correspond to the number of nitrogen atoms in the chemical formula with black = 0N, red = 1N, blue = 2N. The two red peaks with stars in (c) (149.105 and 253.204 Da) have intensities of 260 and 250 respectively and the two red peaks with stars in (d) (181.183 and 253.204) have intensities of 240 and 200 respectively. The noon-6pm panel (c) is shown in Figure 1 (b) of the main text.

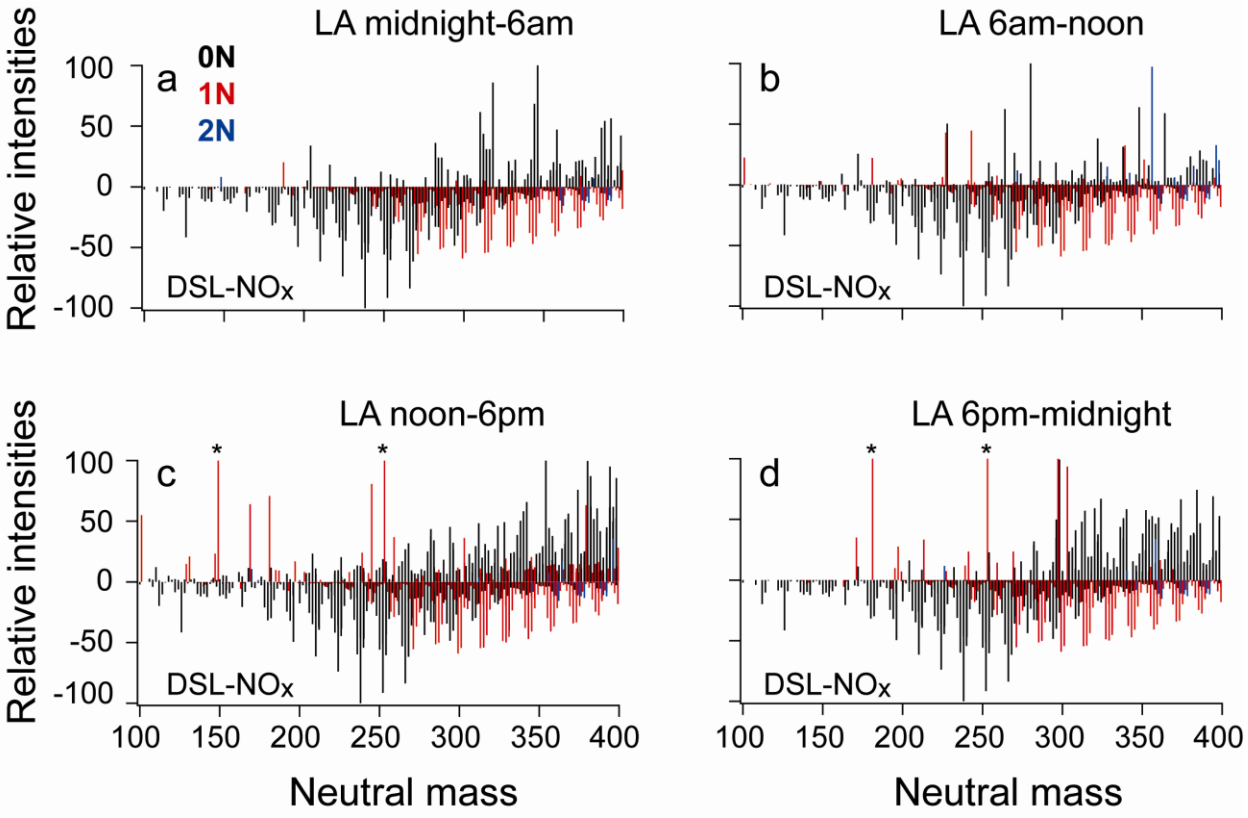

# Appendix C8
# Comparison MS BF to ISO-$NO_x$ chamber

Comparison of the mass spectra for the BF ambient samples to the ISO-$NO_x$ chamber experiment. The ambient mass spectra are on top and the isoprene mass spectra are plotted with negative relative intensities to aid comparison. The colors correspond to the number of nitrogen atoms in the chemical formula with black = 0N, red = 1N, blue = 2N. The starred peaks in (c) and (d) have intensities of 160 and 200 respectively on this scale. The starred peak in the ISO-$NO_x$ spectra at 238.15 Da has an intensity value of 200 on this scale.

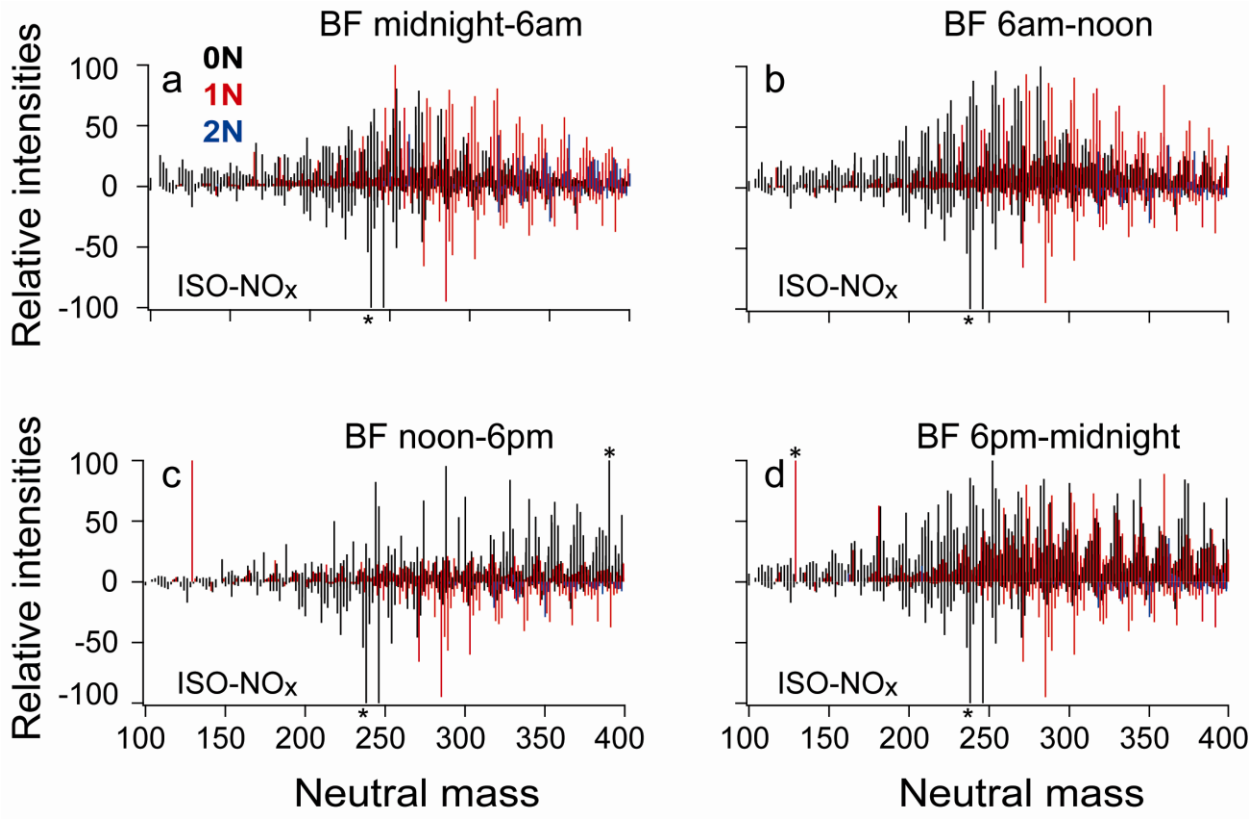

# Appendix C9
# Comparison MS LA to ISO-$NO_x$ chamber

Comparison of the mass spectra for the LA ambient samples to the ISO-$NO_x$ chamber experiment. The ambient mass spectra are on top and the isoprene mass spectra are plotted with negative relative intensities to aid comparison. The colors correspond to the number of nitrogen atoms in the chemical formula with black = 0N, red = 1N, blue = 2N. The two red peaks with stars in (c) (149.105 and 253.204 Da) have intensities of 260 and 250 respectively and the two red peaks with stars in (d) (181.183 and 253.204) have intensities of 240 and 200 respectively. The starred peak in the ISO-$NO_x$ spectra at 238.15 Da has an intensity value of 200 on this scale.

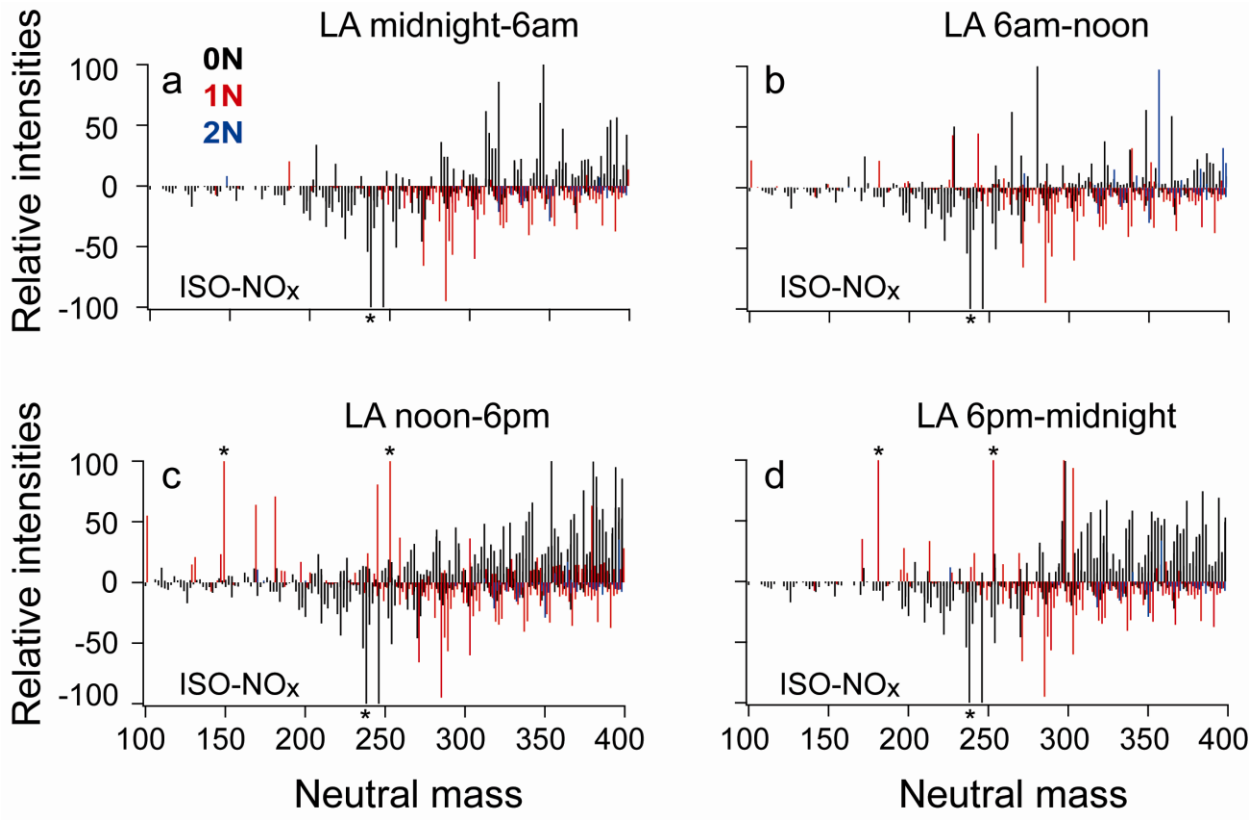

## Appendix C10
## Comparison MS BF to DSL-$NO_x$-$NH_3$ chamber

Comparison of the mass spectra for the BF ambient samples to the DSL-$NO_x$- $NH_3$ chamber experiment. The ambient mass spectra are on top and the diesel-$NH_3$ mass spectra are plotted with negative relative intensities to aid comparison. The colors correspond to the number of nitrogen atoms in the chemical formula with black = 0N, red = 1N, blue = 2N. The starred peaks in (c) and (d) have intensities of 160 and 200 respectively on this scale.

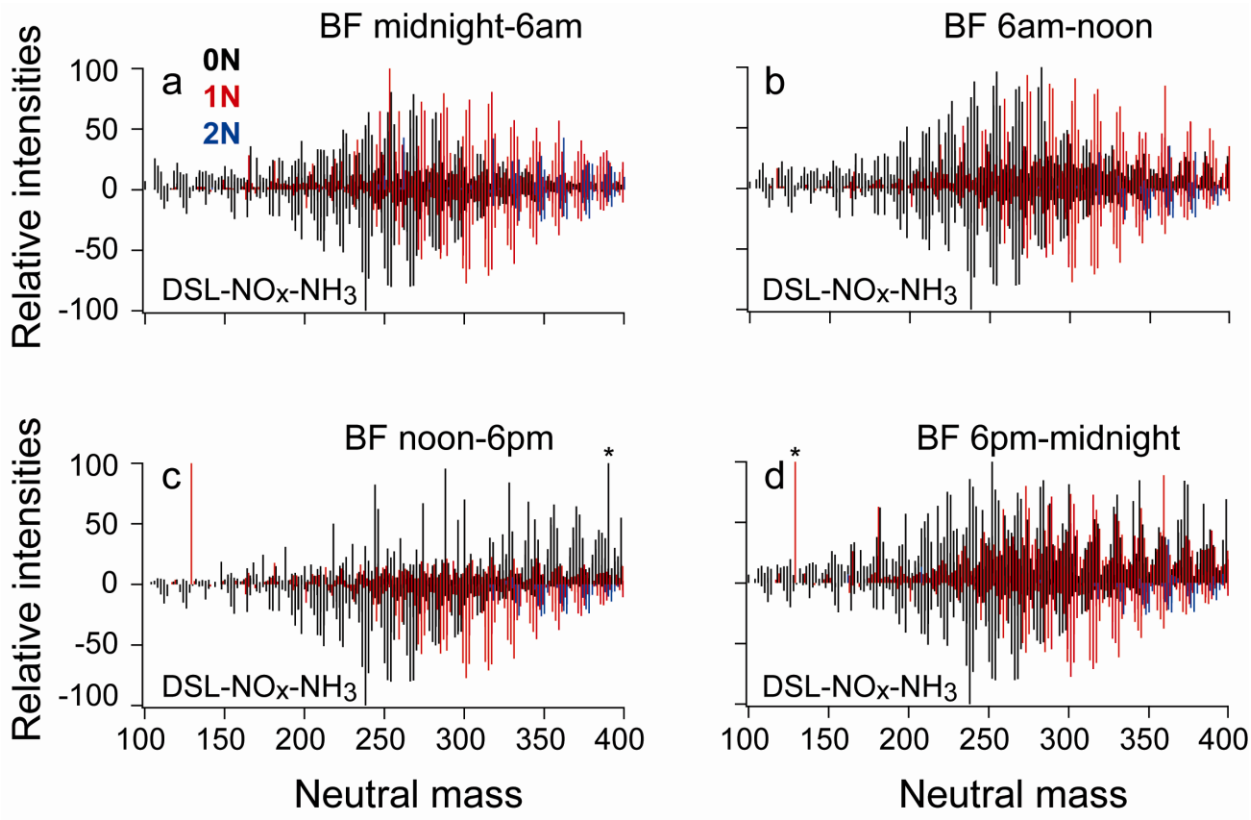

# Appendix C11
# Comparison MS LA to DSL-$NO_x$-$NH_3$ chamber

Comparison of the mass spectra for the LA ambient samples to the DSL-$NO_x$-$NH_3$ chamber experiment. The ambient mass spectra are on top and the diesel-$NH_3$ mass spectra are plotted with negative relative intensities to aid comparison. The colors correspond to the number of nitrogen atoms in the chemical formula with black = 0N, red = 1N, blue = 2N. The two red peaks with stars in (c) (149.105 and 253.204 Da) have intensities of 260 and 250 respectively and the two red peaks with stars in (d) (181.183 and 253.204) have intensities of 240 and 200 respectively.

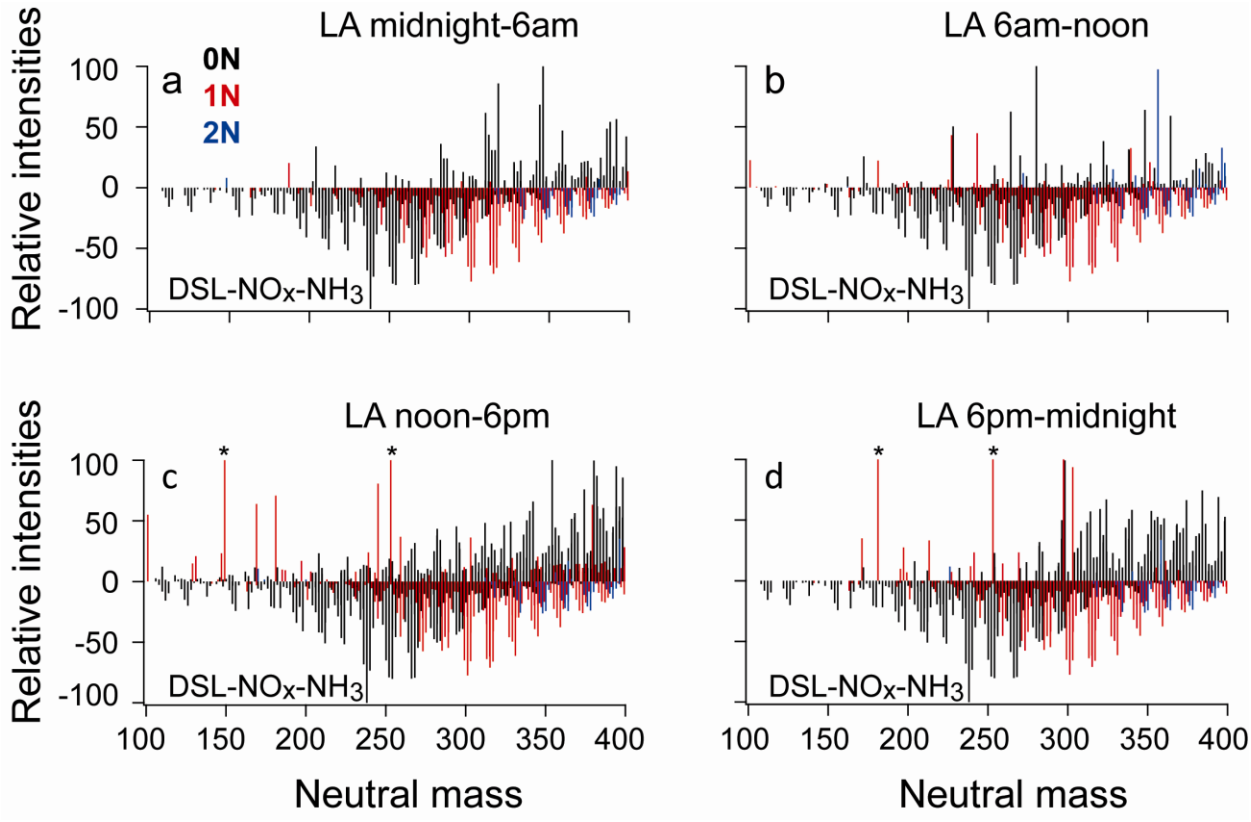

# Appendix C12
# Van Krevelen diagrams for chamber experiments

Van Krevelen diagrams for the three chamber studies showing O/C vs. H/C for each compound. In a) the DSL-$NO_x$ data is shown, b) DSL-$NO_x$-$NH_3$, and c) ISO-$NO_x$. The peaks are colored by the number of nitrogen atoms in the chemical formula with black = 0N, red = 1N, and blue = 2N.

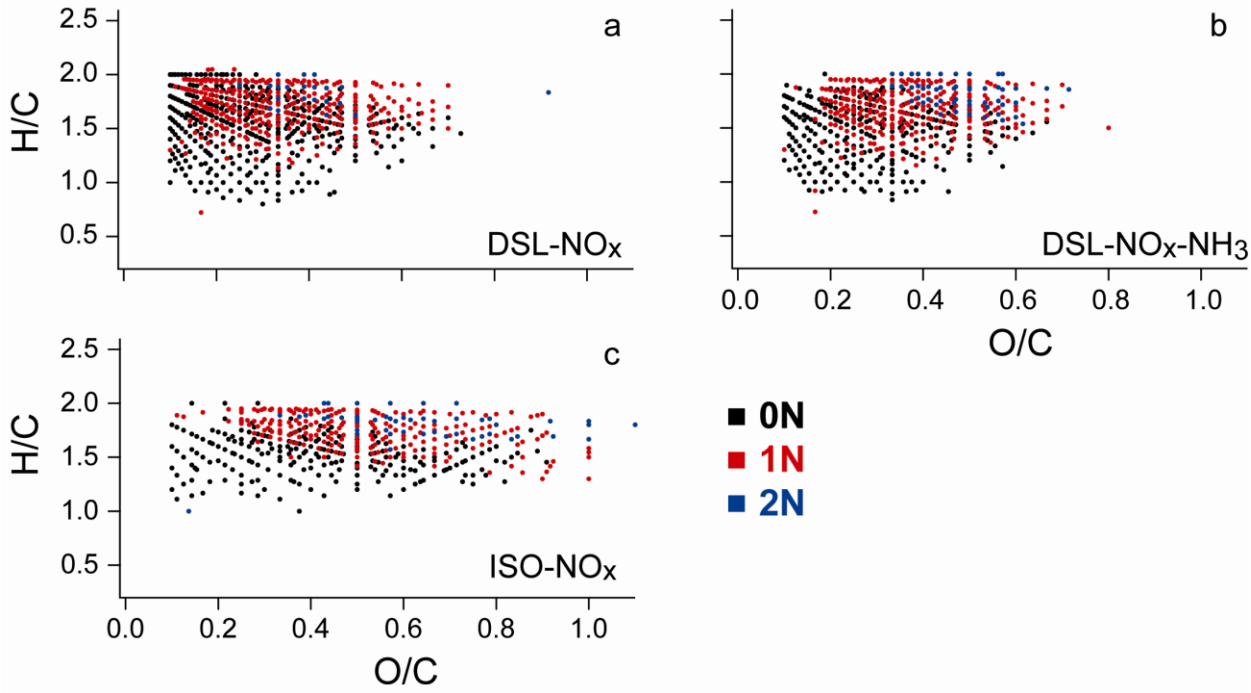

# Appendix C13
# Van Krevelen diagrams for BF samples

Van Krevelen diagrams for the four Bakersfield samples showing O/C vs. H/C for each compound. In a) the midnight-6am data is shown, b) 6am-noon, c) noon-6pm, and d) 6pm-midnight. The peaks are colored by the number of nitrogen atoms in the chemical formula with black = 0N, red = 1N, and blue = 2N.

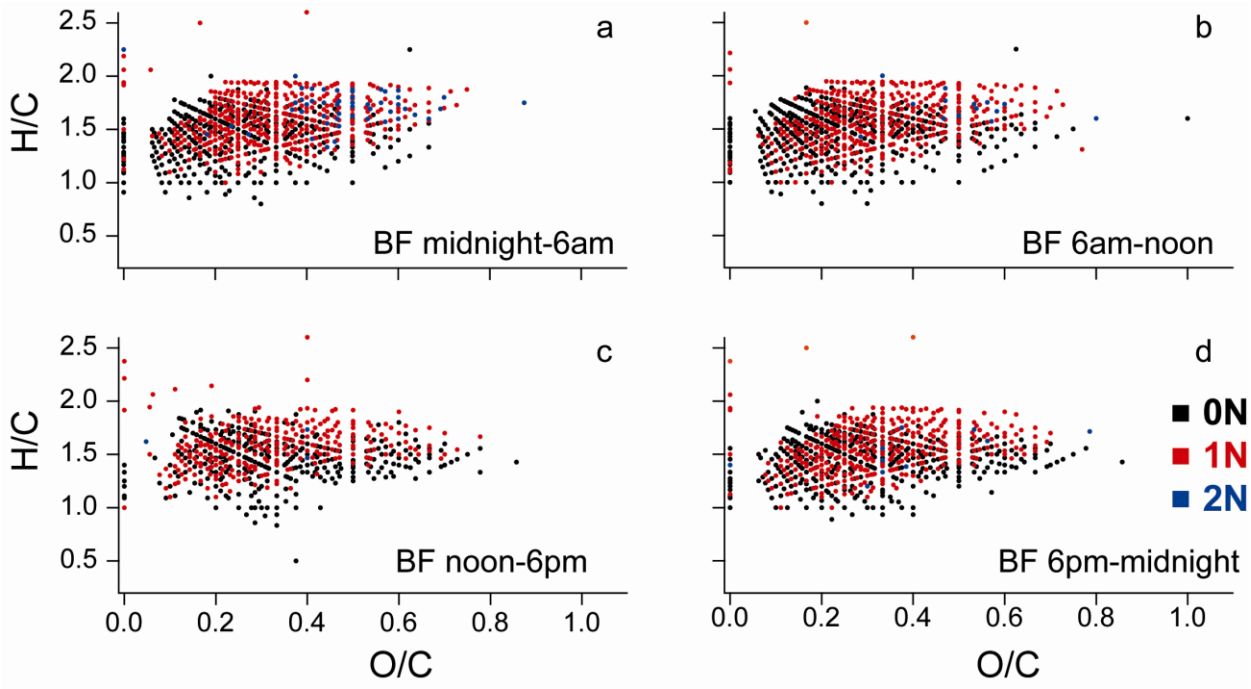

# Appendix C14
# Van Krevelen diagrams for LA samples

Van Krevelen diagrams for the four LA samples showing O/C vs. H/C for each compound. In a) the midnight-6am data is shown, b) 6am-noon, c) noon-6pm, and d) 6pm-midnight. The peaks are colored by the number of nitrogen atoms in the chemical formula with black = 0N, red = 1N, and blue = 2N.

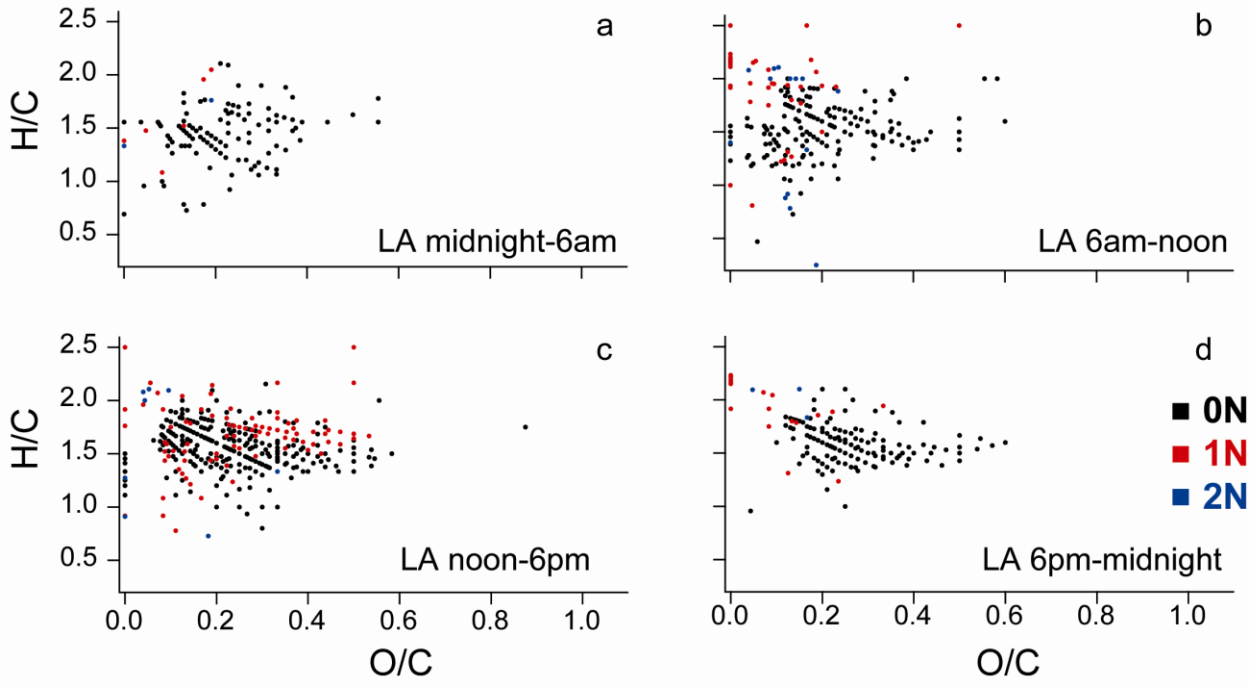

## Appendix C15
## Percent overlap of BF with ISO-$NO_x$ and DSL-$NO_x$

The percent overlap by count of the BF data on the LA data. The highest overlap is observed for the two afternoon LA samples. The equation used to calculate the percent overlap is given by:
% overlap = (number matching peaks /number peaks LA) x 100

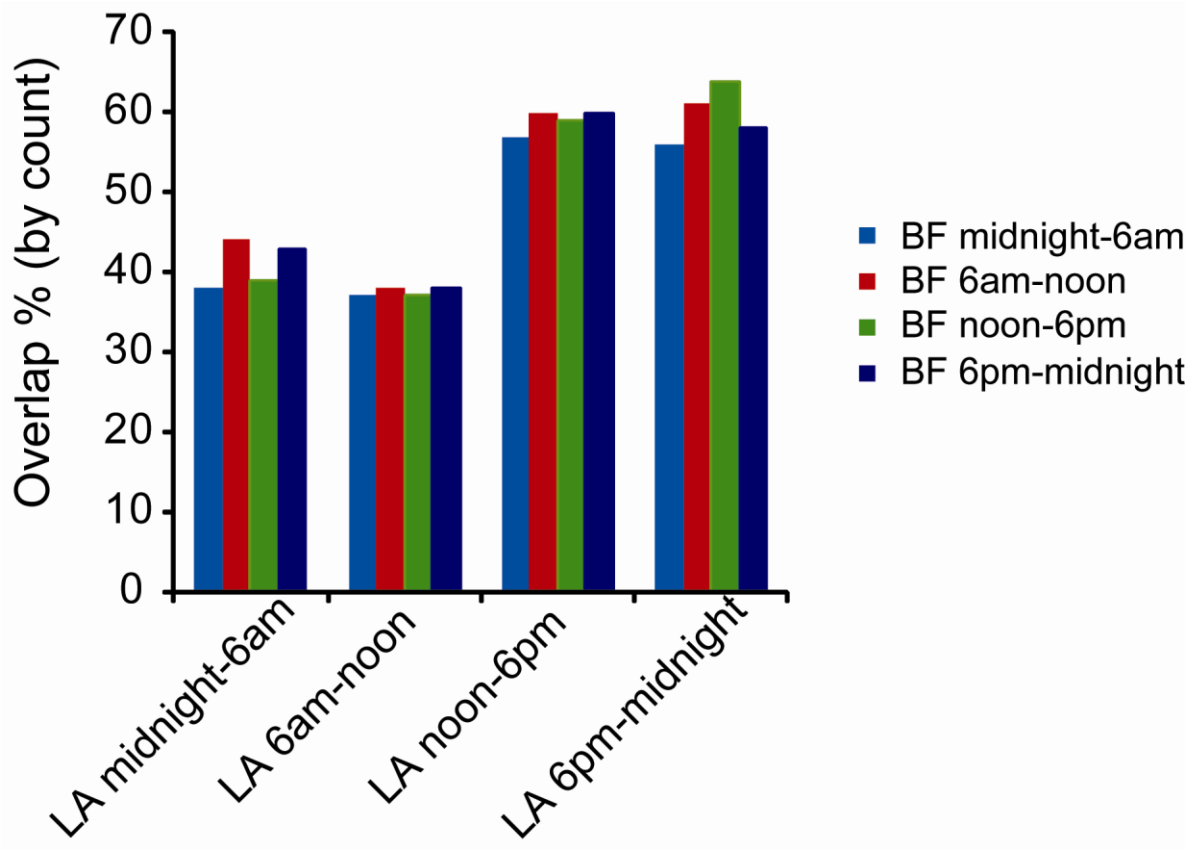

# Appendix C16
# Percent Unsaturation of BF and LA data

Percent unsaturation vs. neutral mass for the BF and LA samples. The circles are the unique data between the two sites for that time period colored by the O/C values of the compounds as indicated in the legend. The black pluses are the common peaks for comparison. The data from (c) and (d) are shown in Figure 4 in the text.

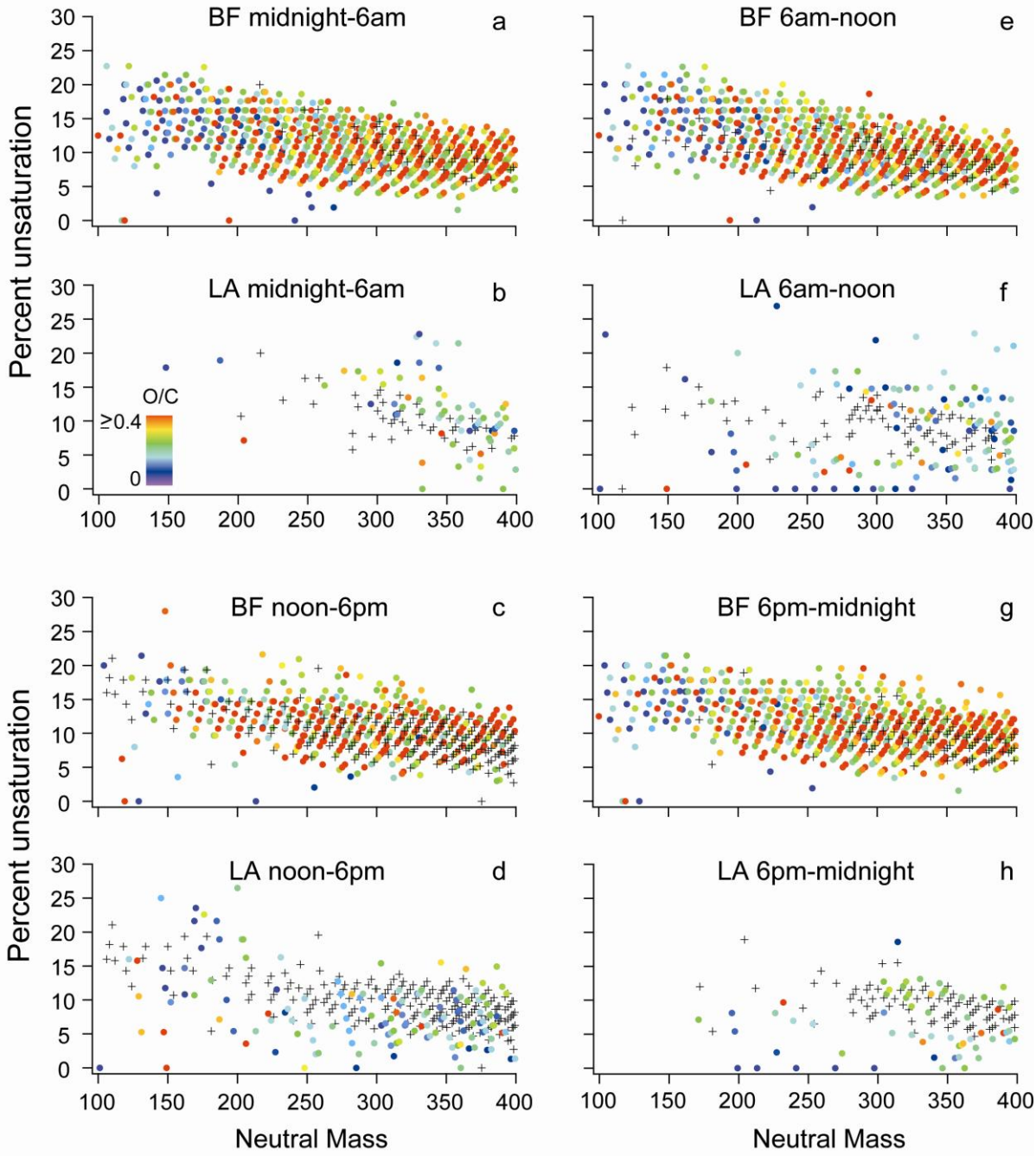

## Appendix C17
## Percent overlap of BF with ISO-$NO_x$ and DSL-$NO_x$

Comparison of the percent overlap of the Bakersfield data with the DSL-$NO_x$ and ISO-$NO_x$. The total percent overlap of the two chamber experiments is shown in black and white. The overlap of the compounds that are unique between DSL-$NO_x$ and ISO-$NO_x$ are shown overlaid with the unique DSL-$NO_x$ in orange and the unique ISO-$NO_x$ in green.

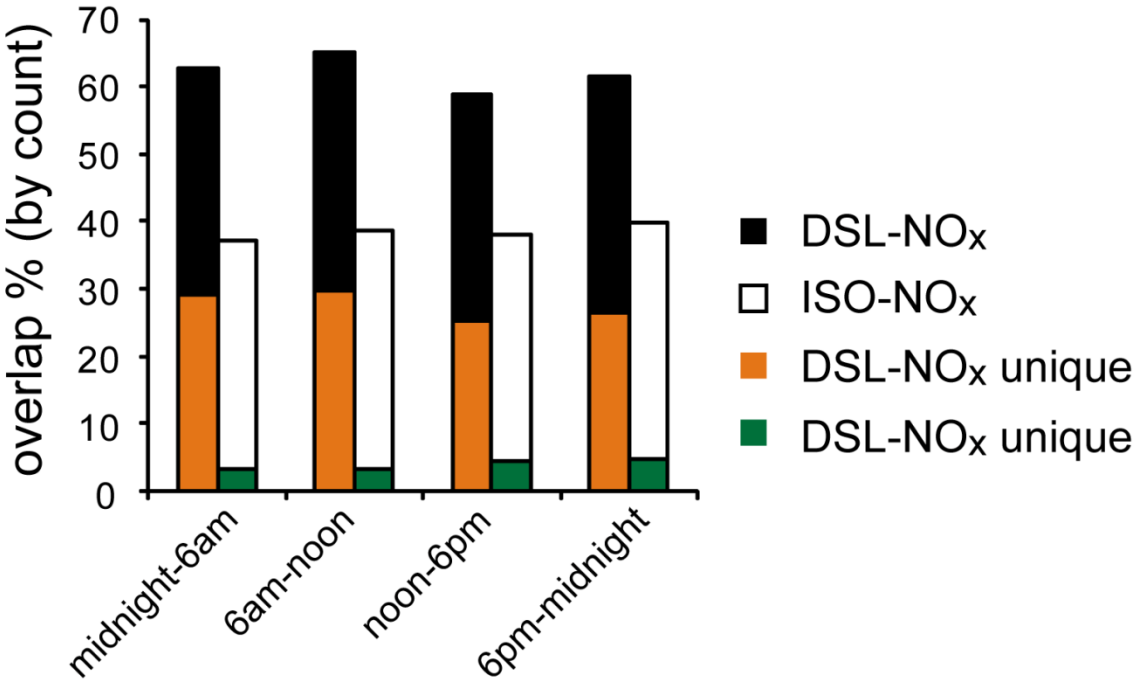

## Appendix C18
## Overlap between BF and unique DSL-$NO_x$-$NH_3$ and DSL-$NO_x$

Comparison of the percent overlap of the unique DSL-$NO_x$ (black) and unique DSL-$NO_x$-$NH_3$ (grey) with the BF sample from (a) the midnight-6am, (b) 6am-noon, (c) noon-6pm, and (d) 6pm-midnight. The data is broken down by the number of nitrogen atoms in the chemical formula. The noon-6pm panel (c) is shown in Figure 5a in the main body of the text with reduced axis.

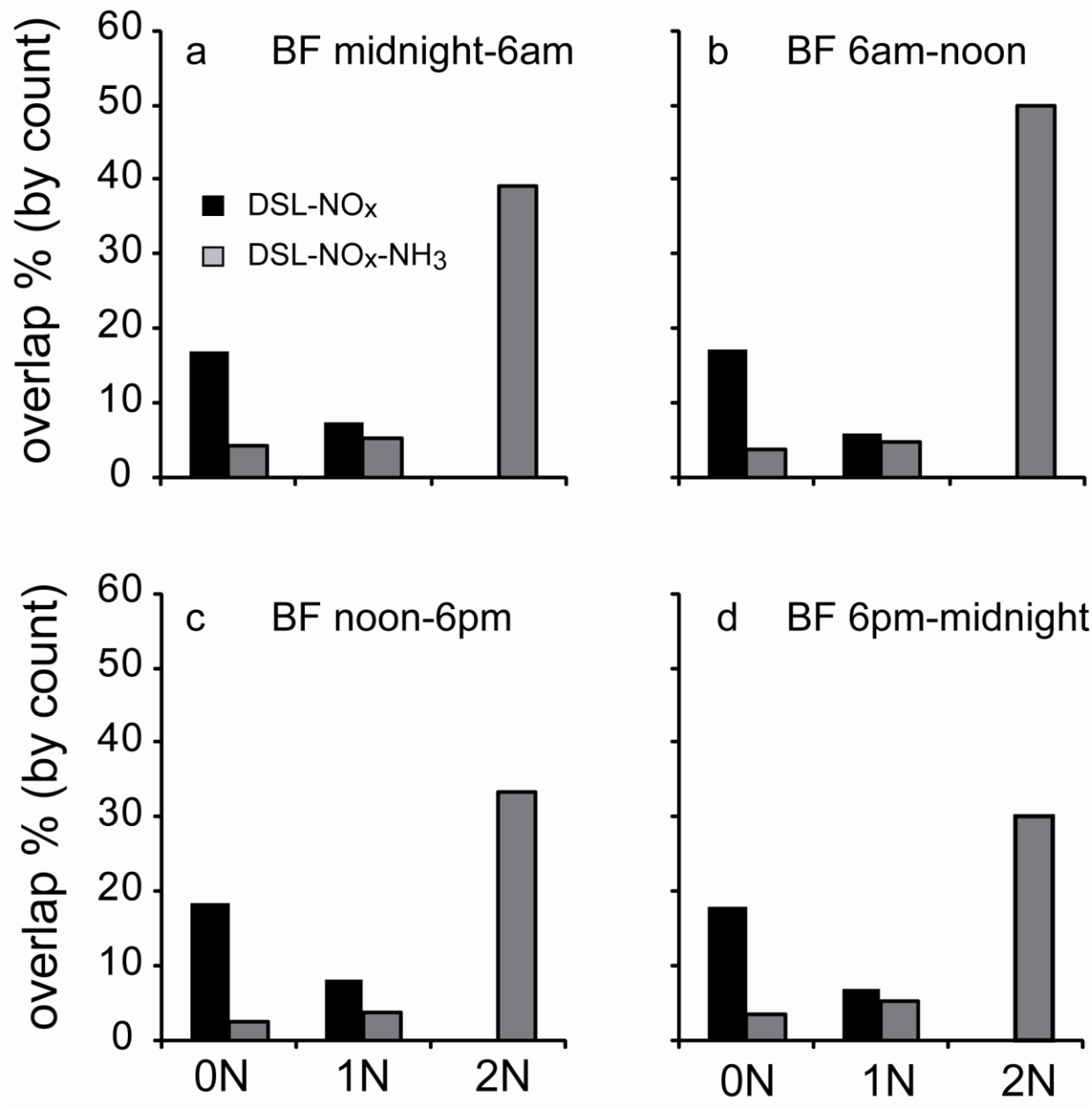

## Appendix C19
## Overlap between LA and unique DSL-$NO_x$-$NH_3$ and DSL-$NO_x$

Comparison of the percent overlap of the unique DSL-$NO_x$ (black) and unique DSL-$NO_x$-$NH_3$ (grey) with the LA sample from (a) the midnight-6am, (b) 6am-noon, (c) noon-6pm, and (d) 6pm-midnight. The data is broken down by the number of nitrogen atoms in the chemical formula. The noon-6pm panel (c) is shown in Figure 5b in the main body of the text.